



Research Doctorate in Life and Environmental Sciences

Curriculum of Biomolecular Sciences

Cycle XXXIV

**Vibrational imaging techniques
in teleost fish research:
new insights into reproduction and
development**

Supervisor:

Prof. Elisabetta Giorgini

Co-supervisor:

Prof. Giorgia Gioacchini

PhD candidate:

Dr. Chiara Pro

ABSTRACT

Fourier Transform Infrared (FTIR) spectroscopy and Raman Microspectroscopy (RMS) are vibrational techniques which have been revealed in the last ten years as excellent tools to study and characterize the chemical composition of several types of materials/compounds in the different physical states. They have the advantage to be label-free, making them objective and reliable approaches within chemical, biological, and biomedical research fields. Moreover, the coupling of last generation spectrometers with optical microscopes, makes it possible to collect in a few minutes and on the same sample, a great amount of information about the macromolecular composition and the distribution of the most relevant biomolecules (such as proteins, lipids, carbohydrates, and nucleic acids) within the analyzed sample. In fact, each macromolecule shows specific vibrational modes corresponding to transitions from adjacent vibrational energy levels, which are reported as peaks in the IR and Raman spectra: the position, width, and intensity of each peak let obtain a complete information on the molecular composition and structure of the sample.

The aim of the present PhD project was to exploit the potential of IR and Raman spectroscopies, in terms of spatial resolution and possibility of obtaining morpho-chemical information, to deepen physiological mechanisms, related to environmental issues, of wild and laboratory model fish species. In particular, the study was focused on: (i) the optimization of a fixation protocol for Raman analysis of fish embryos; (ii) the spectroscopic evaluation of the effects caused by emerging pollutants, such as perfluoroalkyl compounds, on the development of the embryos of the fish model *Danio rerio*, and (iii) on the possible correlation between the fishing area and the structural organization and the macromolecular composition of *Xiphias gladius* oocytes, with a particular focus on the Zona Radiata. The

advantage of using these spectroscopic approaches respect to routine methodologies (including histology, immunohistochemical and biomolecular assays) relies on the unique possibility given by FTIR and RMS, to provide on the same sample and at the same time, punctual information correlating the structural features with the macromolecular composition.

The objectives, methods and results of each chapter are listed below.

1. A new methodological set up for spectroscopic studies on fish embryos.

Aim: defining a specific fixation protocol to analyze Zebrafish embryos by Raman Microspectroscopy. *Methods:* Zebrafish embryos were collected from 1 until 5 days post fertilization (dpf), and immediately fixed using paraformaldehyde 4%, Bouin's fixative, and formol. Embryos were first submitted to a visual inspection by stereomicroscope and then analysed by the XploRA Nano MicroSpectrometer (Horiba Jobin-Yvon) with a particular focus on the yolk region. A x100 long working distance objective and the 532 nm diode laser were used to acquire spectra along the Z axis, going from the surface to 300 μm in depth. Raman spectra were acquired 3 times for 10 seconds in the spectral range 400–1800 cm^{-1} , opportunely pre-processed and analyzed (OPUS 7.5, Bruker Optics, Ettlingen, Germany). *Results:* The Raman analysis carried out on zebrafish embryos, evidenced that the protocol employing formol resulted the optimal one, in term of maintenance of morphological features and quality of Raman spectra.

2. Metabolism alterations in fish embryos exposed to emerging environmental contaminants: what can we learn from molecules vibrational changes?

Aim: monitoring the effects of PFOS and PFOA on the embryo development of *Danio rerio*, by the exploitation of Raman Microspectroscopy. *Methods:* Zebrafish embryos were exposed to PFOS and PFOA (0.02 μM , 0.2 μM , and 2 μM ; Sigma Aldrich, St. Louis, MO) from 2 to 5 dpf and then fixed in Formol (formaldehyde:glutaraldehyde 3:1). The yolk region of zebrafish embryos was analysed by the XploRA Nano MicroSpectrometer (Horiba Jobin-Yvon). A x100 long working distance objective and the 532 nm diode laser were used to acquire spectra along the Z axis, going from the surface to 300 μm in depth. Raman spectra, acquired 3 times for 10 seconds in the spectral range 400–1800 cm^{-1} , were opportunely pre-processed and analyzed (OPUS 7.5, Bruker Optics, Ettlingen, Germany). *Results:* The histological analysis suggested that PFOA and PFOS can cause alterations in the morphological features of 2-5 dpf zebrafish embryos. Moreover, the comparison between Raman spectra of all the treated samples and control ones evidenced that these perfluorinated compounds can alter the yolk composition and uptake.

3. New insights from FTIRI on *Xiphias gladius* reproduction: a correlation between oocytes morpho-chemical features and the fishing area

Aim: highlighting the morphological and macromolecular changes of Zona Radiata in relation to the fishing area. *Methods:* Ovary samples from swordfish females caught in the central (Sardinia and Sicily) and western Mediterranean Sea (Balearic Islands) were submitted to histological (H&E staining) and spectroscopic analysis by using a Bruker INVENIO-R interferometer coupled with a Hyperion 3000 Vis-IR microscope and a bidimensional Focal Plane Array (FPA) detector. IR maps (164 \times 164 μm^2 ; 4096 pixel/spectra) were acquired in transmission mode on the Zona Radiata (ZR) of vitellogenic (VTG) and mature (MAT) oocytes (4000–900 cm^{-1} MIR range; spatial resolution \sim 2.56 μm ; spectral resolution 4 cm^{-1} ; 256 scans).

Results: Differences in the macromolecular composition and morphology of the Zona Radiata of swordfish caught in the different areas were observed suggesting a relation between the physiological features and the fishing area.

CONTENTS

INTRODUCTION

1. Vibrational Spectroscopy: theoretical principles	1
1.1 Infrared spectroscopy	4
1.2 Raman spectroscopy	15
1.3 Biological applications of FTIR and Raman spectroscopies	24
2. Chemicals and endocrine-disrupting chemicals	30
2.1 Polyfluorinated and perfluorinated compounds	31
2.2 Distribution and uptake of poly- and per-fluorinated compounds	33
2.3 Bioaccumulation and toxicology of poly- and per-fluorinated compounds	35
3. Zebrafish (<i>Danio rerio</i>): a laboratory animal model	40
3.1 Zebrafish anatomy	41
3.2 Zebrafish reproduction	42
3.3 Zebrafish as animal model	45
4. Swordfish: a vulnerable fisheries resource	47
4.1 Swordfish anatomy	48
4.2 Swordfish reproduction	50
References	53

CHAPTER 1

A new methodological set up for spectroscopic studies on fish embryos	65
---	----

CHAPTER 2

Metabolism alteration in fish embryos exposed to	
--	--

environmental contaminants: what can we learn from molecules vibrational changes	81
---	----

CHAPTER 3

New insights from FTIRI on <i>Xiphias gladius</i> reproduction: a correlation between oocytes morpho-chemical features and the fishing area	103
---	-----

CONCLUSIONS	123
--------------------	-----

INTRODUCTION

1. VIBRATIONAL SPECTROSCOPY: THEORETICAL PRINCIPLES

Vibrational spectroscopy is a well assessed analytical tool for the characterization of the chemical composition of compounds/matter. It is used to analyse a wide variety of samples, in small quantities and in different physical states. By the analysis of the interaction between the electromagnetic radiation and the chemical bonds, it let identify the functional groups within a molecule.

The electromagnetic radiation is a wave-like and particle-like phenomenon (Figure 1.1). It is created when an atomic particle, such as an electron, is accelerated by an electric field, causing it to move. The movement produces oscillating electric and magnetic fields, which travel at right angles to each other in a light energy package called photon. Photons travel in harmonic waves at the fastest possible speed, $\sim 2.99 \cdot 10^8$ m/s in vacuum, which is the speed of light. Waves have some given characteristics, such as frequency, wavelength, and energy. Each photon carries a quantum of energy, whose value is directly related to the frequency of the electromagnetic radiation (equation of Plank): ν is the frequency of the electromagnetic radiation (measured in hertz, number of waves per second), and h is the Planck's constant (6.63×10^{-34} J s) (*Equation 1.1*).

$$E = h\nu = \frac{hc}{\lambda} \qquad \text{Eq. 1.1}$$

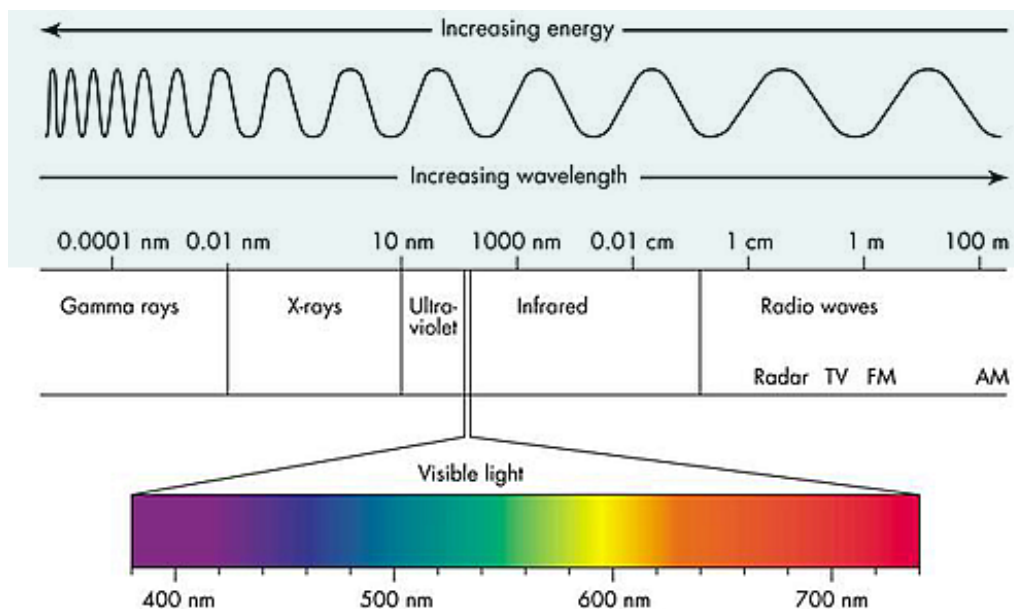


Figure 1.1. The electromagnetic radiation. Representation of the whole electromagnetic spectrum indicating the correspondence between frequency and wavelength (<https://www.cyberphysics.co.uk/topics/light/emspect.htm>).

The term vibrational spectroscopy includes infrared (IR) and Raman spectroscopies. Both are considered non-destructive label-free techniques as they do not require complex procedures regarding sample preparation, they not require added labels or dyes and they do not destroy the sample during the preparation and acquisition. They provide complementary information on the chemical composition of the sample, since they rely on different physical phenomena. In fact, the interaction between matter and the electromagnetic radiation can occur in different ways: absorption (transmission or reflection), as in the case of IR spectroscopy, and scattering, i.e. Raman spectroscopy. Infrared spectroscopy better identifies the asymmetric vibrations of polar groups, while Raman spectroscopy the symmetric vibrations of non-polar groups (Pavia *et al.* 2013).

Vibrational spectroscopy is mainly used for qualitative determination, even if quantitative analyses can be performed, too. The chemical compounds that can be identified and analysed are various, from organic and inorganic chemistry to pharmacology, toxicology, biomedicine, and even forensic and cultural heritage. Moreover, both IR and Raman spectrometers can also be coupled with visible microscopes, enabling the possibility to spectral map non-homogeneous samples, combining morphological and spectral information (Griffiths et al. 2007; Larkin 2011; Nyquist et al. 1971; Stuart 2005).

The vibrations observed in molecules are defined fundamental. They are quantized in specific energy levels, and they can be divided into two main categories: internal and external vibrations. Internal vibrations occur within a single molecule, while external ones arise between two or more units of molecules, and are also called lattice or crystal vibrations.

Internal vibrations can be classified as stretching (ν) and bending (δ) vibrations. A change in the inter-atomic distance along the bond axis is called stretching; in case of geminal bonds, there is a symmetric and asymmetric stretching, respectively if the length of the bonds varies in the same way, or in an alternate way (Figure 1.2A). Conversely, when the motion involves changes in bond angles, the vibration is called bending. There are two types of bending vibrations: in-plane (ip) and out-of-plane (oop) (Figure 1.2B). The first occurs in the plane of the molecule and it can be anti-symmetric and symmetric, named respectively rocking and scissoring. The out of plane-bending shows changes in the bond angles across the plane of the molecule: these vibrations are called wagging and twisting.

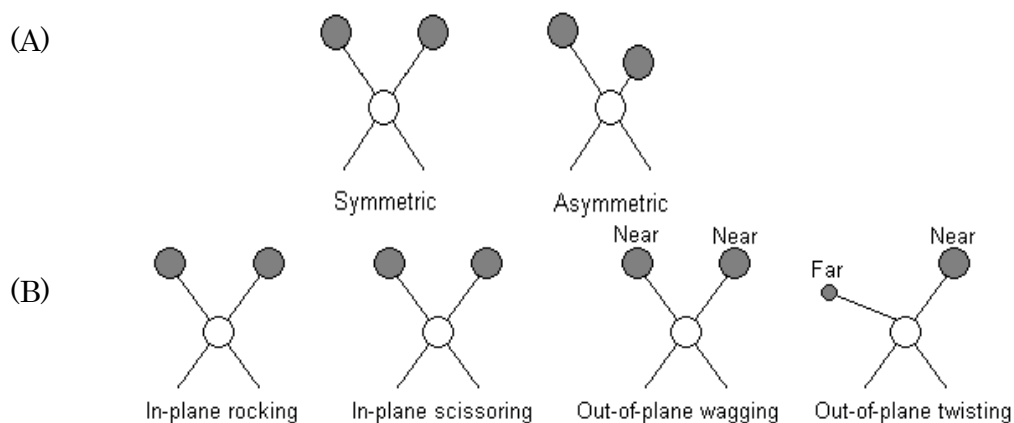


Figure 1.2. (A) Symmetric and asymmetric stretching vibrations with changes along the interatomic bond axis. (B) In-plane (rocking and scissoring) and out-of-plane (wagging and twisting) bending vibrations (<https://teaching.shu.ac.uk/hwb/chemistry/tutorials/molspec/irspec1.htm>).

1.1 Infrared spectroscopy

The infrared range of the electromagnetic spectrum is embraced between the visible and microwave regions and includes the spectral region from 25 μm to 1 mm, which corresponds to the wavenumber range 12.500 – 5 cm^{-1} . It can be furtherly split into Near-IR (NIR) from 12.500 to 4.000 cm^{-1} , Mid-IR (MIR) from 4.000 to 400 cm^{-1} , and Far-IR (FIR) from 400 to 5 cm^{-1} (Figure 1.3).

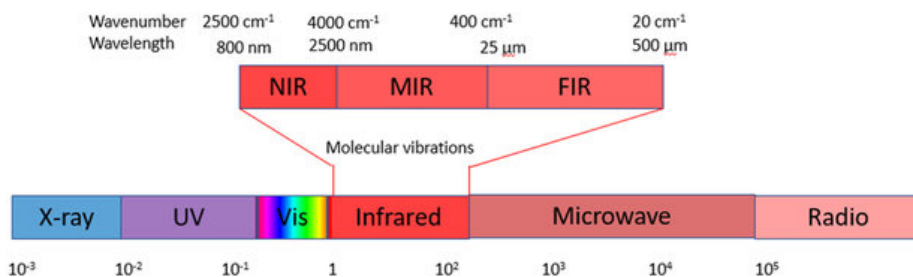


Figure 1.3. IR spectral ranges: NIR, MIR and FIR regions (Fox 2020).

All the regions of the electromagnetic spectrum can be described by a corresponding energy value E ; the relationship between this energy and the frequency of the electromagnetic radiation itself is described by the above defined equation of Plank (*Equation 1.2*):

$$E = h\nu = \frac{hc}{\lambda} \quad \text{Eq. 1.2}$$

It is possible to convert the frequency ν into wavenumbers $\bar{\nu}$, the units employed in IR spectroscopy, by the relationship (*Equations 1.3*).

$$E = hc\bar{\nu} \quad \text{Eq.1.3}$$

where the wavenumber is measured in cm^{-1} and c is the light speed ($2.99 \cdot 10^8$ m/s). From this relation it is evident that an increase in energy corresponds to an increase in wavenumbers.

The harmonic approximation

The vibration between two molecules can be expressed by the Hooke's spring law. The potential energy U of the vibration depends on the constant k and the distance x from the equilibrium position (stretching or compression of the spring) (*Equation 1.4*).

$$U = \frac{1}{2}kx^2 \quad \text{Eq. 1.4}$$

The classical harmonic oscillating spring model can absorb energy at any given wavelength. However, in the case of chemical bonds, IR vibrations must follow the rules of quantum mechanics; hence, the vibrational motion is a quantized function, allowing only certain transitions (*Equation 1.5*):

$$E_n = \left(n + \frac{1}{2}\right) h\nu \quad \text{Eq. 1.5}$$

In the *Equation 1.5*, ν is the frequency of the vibration, n is the quantum number (0, 1, 2, 3, etc...) and h is Planck's constant. $E_0 = \frac{1}{2}h\nu$ is the lowest energy level, $E_1 = \frac{3}{2}h\nu$ the next lowest and so on (Figure 1.4).

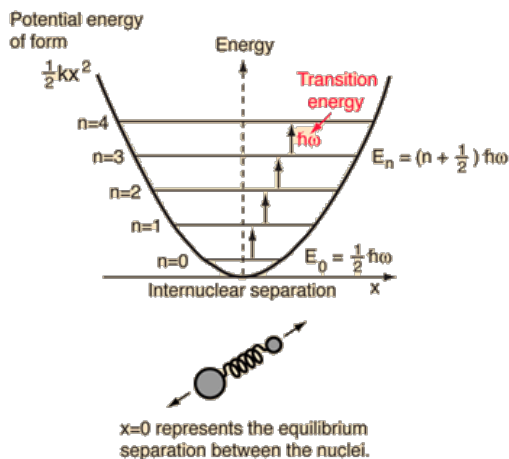


Figure 1.4. The harmonic oscillator model in which the quantized fundamental vibrations are shown (<http://hyperphysics.phy-astr.gsu.edu/hbase/quantum/hosc.html>).

A vibration between two atoms can only compress or stretch to a certain limit before colliding or breaking the bond. The Hooke's equation is changed to include the reduced atomic mass $\mu = \left(\frac{m_1 m_2}{m_1 + m_2}\right)$, the force of the bond k , and the frequency of the vibration (*Equation 1.6*):

$$v = \frac{1}{2\pi} \sqrt{\frac{k}{\mu}} \quad \text{Eq. 1.6}$$

The 1st selection rule declares that vibrations are IR allowed, only if the molecular dipole moment changes during the vibration itself. As regards the 2nd selection rule, only vibrational transitions from one level to the next are allowed; moreover, the most frequent transition is from the fundamental state to the first excited one and, hence, the molecule will absorb an amount of energy equal to $E_1 - E_0 = h\nu$. This means that energy is quantized from the fundamental vibration bond between two atoms in a molecule, which is essential for the harmonic approximation of the energy.

Sometimes, even transitions of $2h\nu$ or $3h\nu$ are observed: these transitions are called overtones and have lower intensity than the fundamental vibration. Moreover, when the vibrating bonds are coupled to a central single atom, some absorptions at high wavenumbers can be observed, named combination bands. The vibrational coupling is influenced by several factors: coupling between stretching or bending vibrations occurs when there is a common atom or bond between the two vibrating groups; the stronger is the coupling, the better the energy of the coupling groups approaches to the anharmonic approximation energy value; no coupling is observed when the groups are separated by two or more bonds.

The Lambert-Beer's law

Infrared spectroscopy is ruled by the Lambert-Beer's law, which is the fundamental law of absorption spectroscopy. Lambert's law states that the fraction of the incident light absorbed is independent by the intensity of the source. Beer's law shows that the absorption is directly proportional to the number of absorbing molecules. Combining the two laws, the Lambert-Beer law is expressed as follows (*Equation 1.7*) (*Smith 2011*):

$$A = \epsilon cl \quad \text{Eq. 1.7}$$

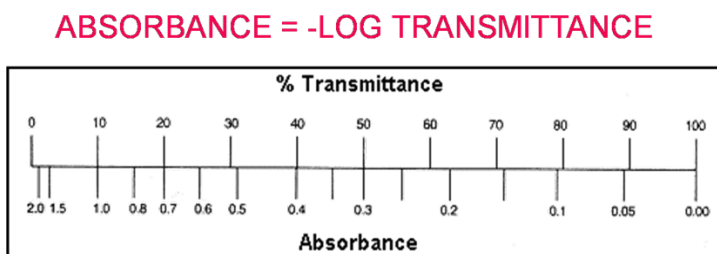
where A is absorbance (dimensionless), c is the concentration of the sample, l is the path length travelled by the light through the sample and ϵ is the absorptivity or extinction coefficient (given in units concentration per path length). The absorptivity ϵ is a fundamental physical property specific for the molecule/bond under investigation. For quantitative analysis absorbance is applied as it is proportional to concentration. For qualitative studies, transmission T can be employed: it gives a directly readable output-signal ratio as difference between sample and no-sample in the pathway of the IR beam, according to *Equation 1.8*

$$T = \frac{I}{I_0} \quad \text{Eq. 1.8}$$

where T is transmittance, I the intensity of the light passed through the sample, and I_0 the intensity of the incident light. The relationship between absorbance and transmission is described by *Equation 1.9*

$$A = -\log T \quad \text{Eq. 1.9}$$

This relationship can also be observed in Figure 1.5. If all the light goes through a sample without any absorption, absorbance is zero, and percent transmittance is 100%; if all the light is absorbed by the molecules of the sample, the percent transmittance is zero, and absorption is 2. Usually, all spectra are conventionally shown in transmittance (%T).



Abs = 0 100% light transmitted

Abs = 1 10% light transmitted

• Absorbance = 0 to 1.0 for minimal error

Figure 1.5. The relationship between Absorbance and Transmission as explained by Equation 1.9

(http://websites.umich.edu/~chem125/softchalk/Exp2_Final_2/Exp2_Final_2_print.html).

IR instrumentation

IR spectrometers are composed by several optical components, including the light source, the interferometer, and the detector. The scheme of a FTIR spectrometer is shown in Figure 1.6. The red line shows the optical pathway of the IR beam in the spectrometer, through the interferometer,

reflected off the mirrors, through the sample compartment (and the sample) to the detector.

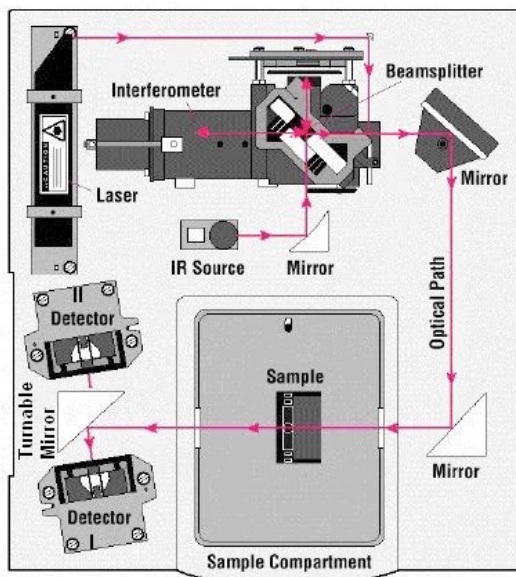


Figure 1.6. Schematic of a FTIR spectrometer with two detectors (https://www.researchgate.net/publication/232441996_Polyoxometalates_Immobilized_onto_Mesoporous_Organically-Modified_Silica_Aerogels_for_Selective_Oxidation_Catalysis_of_Anthracene/figures?lo=1).

Light sources

IR instruments need light sources which can provide radiant energy in the infrared region of the electromagnetic spectrum. There are several conventional light sources, such as the Globar source, the Nernst glower and ceramic filaments. Globar is a silicon carbide rod, which typically reaches temperatures in the range 1200-1800 K (Smith 2011). The Nernst glower is a very small cylinder made of fused oxides, such as zirconium oxide and yttrium oxide, electrically heated at around 1300K; its special feature is that it does not oxidize.

There is also an unconventional very performant light source, which is represented by Synchrotron radiation: it is generated by radially accelerated electrons in dedicated circular buildings named synchrotrons. Synchrotron radiation has a very high brilliance, letting obtain high quality spectra, with a resolution limit of about $3 \mu\text{m}$, near the diffraction limit. It is applied in several techniques, such as X-ray diffraction, crystallography and imaging, small angle scattering.

Interferometer

Modern IR spectrometers have at their core a Michelson Interferometer, which substitutes the old monochromator. The interferometer splits a beam of light into two beams and ensures one of the light beams travels a different path than the other (called Optical Path Difference, OPD, denoted by δ) (Smith 2011).

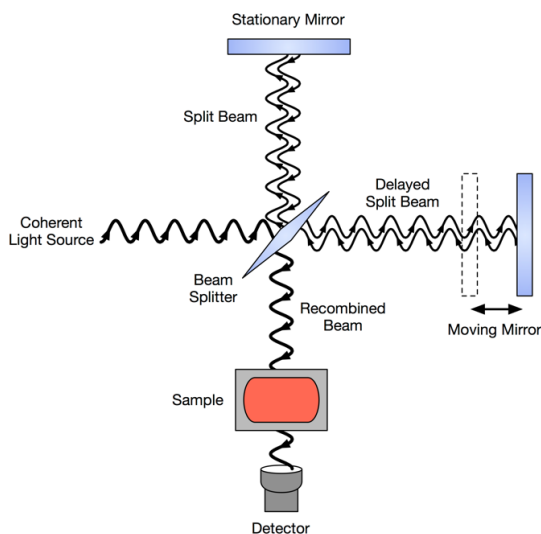


Figure 1.7. Schematic of the Michelson interferometer where the arrows show the optical pathway for the IR beam (<https://stackoverflow.com/questions/29657480/how-to-fourier-transform-an-interferogramm-to-an-ir-spectrum-using-r>).

The interferometer, represented in Figure 1.7, consists of two mirrors located at a straight angle each other and oriented perpendicularly, with a beamsplitter placed at the summit of the straight angle and directed with a 45° angle to each of the two mirrors. The beamsplitter splits the incident beam in two equal parts: the former goes through the beamsplitter to the translating mirror, while the latter is reflected to the fixed mirror. Both the fixed and translating mirrors reflect the incident beam and work at the same time. The two beams are then recombined and transmitted to the detector. When both the mirrors have the same distance from the beamsplitter, the distance travelled by the two light beams is the same, and this is called Zero Path Difference (ZPD), Δ . The relationship between mirror displacement with optical path difference is given by *Equation 1.10*:

$$\delta = 2\Delta \tag{Eq.1.10}$$

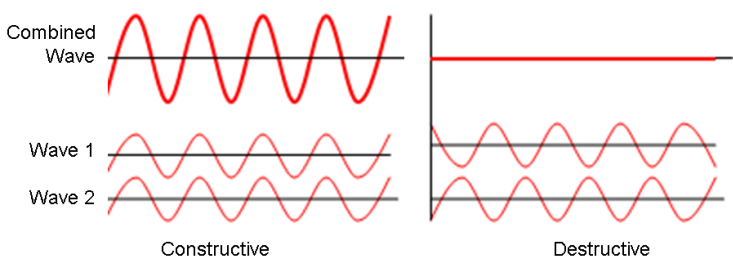


Figure 1.8: Destructive and constructive interference pattern for light travelling in an interferometer (https://en.wikipedia.org/wiki/Wave_interference).

If an optical path difference is introduced between the two light beams, by moving the translating mirror away from ZPD position, the light reflecting from the translating mirror is travelling more than the light reaching the fixed mirror. Light travels a specific wavelength λ in addition, giving a constructive wave pattern, and creating an intense light beam leaving the interferometer. The amplitudes of light are additive, so the

amplitudes of the two light beams travelling between the two mirrors is greater than the single beams.

$$\delta = n\lambda \quad \text{where } n = 0, 1, 2, 3, \dots \quad \text{Eq. 1.11}$$

Where ZPD corresponds to $n = 0$, constructive wave pattern takes place, if OPD is equal to multiples of λ . However, if ZPD is $\frac{1}{4}\lambda$ out of phase, OPD will recombine to give $\frac{1}{2}\lambda$, and a destructive wave pattern signal is generated (Figure 1.8), following from *Equation 1.12*:

$$\delta = \left(n + \frac{1}{2}\lambda\right) \quad \text{where } n = 0, 1, 2, 3, \dots \quad \text{Eq. 1.12}$$

In IR spectroscopy the interferogram observed is a multitude of amplified wave pattern. A typical interferogram is showed in Figure 1.9A. The centerburst is ZPD and it is the highest spike which can be observed in the interferogram: it is caused by the addition of all constructive wave amplitudes. The destructive wave pattern is observed in the wings, where the amplitudes delete each other, giving weak or no signal. This is the originally observed signal in Fourier Transform InfraRed (FTIR) spectroscopy: when the signal reaches the detector, it is mathematically transformed using Fourier Transform, from a function of mirror path differences to a function of wavelength/wavenumbers, giving birth to the well-known IR spectrum made of a series of subsequent peaks (Figure 1.9B).

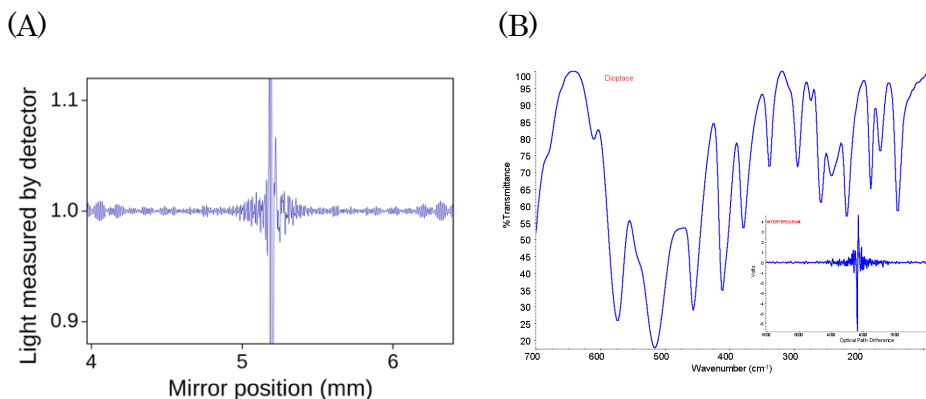


Figure 1.9: (A) Interferogram collected of the background, with OPD as a function of voltage. ZPD is the highest amplitude of constructive waves (<https://en.wikipedia.org/wiki/File:FTIR-interferogram.svg>). (B) FTIR spectrum and its interferogram (inserted) collected in transmission mode. The Cooley-Tukey algorithm transforms the interferogram into a readable IR spectrum (<https://stackoverflow.com/questions/29657480/how-to-fourier-transform-an-interferogram-to-an-ir-spectrum-using-r>).

Detector

When the interference reaches the detector, it produces an interferogram, which is the sum of sinusoidal waves. Each wave contains information about the wavenumber of a given infrared peak and amplitude information about the peak intensity at a specific mirror position (*Smith 2011*). So, the temperature fluctuations in voltage are measured by the interferogram by the detector and result as a function of OPD. Its transformation into transmittance occurs by applying the Fourier transformation (FT), a function of wavenumbers. Joseph Fourier, a French mathematician, first developed the FT in the 19th century and then, in the 1960, the Cooley-Tukey algorithm was designed: it is the IR spectroscopy algorithm applied nowadays.

Several detectors can be employed, depending on the nature of the sample and the type of acquisition. The most widespread detector is a pyroelectric bolometer named DTGS (Deuterated TriGlycine Sulphate). The

changes in the amount of infrared radiation reaching the detector are registered, causing a temperature change in the DTGS element itself. This impairment can be quantified because the change in temperature causes a modification in capacitance which can be measured by a voltage gap by the detector element. The DTGS detector is cheap, simple, and stable, even if less sensitive and slower than other detectors available. It is used for the analysis of homogeneous samples.

In the case of instruments equipped with Vis-IR microscopes, the MCT (Mercury-Cadmium-Telluride) detector is usually used (Figure 10A). It is more expensive respect to the DTGS, since it needs to be cooled using liquid nitrogen, but it has the great advantage of allowing to analyse non-homogeneous samples, such as tissues and cells, by acquiring the IR spectrum on selected areas of ca. $10 \times 10 \mu\text{m}$. It is usually applied for single point investigations. In case of hyperspectral imaging analysis, the most used detector is the FPA (Focal Plane Array) (Figure 10B): it is a focal plane array, detector, also working at liquid nitrogen temperature, which let acquire simultaneously 4096 spectra, allowing to perform imaging maps of the sample. Each array has a $164 \cdot 164 \mu\text{m}$ -side acquired area, 4096 pixel/spectra, and a spatial resolution of $2.56 \mu\text{m}$ for each pixel.

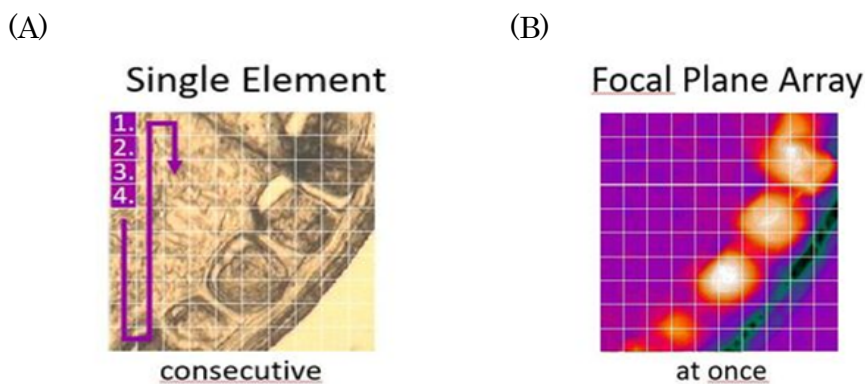


Figure 1.10: Images of MCT (A) and FPA (B) acquisition systems (<https://www.bruker.com/it/products-and-solutions/infrared-and-raman/ft-ir-microscopes/what-is-ft-ir-imaging.html>).

1.2 Raman spectroscopy

IR and Raman spectroscopies are usually considered complementary tools, due to the rule of mutual exclusion, which states that in a symmetric molecule with a centre of inversion, normal vibrational modes cannot be both infrared and Raman active. In contrast to IR spectroscopy, Raman spectroscopy uses a monochromatic light source to exploit the phenomena of the inelastic scattering, to investigate the chemical content of a sample (*Bonnier and Byrne 2012*). Raman spectroscopy has the advantage of allowing to investigate a wide variety of samples, in every condition, also hydrated, due to the weak contribution of water in the Raman spectrum, and with no need of preprocessing protocols (*Byrne et al. 2016; Cheng et al. 2004*).

Raman spectroscopy is based on light scattering, which can be seen as the redirection of light when a wave interacts with an obstacle. The interaction between the sample and the wave causes the electrons inside the molecule to be perturbed in a periodical way and with the same frequency (ν_0) because of the electric field of the incident wave which forms an induced electric dipole moment. The scattered light is the result of the disturbance of the electronic cloud which is then propagated. Two categories of scattering

processes can be distinguished: the elastic and the inelastic scattering (Figure 1.11). The elastic scattering occurs at the same frequency (ν_0) of the incident wave and it is called Rayleigh scattering. Conversely, the inelastic scattering of light has a different frequency (ν) compared to the incident light and it is known as Raman scattering. The inelastic scattering was observed as a frequency shift in the spectrum of scattered light compared to incident light, and it was experimentally observed in 1928 by Raman and Krishnan (*Raman et al. 1928*). Because of this, this frequency shift is today known as the Raman shift and can be calculated by the *Equation 1.13*

$$\Delta(\text{cm}^{-1}) = 10^{-7} \left(\frac{1}{\lambda_{\text{excitation}}} - \frac{1}{\lambda_{\text{Raman}}} \right) \quad \text{Eq. 1.13.}$$

Δ is the Raman shift, $\lambda_{\text{excitation}}$ is the wavelength of the excitation source and λ_{Raman} is the corresponding Raman wavelength.

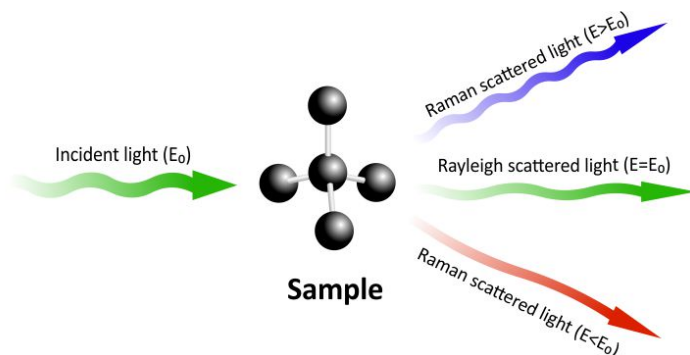


Figure 1.11. Light scattering by an induced electric dipole (<https://integratedoptics.com/Raman-Spectroscopy>).

The Raman effect can be explained as the interaction of the incident radiation of the electric field E with a molecule, which induces an electric dipole moment P (Figure 1.12) (*Equation 1.14*).

$$P = \alpha E \quad \text{Eq. 1.14}$$

where P is the dipole moment, α is the electric polarizability of the molecule and E is the amplitude of electrical field caused by the incident electromagnetic wave. Polarizability is an intrinsic property of the molecules, and it depends only on the electronic structure and the nature of the chemical bonds of the molecule.

Raman scattering can be simply described using the classical electromagnetic theory. First, polarization and scattering intensity have linear dependence on the laser intensity. Second, only vibrations which change the polarizability of the molecule are Raman active. The changes in frequency, or Raman shifts, can be positive or negative with respect to the laser frequency. In fact, besides the Rayleigh scattering in which no energy exchange occurs between light and the surface of the sample, light can be scattered by the molecule with higher frequencies (anti-Stokes Raman scattering) and lower frequencies $\nu_0 - \nu_i$ (Stokes Raman scattering): the former produces outgoing scattered photons with an increase in frequency $\nu_0 + \nu_i$, while the second one photons with a decrease in frequency $\nu_0 - \nu_i$ (Turrell 1996; Turrell et al. 1996) (Figure 1.12). More in detail, as regards the anti-Stokes scattering, the molecule is on an excited vibrational state, and it will relax back to the ground state gaining energy. Conversely, in the Stokes scattering, the molecule is on the ground state and must be excited to a virtual state by the radiation; it is subjected to a relaxation to a vibrational level at a ground state, with the result of an energy loss.

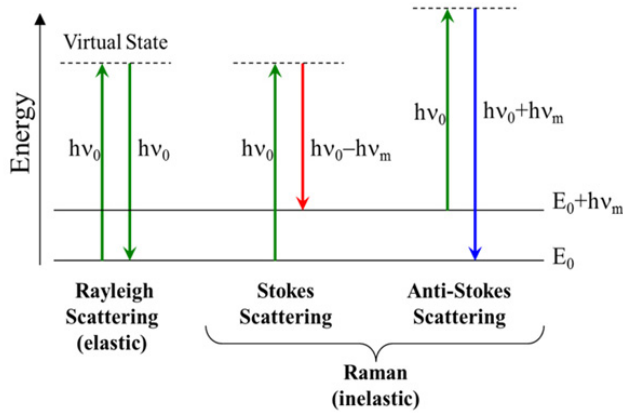


Figure 1.12. Jablonski energy diagram for Raman scattering (<https://bwtek.com/raman-theory-of-raman-scattering/>).

As regards the proportion between the amount of elastic and inelastic scattering, only a small part (10^{-6} of scattered photons) of incident photons undergo inelastic scattering. The ratio between the Stokes and anti-Stokes scattered light depends by the population of the vibrational ground and excited states and can be calculated using Boltzmann's equation (Winefordner 2005):

$$\frac{I_{Stokes}}{I_{anti-Stokes}} = \left(\frac{\nu_0 - \nu_i}{\nu_0 + \nu_i} \right)^4 e^{\frac{h\nu_i}{k_B T}} \quad Eq. 1.15$$

where T is the absolute temperature and k_B is the Boltzmann constant. Equation 1.15 shows the proportionality of Raman intensity with the fourth power of the frequency. The intensity of the Raman signal is increased by several orders of magnitude due to the resonance regime, (Czernuszewicz and Zaczek 2011; Okada et al. 2012) so that it is possible to provide the presence of certain analytes in very small concentration (Turrell, Delhaye, and Dhamelincoirt 1996).

Raman instrumentation

A typical Raman microspectrometer, as described in the image, consists of several components (*Approach et al. 2005; Winefordner 2005*) (Figure 1.13).

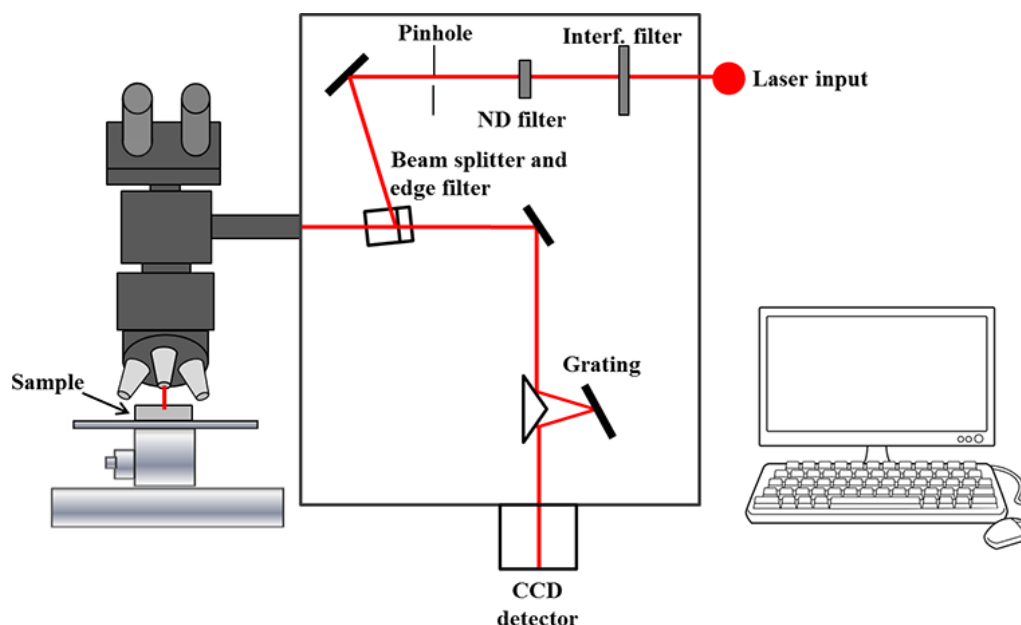


Figure 1.13. Schematic diagram of a Raman microspectrometer (<https://courses.lumenlearning.com/labmethods/chapter/part-of-a-raman-spectrometer/>).

Light source

The intensity of the Raman scattered light is proportional to $\frac{1}{\lambda^4}$. Because of this, Raman spectroscopy lasers are in the visible range of electromagnetic wave (400-660 nm). In fact, this allows higher efficiency of the CCD (Charge Coupled Device) detectors used for the detection of the Raman scattered light. The main disadvantage connected to the use of visible lasers in the case of Raman measurements of biological samples is the high probability to excite fluorescence emission, resulting in photo-sensibilization

or to damage the sample, degrading cells and tissues (*Puppels et al. 1991*). In addition, fluorescence emission can give place to a large background signal that can make the Raman spectrum unreadable. The Raman microspectrometer spatial resolution achieved is also based on the wavelength of the laser. Using confocal configuration, the resolution in the sample plane (*i.e.* normal to laser beam), is (*Diaspro 2002*):

$$r_{x,y,confocal} \approx \frac{0,61\lambda}{N.A.}, r_{z,confocal} \approx \frac{1,67\lambda}{(N.A.)^2} \quad \text{Eq. 1.16}$$

where λ is the wavelength of the laser and N.A. is the numerical aperture of the objective.

Sample illumination and signal collection

The latest generation Raman spectrometers are equipped with optical microscope objectives which allow efficient light collection in case of microscopic samples investigation. These objectives are a key component of the Raman microspectrometer and allow the possibility to focus the laser to a small spot maximizing the collection of the signal, increasing spatial resolution. The numerical aperture (N.A.) is an important defining parameter for a microscope objective and it describes the ability of an optical system to gather light. It is expressed by the *Equation 1.17*.

$$N.A. = n \sin \alpha \quad \text{Eq. 1.17}$$

where n is the refractive index of the medium between the sample and the objective, and α is the half angle of the cone of light. Raman objectives can be dry objectives (with $n=1$), where the maximum achievable half angle is 720° , with a calculated yield in N.A. of 0.95 (*Puppels et al. 1991*), or immersion objectives. Immersion objectives can be water or oil immersion objectives; the former is used more than the latter because oil can give rise to Raman bands that can overlap the Raman bands of the sample. As usual, immersion objectives are designed for higher light collection efficiency and

for observation of biological samples through a cover slip glass with a different refractive index.

Monochromators

Dispersive Raman spectrometers spatially separate the scattered light into light with different wavelengths, that are then throw simultaneously to an CCD detector. The schematic description of a Czerny –Turner monochromator is shown in Figure 1.14. It is made up by two concave mirrors, which collimate the Raman scattered light, and a reflective diffraction grating; the diffracted image is collected by the second mirror and focused on the CCD detector.

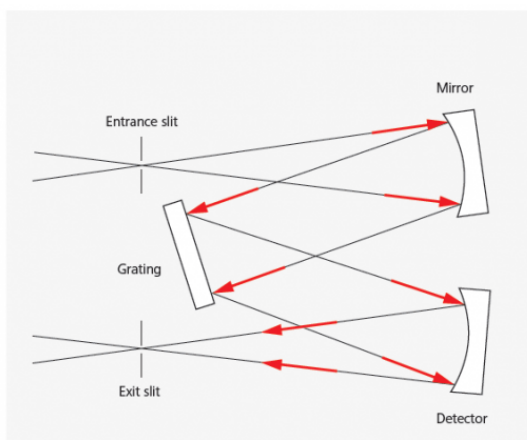


Figure 1.14. Schematic description of Czerny-Turner monochromator. (<https://www.tec5usa.com/product/plane-gratings/>)

The choice of a Raman microspectrometer must take into account many parameters: the flux of light (Φ) passing through the spectrometer, the focal length of the mirrors and the diffraction grating efficiency. *Equation 1.18* defines the wavelength for grating maximum efficiency:

$$\lambda_B = \frac{2d}{m} \sin \theta_B \quad \text{Eq. 1.18}$$

where θ_B is the angle between the face of the grooves and the plane of grating, m is diffraction order and λ_B is the distance between the grooves. Linear dispersion describes the spread of the wavelength domain within the plane of focusing mirror, and it is defined by the Equation 1.19 (Stimson et al. 1952):

$$\frac{d\lambda}{dx} = \frac{\cos\beta}{knf} \quad \text{Eq. 1.19}$$

where β is the angle of the diffracted light corresponding to the wavelength λ , f is the focal length of focusing mirror, k is the diffraction order and n is groove density of the grating. The linear dispersion is inversely correlated to both the focal length and/or the groove density of the diffraction grating. Higher dispersion results in a smaller $\frac{d\lambda}{dx}$ and gives a better spectral resolution, and an increased spread-out of the spectral domain on the CCD. Consequently, this leads to smaller spectral coverage by the CCD.

Detector

The CCD is the most used detector (Figure 1.15). It is a bidimensional detector where each element, called pixel, collects a different band of the spectrum. It works like the IR detectors, recording and manipulating the electric signal and converting it into a digital value. Each detector has a limited number of pixels (256, 512, or 1064), a much lower quantity than the number of spectral features to detect.

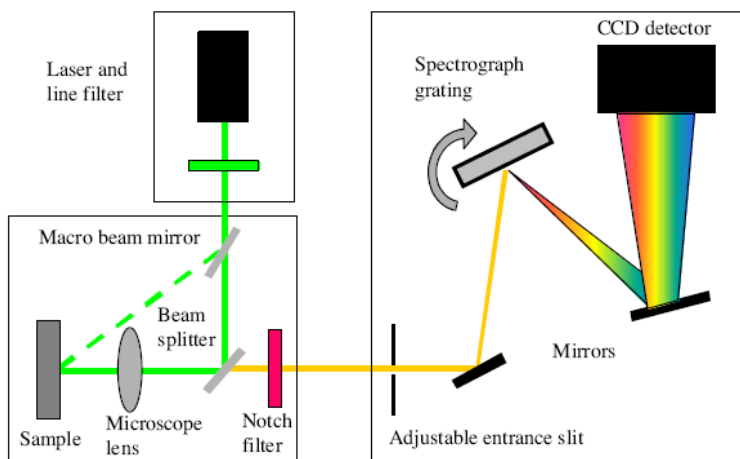


Figure 1.15. Description of the light path inside the Raman spectrometer (<https://www.sas.upenn.edu/~crulli/TheRamanSpectrophotometer.html>).

The selection of the CCD detector is very important, because it will determine the sensitivity, the spectral coverage, and the speed of the acquisition, which depends on the laser wavelength used for the excitation of the sample and on the characteristics of the spectrometer type. CCD performances are influenced by several parameters, such as the format, quantum efficiency, readout noise, dark current and dynamic range.

The coupling of a Raman spectrometer with an optical microscope, let observe and acquire specific areas of interest. In fact, by the fine regulation of X and Y axis, it is possible to map zones which can be in the range of few to hundreds of μm^2 , according to the laser and the objectives, which are usually 10x, 20x, 50x, 80x and 100x. Moreover, it is also possible to scan the sample in depth (i.e. in the Z-axis). Hence, the choice of the proper laser and objectives let obtain a profile of a layered sample (Figure 1.16).

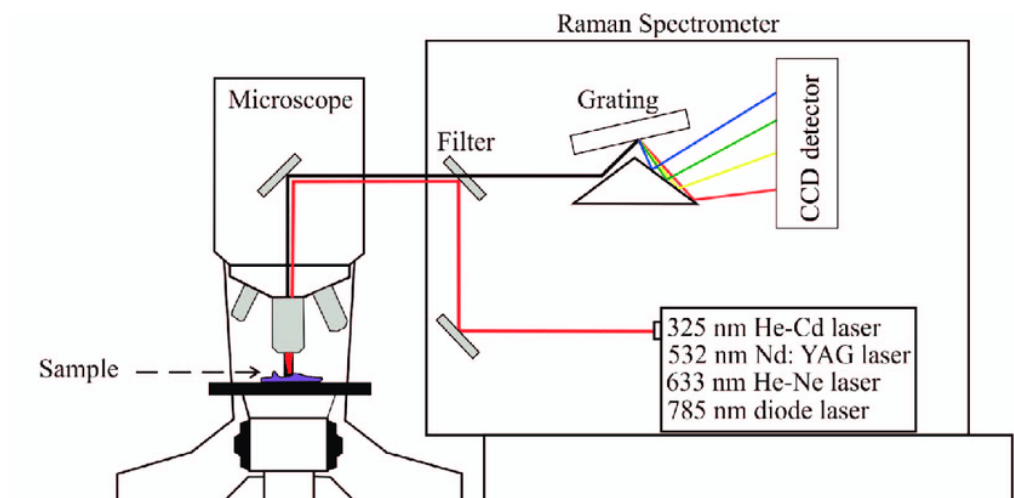


Figure 1.16. A schematic diagram of a modern Raman spectrometer (Chou et al. 2017).

1.3 Biological applications of Infrared and Raman spectroscopies

Vibrational techniques are widely applied in life sciences. In fact, the possibility to study non-homogeneous biological samples, such as cells and tissues, in a non-invasive, label-free and highly specific way makes these techniques very interesting from a scientific point of view. Moreover, spectral information on biological samples can be obtained both in transmission and reflection modes, by performing single point or hyperspectral imaging.

It is noteworthy that, even if biological samples are composed by several complex macromolecular components, each of them presents well evident absorption peaks in specific and different ranges of the spectrum. Hence, the analysis of IR and Raman peaks in terms of position, intensity and width provides relevant information on the chemical composition of the sample, allowing the identification and characterization of functional groups, bonding types and molecular conformations of the most important biological molecules, such as proteins, lipids, carbohydrates, and nucleic

acids (Barth 2007; Lyng et al. 2007; Mantsch et al. 1996; Pilling et al. 2016; Stuart 2005; Stuart 2006). This spectral approach can be used to detect biochemical alterations in tissues and cells, if affected by pathologies or when treated with external agents, and hence to identify the spectral markers which can be ascribable to a specific pathology or alteration (Larkin 2011; Owens et al. 2014).

The IR spectrum of a biological sample with the identification of the main peaks and their biochemical attributions is showed in Figure 1.17.

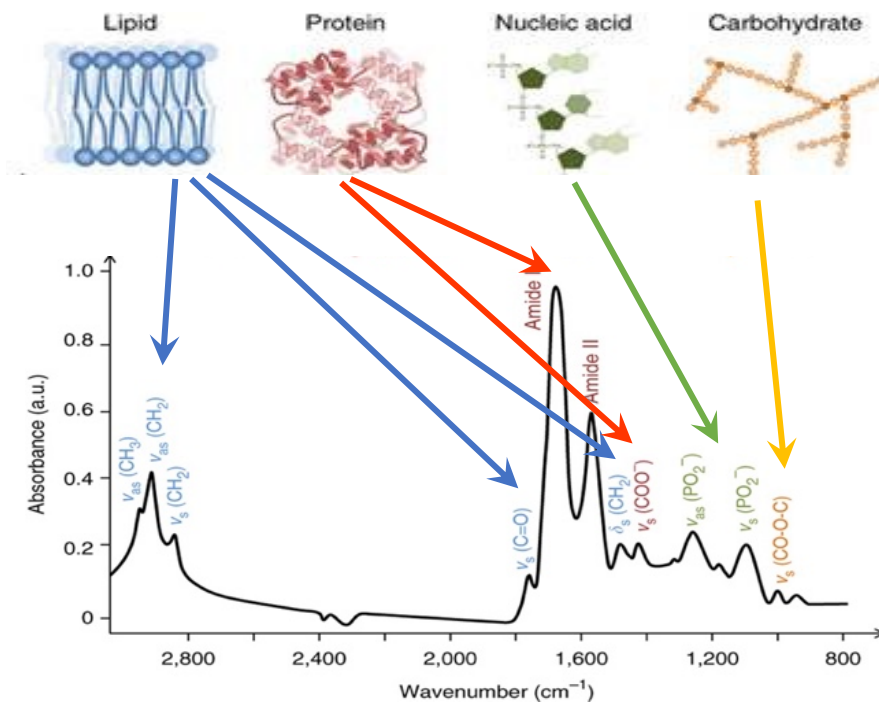


Figure 1.17. IR spectrum of a biological sample. The main peaks attributable to the most relevant biomolecular components are indicated together with the vibrational modes and the biological meaning (<https://www.nature.com/articles/nprot.2014.110>).

Due to the huge amount of data deriving from the vibrational analysis, it is usually necessary to apply statistical post-processing procedures, including multivariate and univariate analyses (*Bonnier et al. 2012; Byrne et al. 2016; Walsh et al. 2009*). Moreover, since IR vibrational modes of chemical bonds require frequencies which differ from each other for only few cm^{-1} , IR bands are often composed by several underlying bands; hence, the analysis of the spectra needs curve fitting procedures, to identify all the sub-bands, in terms of position, area, height and half-band width.

IR spectroscopy, as said before, through the application of a continuous range of frequencies, allows the assessment of the interaction between matter and electromagnetic radiation. Specifically, the most used range is the mid-IR region ($4000\text{--}400 \text{ cm}^{-1}$) in which it is possible to detect the fundamental vibrations, mainly stretching and bending, of biomolecules.

The possibility of exploiting IR spectroscopy on non-homogeneous biological samples is due to the coupling of IR spectrometers with visible microscopes. The investigation of the sample by the television camera allows to identify the areas of interest, which will be investigated by the IR spectrometer. Depending on the detector adopted for the analysis, we can find Fourier Transform InfraRed Microspectroscopy (FTIRM) and Fourier Transform InfraRed Imaging (FTIRI) spectroscopy. The former, usually carried out on cellular samples (*Giorgini et al. 2011; Notarstefano et al. 2021; Sabbatini et al. 2013*), is exploited by using a MCT detector and allows a single point analysis with a spatial resolution of ca. $10 \mu\text{m}$. Conversely, FTIRI is more suitable for the investigation of tissue samples: by the FPA detector, it is possible to achieve IR images $164 \times 164 \mu\text{m}$ size, composed by 4096 spectra with a spatial resolution of $2.56 \mu\text{m}$; a multivariate statistical analysis is usually performed on IR images, using proper programs with statistical tools which can discriminate or highlight differences or similarities among the given spectra (*Lasch et al. 2004; Wang et al. 2008*).

This hyperspectral imaging analysis can lead to the detection of subtle biochemical changes caused by specific pathologies, both benign and malignant, very useful for early diagnosis in life sciences (*Akbari et al. 2011; Anastassopoulou et al. 2009; Carnevali et al. 2017; Conti et al. 2009; Fabian et al. 2006; Giorgini et al. 2018; Lyng et al. 2015; Movasaghi et al. 2008; Notarstefano et al. 2022*). FTIRI has also the advantage of enabling the analysis of large sample areas in short time, allowing the identification of pathological areas present in the tissue (*Baker et al. 2014; Gazi et al. 2007; Giorgini et al. 2015; Krafft et al 2006*) For FTIRI analysis, tissue samples, deriving from biopsy or surgical excisions, must be 5-10 μm thick, so the light can pass through the sample.

As for FTIR spectroscopy, also Raman spectrometers are usually coupled with visible microscopes, thus enabling applications of Raman MicroSpectroscopy (RMS) to study the biochemical features of biological samples such as cells and tissues (*Butler et al. 2016; Chan et al. 2008; Matthäus et al. 2008; Naumann 2001; Romeo et al. 2006*). As already mentioned, Raman spectroscopy relies on the light scattering phenomenon produced by a monochromatic visible light (*Keating et al. 2013*). Moreover, the main advantage of Raman spectroscopy is that the sample does not require to be dried before the analysis. In fact, RMS can be exploited on cells and tissues under physiological conditions because water does not affect the acquisition in a negative way, as happens with IR spectroscopy (*Notingher et al. 2003*).

One of the several biological topics on which FTIR and RMS have been successfully applied is represented by reproductive biology. Many works have been published about, ranging from human to animal reproduction. More in detail, female gametes coming from oviparous and mammal species have been biochemically characterised by applying vibrational techniques (*Giorgini et al. 2014; Giorgini et al. 2012*). FPA-FTIR has been exploited to

investigate the effects induced by aging on human oocytes: IR images were acquired on single oocytes, focusing on the different morphological and quantitative distribution of lipids, proteins, and nucleic acids (*Gioacchini et al. 2014*). As concerns RMS, female gametes have been studied in few cases, focusing on the architecture of oocytes belonging to different species, on the different maturation stages during oocyte maturation, on mice oocytes subjected to aging phenomena, or on the structure of zona pellucida of oocytes (*Bogliolo et al. 2012; Bogliolo et al. 2020; Davidson et al. 2013; Heraud et al. 2017; Rusciano et al. 2010; Wood et al. 2008*).

Vibrational techniques have been also applied to study both commercial and wild fish species as well as fish models. Recently, some studies have been published on FTIRI analysis of the effects of different feeding regimes on liver and gut samples from Rainbow trout (*Oncorhynchus mykiss*), Gilthead Seabream (*Sparus aurata*), and Siberian sturgeon (*Acipenser baerii*) (*Randazzo et al. 2021; Randazzo et al. 2021; Zarantoniello et al. 2021*). Zebrafish (*Danio rerio*) is considered as a tool for developmental biologists since 1970s, thanks to its transparent embryos and rapid organogenesis. In this framework, ovary sections and single oocytes of zebrafish have been analysed by FTIRI, to investigate the oocyte maturation processes through specific spectroscopic features related to the distribution and macromolecular composition of vitellogenin and lipovitellin. FTIRM was also exploited to evaluate the effects of food additives, such as *Lactobacillus rhamnosus* and melatonin on zebrafish liver and gonads (*Gioacchini et al. 2012; Gioacchini et al. 2014; Giorgini et al. 2010*). As regards wild fish species, the different maturation stages of swordfish oocytes have been analyzed for the first time in 2019, by coupling FTIRI data with histological analysis. The morphological, topographical, and biochemical distribution of the most relevant biocomponents, such as lipids, proteins, and carbohydrates, was evidenced, highlighting the differences among

previtellogenic, vitellogenic, mature and atretic follicles. In addition, cortical alveoli, yolk vesicles, oil droplets and Zona Radiata have been outlined to complete the study (*Carnevali et al. 2019*).

2. ENDOCRINE - DISRUPTING CHEMICAL CONTAMINANTS

Nowadays, the presence of chemicals must be considered ubiquitous all over the world: they can be found in every man-made product, from personal care and health products, to clothes, merchandises, and every day-use good, from engineering to infrastructures goods. The chemical industry is one of the main economic sectors with major expansion perspective, according to the Organization for Economic Co-operation and Development (OECD) Environmental Outlook to 2030. It is estimated that about 75% of worldwide chemical output is produced by OECD countries, with a long-term increasing trend in Asian countries like India and China, too (*OECD environmental outlook to 2030 2008*). A category of compounds has come to the fore in the last decades: the endocrine-disrupting chemicals, worldwide known as EDCs. They are a group of molecules, chemically miscellaneous by activity and composition, applied and used in a wide range of items, and found to be cause of disease, morbidity, and health impairment in human and animal populations worldwide. The European Union defined them as “exogenous substance that causes adverse health effects in an intact organism, or its progeny, secondary to changes in endocrine function”. Recent studies predict lifelong effects in terms of outcoming diseases, due to the exposure of these compounds (*Trasande et al. 2016; Trasande et al. 2015*). Therefore, it is necessary to monitor, evaluate and assess as soon as possible the hazardous effects related to the exposure to EDCs, with the development of new methodologies or with the improving of the existing ones. There are nearly 85,000 man-made chemicals in the world, and people get in touch with many of them every day. Only about 1% of them have been studied for safety; and about 1000 of these chemicals may be EDCs, if we base on their similarity

with existing EDCs. The most common EDC types and product categories are brominated flame retardants (BFRs), polychlorinated biphenyls (PCBs), phthalates, bisphenol A (BPA), pesticides and herbicides and per- and polyfluoroalkyl compounds (PFCs) (<https://www.endocrine.org/topics/edc/what-edcs-are>).

2.1 Polyfluorinated and perfluorinated compounds

The polyfluorinated compounds (PFCs) are environmentally persistent compounds with a long carbon backbone, partly (*poly-*) or fully (*per-*) fluorinated, presenting either a carboxyl, alcohol, or sulfonate terminal group (*Conder et al. 2008*). Along with all the previous presented classes of substances, thousands of chemicals are included in this family of compounds. The most represented are the perfluorosulfonates (PFSAs), which comprise the perfluorooctane sulfonate (PFOS), and the perfluorocarboxylic acids (PFCAs), including perfluorooctanoic acid (PFOA) (Figure 2.1) (*Lindstrom et al. 2011*). PFCs are manmade chemicals with an extreme stability and unique physico-chemical features, making them very useful for several applications: they are used as oil and water repellents and in water and stain proof coatings of commonly used products, aqueous film forming foams, and thermally stable lubricants (*Lehmler 2005; Lindstrom et al. 2011*).

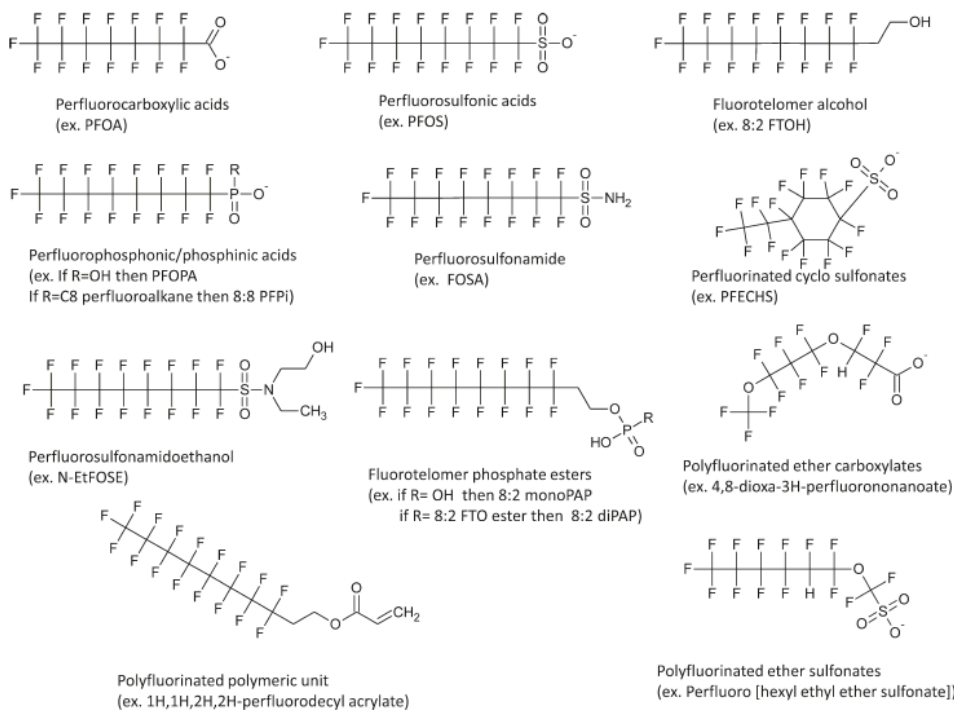


Figure 2.1. Generic structures for polyfluorinated compounds (Lindstrom, Strynar, and Libelo 2011).

The two most studied PFCs are PFOS and PFOA, which have the following chemical formulas: $C_8F_{17}SO_3^-$ and $C_8F_{15}COO^-$, respectively (Suja *et al.* 2009). These compounds do not break down when they are released into the environment, and they continue to accumulate over time, in a bioaugmentation chain. PFOS is toxic and extremely resistant to degradation, having long half-lives in animals and in humans (half-life of ~4 years). His continuous exposure may cause adverse health effects, resulting mainly in decreased body burdens, who produces adverse outcomes. PFOS has already been included among the Persistent Organic Pollutants (POPs) by the Stockholm Convention (*Secretariat of the Stockholm Convention. The new POPs under the Stockholm Convention. 2011*), while PFOA is still under evaluation for inclusion in the POPs list (*Stockholm Convention on Persistent Organic Pollutants (POPs) 2017*).

2.2 Distribution and uptake of poly and perfluorinated compounds

The distribution of PFCs is ubiquitous. Although their moderate water solubility, they have been found in surface water and groundwater. In Italy, PFAs were found in drinking water, and serum analysis brought to the identification of PFAs levels in blood: those levels reflected the actual period of exposure, going from months to years, and were related to a slow decrease in body weight (*Ingelido et al. 2018*). In particular, PFOA has been detected in high concentrations in USA (Tennessee and Ohio River, ~500 ng/l), in Germany (Alz River, ~56 µg/l) and in ocean waters (~100 pg/l) (*Loos et al. 2008*). PFOS has been detected in all the tested animal species, tissues, and locations (*Houde et al. 2011*). In the last 10 years, since the problem has emerged, many studies have been conducted in the aquatic system, to achieve data about the contamination of PFCs in the aquatic biota. A wide range of regions and habitats has been tested and analyzed to evaluate the possible risk of intake of these chemicals by humans: PFCs present in water move up the food chain until fishes to humans, providing one of the principal sources of dietary PFOS exposure (Figure 2.2).

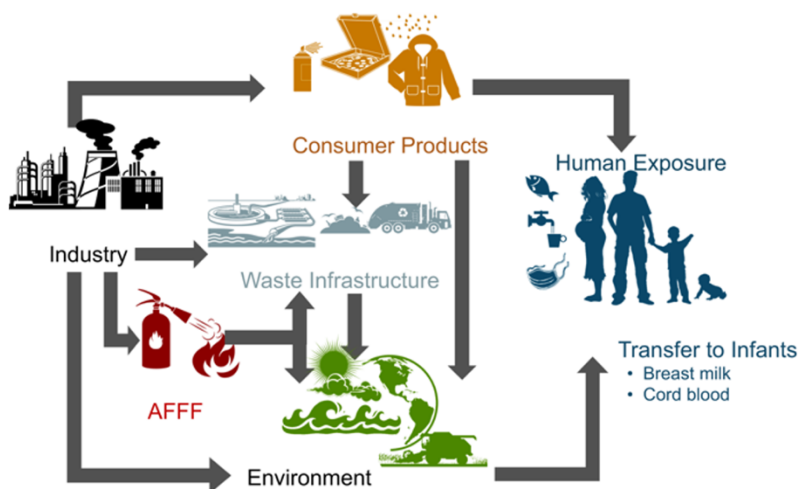


Figure 2.2. Potential major exposure pathways of PFAS to humans (Sunderland et al. 2019).

Studies have been conducted in Sweden, in the Lake Vattern, showing a median intake from seafood of 2.7 ng/kg body weight, in Italy, in Lake Maggiore, suggesting the presence of PFOS in all the analyzed muscles of *Coregonus lavaretus* and *Perca fluviatilis* (Berger et al. 2009; Squadrone et al. 2014). The total exposure to PFOS resulting from research carried out in 2008 arises in a daily exposure of 60 ng/kg body weight for persons who assume an average amount of fish or 200 ng/kg body weight for those who assume large amounts of fish; considering PFOA, the daily uptake was estimated at 2 ng/kg body weight/day, and 6 ng/kg body weight/day for those who eat larger amounts of fish products (*Perfluorooctane sulfonate (PFOS)*, *perfluorooctanoic acid (PFOA)* and their salts *Scientific Opinion of the Panel on Contaminants in the Food chain. 2008*).

2.3 Bioaccumulation and toxicology of poly and perfluorinated compounds

Among the EDCs, PFCs are the latest discovered and still under study. PFCAs and PFASs belong to the PFCs class of compounds and present a fluorinated carbon backbone terminated by a carboxylate or sulfonate, respectively. They are mainly present in the environment in the anionic form, because of their low acid-dissociation constant (pKa) values. In addition, the simple linear configuration seems to be the most detected isomer form in biota, determining a slow elimination rate (*Loveless et al. 2006*) and higher exposure concentrations (*Conder et al. 2008*). Perfluorinated molecules are partly hydrophilic and partly lipophilic, due to their molecular structure: they possess a variably long lipophilic core linked to a carboxylate or sulfonate hydrophilic functional group, making them amphiphilic, as shown in Figure 2.1. Because of this duality, perfluorinated molecules resulted from several studies to possess a proteinophilic nature, showing the capacity to bind to serum albumin and other cytosolic proteins (*Han et al. 2003*). In addition, other studies disclosed that protein-rich tissues, mainly liver and blood, are the principal reservoir of perfluorinated molecules in humans (*Houde et al. 2006; Martin et al. 2003*). Given their amphiphilic nature, PFASs present a good mobility in water environments too. Their bioaccumulation potential is related to chemicals' kinetic behavior, which depends on: (i) fast oral absorption (> 90% in 0.25–1.5 h); (ii) binding to both plasma and liver proteins, which represent the bioaccumulation reservoir; (iii) lack of biotransformation; (iv) very slow urinary excretion with renal resorption (*Loos et al. 2008*). Oral uptake of PFOS and PFOA is rapid and complete: when using a radioactively labelled PFOS and PFOA, 95% and 93% of the administered dose resulted to be resorbed by male rats within 24 h (*Stahl et al. 2011*). Considering metabolism, still no data have been reported for PFOA and PFOS, and excretion is the only way these molecules

can be eliminated from the organism with. The binding to proteins results in binding to albumin: the consequence is a low rate of glomerular filtration, as far as albumin is not subjected to this process. The half-time of PFOS is, thus, more than 90 days in rats, while the half-life for PFOA is much shorter: 2-4 hours for female rats and 4-6 days for male rats (*Lau et al. 2007*).

Acute, subacute and subchronic toxicity studies have been performed in rats for both PFOS and PFOA. They demonstrated a moderate acute toxicity, with a lethal dose with 50% lethality (LD₅₀) for PFOS of 251 mg/kg body weight and for PFOA of 430 to 680 mg/kg body weight per day (*Stahl et al. 2011*). Subacute and/or subchronic toxicity studies showed the insurgence of a variety of primary effects which vary on the animal species: hypertrophy and vacuolization of the liver, reduction of serum cholesterol, reduction of triglycerides in serum, reduction in body weight gain or body weight, and increased mortality (*Lau et al. 2007*). Several main disease categories are found to be linked to PFCs exposure: alteration of cholesterol levels, disruption of thyroid function, harming of liver and kidney function, alteration of the immune response, raising risk of ulcerative colitis, harming of reproductive health, increasing risk of birth defects, decreasing infant birth weights, developing of tumors and cancer (<https://www.endocrine.org/topics/edc/what-edcs-are>). As just said, the effects produced by PFOS and PFOA include developmental toxicity, when the mother animal was exposed during pregnancy. Due to their capacity to mimic fatty acids, PFCs can affect our biology interfering with the hormone systems. One of the main effects of PFOS and PFOA is the alteration of the thyroid gland function, due to a decrease of the T4 concentrations with respect to control animals, or to the competition between PFCs and the thyroid hormone transport protein transthyretin, and the influence of the neuroendocrine system, resulting in food intake and body weight reduction, ovarian cycle affection, corticosterone concentration increase, and leptin

concentration in blood serum decrease (Figure 2.3) (Olsen et al. 2007; Yu et al. 2009).

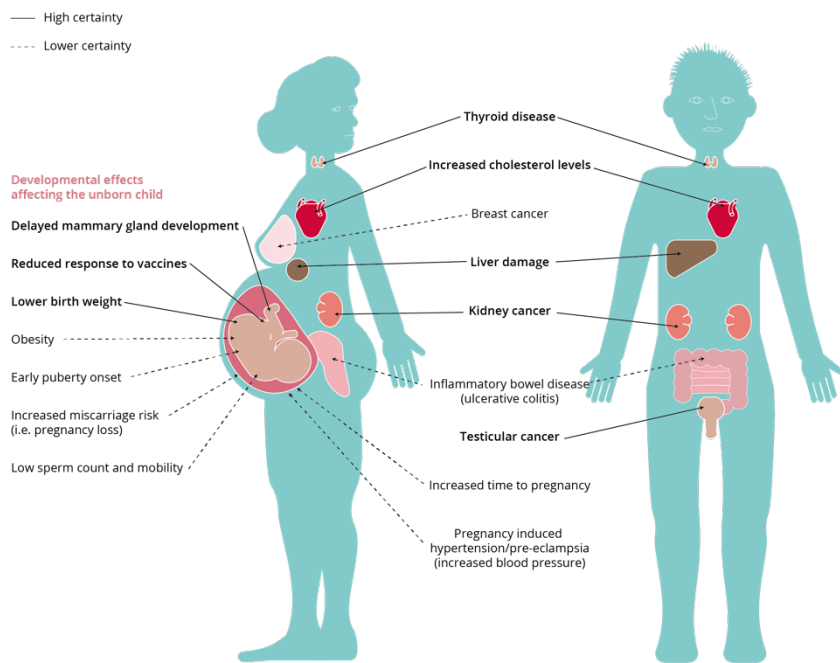


Figure 2.3. Effects of exposure to per-and polyfluoroalkyl substances on human health (Fenton et al. 2021).

In addition to thyroid hormone, PFCs can alter the biosynthesis of gender-specific steroid hormones: male rats have been tested with the administration of PFOA for 14 days, and the results were the reduction of serum and testicular testosterone, and an increase in estradiol levels in blood serum (Lau et al. 2007). Steroid hormones are not only involved in the gametogenesis, but it also regulates cell proliferation, which is involved, when deregulated, in carcinogenesis. Actually, PFOA resulted to trigger the promotion of carcinomas in liver of rainbow trout, in an estrogenic driven pathway; in fathead minnow, it caused an increase in vitellogenin and estrogen receptor b in male liver, and a degeneration of the ovaries in females. Recently, *in vitro* studies of cell lines treated with single and mixed

PFAS revealed the ability of these compounds to trigger proliferation using a non-classic estrogenic receptor signaling pathway (*Weiss et al. 2009*).

Having an affinity in binding proteins, many effects have been widely observed in liver in several species. The presence of PFCs, fatty acids-mimick, is correlated with an increase in the production of enzymes for fatty acid recovery, ketone bodies formation, and a decrease in protein synthesis for liponeogenesis. This can be partly correlated with the occurrence of liver tumours. In *in vitro* hepatocells, PFOA and PFOS administered in doses from 50 to 200 $\mu\text{mol/L}$ gave rise to the production of reactive oxygen species (ROS), to the alteration of the membrane potential of the mitochondria and to cell apoptosis. In addition, the activity of the superoxide dismutase, catalase, and glutathione reductase was increased (*Hu and Hu 2009*). A more recent study displayed that PFOS and PFOA did not damage DNA and their effects were not dose-dependent (*Eriksen et al. 2010*).

Water compartment is important not only for humans, but also for fishes. PFCs are usually searched in drinking water, or in fish species, since PFCs can reach humans through these sources (*Stahl et al. 2011*). PFOS was shown to be more toxic than PFOA in studies of freshwater organisms such as water flea, water snails, shrimp, and planaria. The lowest LC_{50} for fish is a 96-h LC_{50} of 4.7 mg/L to the fathead minnow *Pimephales promelas* (*Stahl et al. 2011*). Despite all these data, PFCs and their effects are poorly characterized by using the vibrational techniques. On the other side, FTIRM and RMS are widely applied in life sciences to study the biomolecular composition and building of cells (*Giorgini et al. 2014; Lyng et al. 2015; Matthäus et al. 2008*). FTIRM has been used to evaluate the injury occurred in liver and ovary, caused by the administration of EDCs or other chemicals, or by biological processes (e.g. aging). All these options have been exploited by the groups headed by Giorgini and by Carnevali, using human (*Gioacchini et al. 2018; Gioacchini et al. 2014*), zebrafish (*Carnevali et al. 2010;*

Gioacchini et al. 2014; Giorgini et al. 2010; Giorgini et al. 2012; Santangeli et al. 2017; Santangeli et al. 2018) Sparus aurata (Carnevali et al. 2017), Fundulus and heteroclitus (Lombardo et al. 2012; Lombardo et al. 2014) as model.

3. ZEBRAFISH (*Danio rerio*): A LABORATORY ANIMAL MODEL

Zebrafish (*Danio rerio*) is a freshwater fish, traditionally popular inhabitant of home aquariums (*Engeszer et al. 2007; Rosenthal et al. 2002*). It originates from South Asia, where it evolved around 320 million years ago, and, thus it uses to live in tropical areas, populating slow-moving water basins such as rivers and small streams or small pools and rice paddles (*McClure et al. 2006*). Its behavior is different from wild to laboratory conditions, as it happens for many species. Wild zebrafish is considered an eurythermic species, with a high adaptability to physical-chemical variations of the environment: it is shown to well tolerate temperature fluctuations in the range 16.5-38.6°C (*López-Olmeda et al. 2011*), and water pH values from 5.5 to 9 (*Ribas et al. 2014*), together with electrolyte concentration variations (*OECD guideline for testing of chemicals: Fish, Short-term Toxicity Test on Embryo and Sac-fry Stages 1998*). Laboratory conditions, on the contrary, are set in a tight range, maintaining in the optimal range of values for a tropical fish: temperature is kept in a 26-28°C range, with a pH going from 7 to 8 (*Avdesh et al. 2012; Lawrence et al. 2012*).

Feeding too is influenced by the living environment. Zebrafish is an eutyphagous omnivore: in wild conditions its diet is made of zooplankton and insects, and even of phytoplankton, filamentous algae, and invertebrate eggs, as results from gut analysis (*Spence et al. 2008*). In aquariums, zebrafish is provided with different kinds of food, depending on its developmental stage: larvae, juveniles and adults need specifically formulated diets, in the shape of microparticles or dried feeds (*Lawrence 2007*). In addition, there is a difference in the fish placement for feeding between the wild and the in captivity one: wild zebrafish feeds in the water

column, while in captivity ones do not seek for food in the bottom of the tank, thus causing the accumulation of uneaten food and, consequently, a decrease in water quality (Spence et al. 2008).

3.1 Zebrafish anatomy

Zebrafish owes its name to the dark blue and silvery vertical stripes flanking its body (MacRae et al. 2003). Males and females differ from each other in body size and livery colour: males display darker blue stripes with a pink tint in between and are leaner than females, whose abdomen is often whiter and more protruded, especially before laying eggs (Figure 3.1)

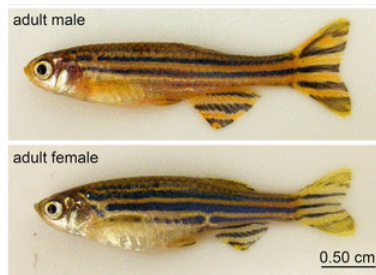


Figure 3.1. Comparison between male and female Zebrafish [from ourmarinespecies.com].

Zebrafish is a small fish belonging to the Cyprinidae family, to the Rasborinae subfamily and to the genus *Danio* (MacRae et al. 2003; Ribas et al. 2014). It reaches a maximum length of 3-5 cm. Considering the anatomy of zebrafish, and of fishes in general, they possess most of the tissue/organ types of mammals except breast, prostate and lung (Spitsbergen et al. 2003). The digestive apparatus of zebrafish consists of the intestine, which is located in the abdominal cavity, and is formed by a long tube that folds twice (Menke et al. 2011). It is not possible to distinguish stomach, small intestine, or large intestine even if the morphology of the mucosa columnar epithelial

cells and the number of goblet cells (responsible for nutrient absorption) possesses differences, suggesting functional differentiation. Liver is formed by three lobes not well organized in lower structures, and lies along the intestine; like in mammals, it is responsible of the homeostasis of the body and of carbohydrates, proteins, lipids, and vitamins metabolism (Figure 3.2).

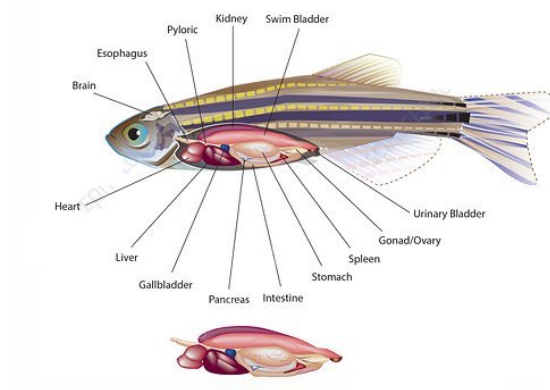


Figure 3.2. Zebrafish anatomy [from sciencephoto.com].

3.2 Zebrafish reproduction

Although zebrafish are not of economic importance as a source of food, they have become increasingly important in research studies as model systems: they are particularly important in developmental biology, biomedicine, and neurophysiology. Zebrafish has many important features that make it one of the most exploited animal model, such as short life cycle compared to other farmed fish species: it reaches reproductive competence at 3 months (Figure 3.3) (Ribas *et al.* 2014; Ulloa *et al.* 2011).

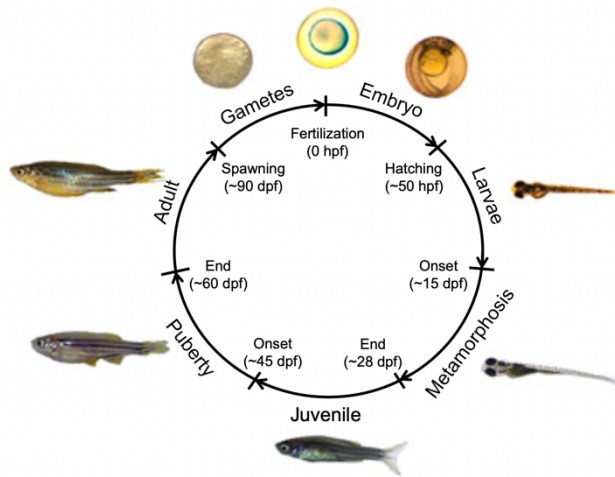
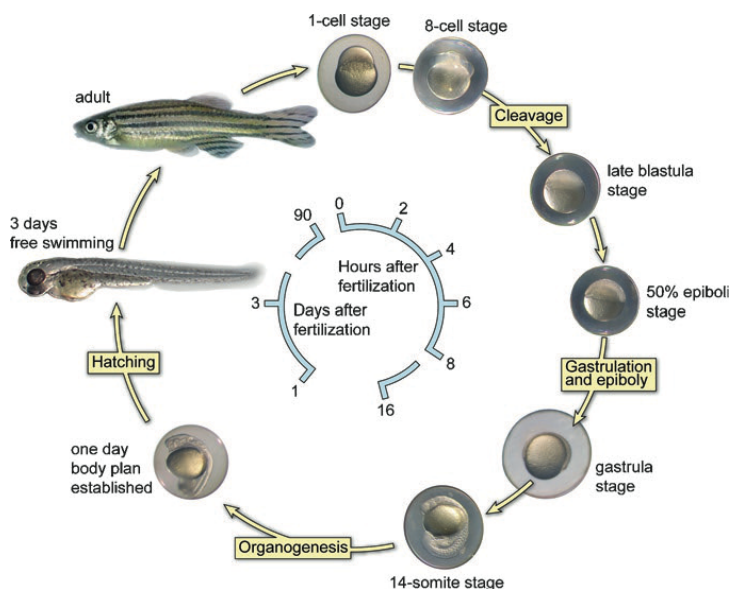


Figure 3.3. Zebrafish life cycle. Representative events separating different stages are shown. hpf, hours post-fertilization; dpf, days post-fertilization (Ribas et al. 2014).

Zebrafish, as said before, shows a sexual growth dimorphism: there are differences in body-size, shape and pigmentation between the male and female, making it easy to distinguish them in adult specimens. Whereas the zebrafish female tends to be larger in size with a rounded and whitish in colour belly, zebrafish male is slenderer, with a golden appearance on its belly. Males also have a golden appearance on their pelvic and ventral fin, while adult females have a small genital papilla located in front of the anal fin (Parichy et al. 2009). Zebrafish females have an asynchronous ovary, thus meaning that they have oocytes at different maturation stages at the same time in the ovaries (Clelland et al. 2009). Reproduction of zebrafish depends on temperatures and food availability. For this reason, wild animals have a spawning season once a year, in the late summer period, when temperatures are high and food abundant (Talling et al. 1998). On the contrary, in laboratory conditions, in a constantly monitored environment, maintained at set temperature and with constant fish supply, females are able to spawn every 10 days (Niimi et al. 1973). Since light stimulates the fish to mate, in

the wild zebrafish usually spawn short after daybreak (*Oecd Guideline For Testing Of Chemicals: Fish, Short-term Toxicity Test on Embryo and Sac-fry Stages 1998*). Each time zebrafish spawns, hundreds of eggs are produced. The clutch in captivity is more frequent than in wild, and even larger in dimensions and number of eggs (*Ribas et al. 2014; Spence et al. 2008*).



*Figure 3.4. A schematic representation of the embryonic developmental stages of zebrafish. The cycle starts at the top with a fertilized single stage. The embryos develop quickly to a 14-somite stage within 16 h. After 24 h, the complete body plan of the embryo has been established meaning that all organs are present. Two days after fertilization, the embryos hatch and become free swimming. Zebrafish are adult at 3 months of age and fertile (*Willemsen et al. 2011*).*

Zebrafish embryogenesis is rapid, with embryos developing and becoming larvae within four days after fertilization (*Kimmel et al. 1995*). In zebrafish embryogenesis seven periods have been detected, each of one occurring during the first 72 hours post fertilization (hpf) (*Kimmel et al. 1995*). Organogenesis starts during the first 24 hpf, and by 96 hpf most organs are fully developed (*Delvecchio et al. 2011; Stern et al. 2003*). Hatching phase marks the end of the embryogenesis, and it usually takes place throughout the third day of development, about 72 hpf (*Kimmel et al.*

1995) (Figures 3.3 and 3.4). In the 24 hours following the hatch, the early larvae drain almost all the yolk sac's content, the swim bladder inflates, and the larvae starts to swim actively around: they are able of swimming and seeking for food independently (*Kimmel et al. 1995*). The larval stage lasts up to 14-20 days, with a total length of approximately 5 mm; then, some changes occur transforming the larvae in juvenile fish, about 4 weeks after: the gut tube shifts to a more ventral position, the scale starts developing and the pigmentation patterns emerge (*Ledent 2002; Parichy et al. 2003*). At about 3-4 months of age, both wild and captivity-grown zebrafish reach reproductive maturity, with similar sizes (*Lawrence et al. 2012*).

3.3 Zebrafish as laboratory animal model

Zebrafish was recognized as a tool for developmental biologists in the 1970s. From the 1990s, it was used for the first vertebrate large scale mutagenesis screening, yielding thousands of mutations, some of which summed up human *diseases* (*Chakraborty et al. 2009*). Several unique advantages make zebrafish a convincing tool for drug discovery and developmental studies, not only for fish but also for humans. First, zebrafish is characterized by high fecundity, producing large numbers of embryos: each mature female can produce 200-250 eggs per mating. In captivity, mating is not seasonal, allowing a huge egg production. In addition, maintenance and husbandry costs are considerably lower than those for mammals. Second, embryogenesis is rapid. As mentioned before, the whole-body structure of the embryo is established by 24 hpf and most of the internal organs like heart, liver kidney and intestine are totally developed by 96 hpf (*Westerfield 2000*). Third, zebrafish larvae are transparent: this means that all the cells, organs and tissues can be easily *in vivo* visualized and real-time investigated (*Eisen 1996; Fishman 1999*). Fourth, genetic tools are available for zebrafish, such as whole genome sequenced, transcriptomic profile of several organs and

large-scale mutagenesis (*Driever et al. 1996; Haffter et al. 1996*). Fifth, zebrafish embryos can be used in toxicology studies to screen compounds detrimental effects by using only small volumes. Compounds can be directly added to water, and they are ingested and absorbed by embryos once they are able to swallow. Thus, little amounts of expensive metabolites or new targeted drugs or toxic substances can be rapidly evaluated. Compound screening, target identification, target validation, assay development and drug toxicity study can be performed, due to the given reproducible effects. Sixth, zebrafish share a largely conserved physiology and anatomy with mammals, allowing the translation from a system to the other. Seventh, there is a high degree of conservation between human and zebrafish genomes (approximately 75% similarity). This allows genetic analysis on a great number of genes to be performed, thanks to its complete genome sequence (*Genome, Map, and Expression <http://www.ncbi.nlm.nih.gov/genome/guide/zebrafish/>; Howe et al. 2013*). In addition, zebrafish has a high similarity degree with most of the fish species, and it can be used to replace fish species of economic importance in the biology of reproduction processes studies (*Dahm et al. 2006; Weltzien et al. 2004*).

4. SWORDFISH: A VULNERABLE FISHERIES RESOURCE

Swordfish is an epipelagic and large fish: reaching maximum weights of 500 kg and lengths of nearly 4.5 m, swordfish is one of the largest species of bony fishes (Figure 4.1). In the Mediterranean Sea, individual fish rarely weigh more than 230 kg, but can weigh up to 320 kg in the Atlantic Ocean (Nakamura *et al.* 1998). The maximum age for this species is estimated at 10 years in the Mediterranean (Alçlı *et al.* 2012), but some studies have shown that swordfish can live up to 15 years. Swordfish is one of the open ocean's fastest and strongest predators and an important fishery species everywhere it lives. It belongs to the Xiphoidei suborder, to the Xiphiidae family and to the *Xiphias gladius* Linnaeus genus.

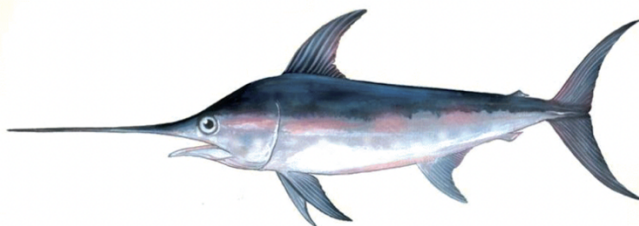


Figure 4.1. Drawing of an adult swordfish (*Xiphias gladius*) (ICCAT 2007) By Wendy Williams, Fisheries and Oceans, Canada.

Swordfish has a large-scale geographical distribution, and it uses to live in a wide variety of climates, from temperate to tropical and subtropical regions, between the latitudes 45° N and 45° S (Palko *et al.* 1981). It prefers to inhabit waters with sea surface temperatures (SST) ranging from 10°C to 28°C, however, thanks to its thermogenic organ, this fish species tolerates can high environmental temperature variations, ranging from 4° to 28 °C (Abascal *et al.* 2015; Neilson *et al.* 2014). In addition, swordfish is highly migratory and capable of long-distance movements (Dewar *et al.* 2011;

Neilson et al. 2007; Sedberry et al. 2001). Swordfish migration is complex and multi-directional: it is characterized by seasonal patterns in the horizontal movement, mainly due to feeding and spawning, and daily vertical way behavior, with fish staying in the mixed layer at night and descending to high depths during the daytime (*Abascal et al. 2015; Evans et al. 2014*). Swordfish is an opportunistic predator that feeds on pelagic vertebrates and invertebrates. Its diet is mainly based on cephalopods, followed by teleost fishes (*Chancollon et al. 2006; Gorni et al. 2012*). Due to its worldwide geographical diffusion, the management of the swordfish fishery is very complex. In the Atlantic and Mediterranean regions, the International Commission for the Conservation of Atlantic Tunas (ICCAT) is the reference regional fisheries management organization, which manage the swordfish as three separate stocks, North Atlantic, South Atlantic and Mediterranean according to multiple lines of evidence including tagging. In the Mediterranean Sea, fishery has a long tradition towards swordfish. Unfortunately, this led to severe overfishing because of the combination of poorly effective measures and swordfish's life history traits, such as spawning dynamics, larval recruitment, seasonal migration, long distance movements (*Gorni et al. 2012*). In 2016, a recovery plan was established by ICCAT. It included measures such as total allowable catches (TAC), fleet capacity limitations, closed fishing season, maximum number of hooks on longlines and a minimum size at catch (*ICCAT 2017*).

4.1 Swordfish anatomy

Swordfish's most evident feature is its flattened bill that looks like a sword, as its name implies. Swordfish's body is stout and rounded with large eyes. On the dorsal side, two fins are located: the first dorsal (back) fin is tall and crescent-shaped, while the second dorsal fin is much smaller. The absence of pelvic fins, teeth and scales, and a single pair of caudal keels are

peculiar features that distinguish swordfish from istiophorid billfishes (sailfish, marlins, and spearfishes) (Nakamura 1985). In addition, swordfish has a broad, crescent-shaped tail. Swordfish coloration is peculiar: the back and flanks are brown-black, and they tend towards light brown on the ventral part; the first dorsal has a blackish brown membrane; other fins are brown or blackish brown (ICCAT 2007). The internal structure includes no branchiospines, large gills and the presence of a swim bladder. Swordfish, during the pre-adult phase, undergoes drastic changes in body shape: juveniles have a long, thin and snake-like body and show teeth and scales that disappear when the animal reaches adulthood (Figure 4.2) (Nakamura 1985). Swordfish shows a sexual dimorphism of growth: males grow more slowly and reach a lower asymptotic (the size that the fish of a population would reach if they were to grow indefinitely) size than females. Growth is very rapid during the first year of the lifecycle and then slows down considerably. Studies have also concluded that Mediterranean swordfish reach a lower asymptotic size than Atlantic swordfish (Ehrhardt 1992; Megalofonou et al. 1995; Tserpes et al. 1995; Alçlı et al. 2012).

(A)



(B)

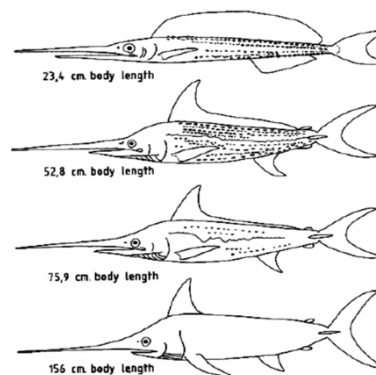


Figure 4.2. A. Dimensions of a juvenile swordfish (photo by Juan C. Lévesque) B. Morphological changes affecting the swordfish's body as it grows (ICCAT 2007 n.d.; I. Nakamura 1985).

4.2 Swordfish reproduction

The reproductive biology of Atlantic and Mediterranean swordfish has been studied. The measure of the gonad somatic index (GSI), oocytes and oocyte cytology, the distribution of eggs and aged young larvae and of the spawning areas have been characterized (*Arocha 2007; Neilson et al. 2013*). Swordfish is a sexually dimorphic and gonochoric species, but no external character distinguishes males from females (*Palko et al. 1981*). Female maturation, generally, occurs later and at a bigger size than the male, even if there are large differences in the maturation age, which takes place in a living-area dependent way (*Arocha 2007; Neilson et al. 2013*). Swordfish spawning is closely related to SST greater than 23- 24°C. As a consequence, given the strong dependence from the environmental conditions, spawning occurs in locations which show a distinctive seasonal pattern. In the Mediterranean Sea, spawning takes place in a short time-window, going from June to the end of August in three main areas, one for each region of the basin (eastern, central and western Mediterranean) between 35° and 40° N. More in detail, the three regions are: the Balearic Islands, the south of the Tyrrhenian Sea and the Strait of Messina and the Ionian Sea (*Arocha 2007*). In addition, in the Eastern Mediterranean Sea, swordfish migrates towards the Eastern Levantine for spawning, concentrating in a region between the islands of Cyprus and Rhodes (*Tserpes et al. 2001; Tserpes et al. 2008*). In winter, Mediterranean swordfish migrates to Moroccan Atlantic waters and to the waters west of the Strait of Gibraltar (out to 15° W) reaching the eastern North Atlantic Sea, and then returns back to spawning grounds in the Mediterranean Sea (*Pujolar et al. 2002*).

Males have an unrestricted lobular testis, (*Uribe et al. 2015*). The female swordfish has asynchronous ovaries, thus meaning that oogonia and oocytes at several stages of development are simultaneously present, showing a long spawning period (>90 days) (*Arocha 2007*). Ovary consists of

a thick muscle wall that surrounds ovigerous lamellae containing oogonia and oocytes. The female has an average production of 1.6×10^6 eggs in the Mediterranean Sea and of 3.9×10^6 eggs per female in the North Atlantic Ocean, with a diameter ranging from 1.6 to 1.8 mm (*Idrissi 1986*). The eggs are floating and transparent with a large oil droplet and a very small yolk.

The different stages of oocyte have been described and characterized using regular histology (*Abid et al. 2019; Arocha 2002; Corriero et al. 2004; Farley et al. 2014; Macías et al. 2005; Marisaldi et al. 2020; Poisson et al. Fauvel 2009; Young et al. 2003*), immunohistochemistry, histochemistry (*Corriero et al. 2004; Ortiz-Delgado et al. 2008*), Fourier Transform Infrared (FTIR) Imaging spectroscopy (*Carnevali et al. 2019*), transmission (*Minniti et al. 2005*) and electron (*Corriero et al. 2004*) microscopy. Depending on their dimensions and of their internal structure and composition, oocytes can be distinguished in different classes. Oogonia ($<15 \mu\text{m}$) constitute the first step of development: they have a globular nucleus with finely dispersed chromatin, a single eccentric nucleolus and small basophilic granules. Then, oogonia enter into the first prophase of meiosis to yield pre-vitellogenic oocytes; they can be further divided in three classes: the chromatin nucleus stage ($15\text{-}120 \mu\text{m}$), the perinucleolar stage ($100\text{-}190 \mu\text{m}$), and the lipid/cortical alveoli stage ($175\text{-}300 \mu\text{m}$), these previtellogenic oocytes are characterized by a large nucleus with chromatin strands, a variable number of peripheral nucleoli and an increasing ooplasm basophily, a starting thin zona radiata of proteinaceous nature, placed between the oolemma and the follicular cells, and lipid droplets, composed by neutral lipids derived from triglycerides-rich serum lipoproteins, at the inner to peripheral part of the cytoplasm. The subsequent step is the vitellogenic stage ($275\text{-}500 \mu\text{m}$): in this phase oocyte growth is mainly due to uptakes of vitellogenin, vitamins and other elements that form the main component of the yolk globules. In this phase zona radiata increases in thickness and becomes evident, Finally, the

oocyte enters the maturation phase (900-1200 μm): the nucleus (germinal vesicle) migrates toward the animal pole, marking meiosis resumption, the lipid and yolk globules merge, and hydration process occurs. The last step is the hydrated phase (>1300 μm): extensive hydration and detachment of follicular cells occur, preceding ovulation. ovarian

According to the histological criteria described in Table 4.1, the ovarian developmental classes of the swordfish are: immature, developing, spawning capable, regressing and regenerating.

Table 4.1. Classification of the swordfish females according to the standardized terminology (Brown-Peterson et al. 2011).

Stage	Histological features
Immature (i.e. never spawned)	Oogonia and previtellogenic oocytes present. No atresia. Thin ovarian wall, no muscle bundles and compact oocytes.
Developing	Previtellogenic, lipid stage and vitellogenic oocytes and some atresia can be present. No evidence of POFs or fully-grown vitellogenic oocytes.
Spawning capable	Fully-grown vitellogenic oocytes and/or POFs present. Migrating-nucleus oocytes and hydrating oocytes can be present (actively spawning subphase). Some atresia of vitellogenic oocytes present.
Regressing	Vitellogenic oocytes and/or lipid stage oocytes. Extensive atresia (any stage) present (>50% of vitellogenic oocytes).
Regenerating	Oogonia and previtellogenic oocytes present. Muscle bundles and thick ovarian wall.

References

- Abascal, F J et al. 2015. "Tracking of the Broadbill Swordfish, *Xiphias Gladius*, in the Central and Eastern North Atlantic." *Fisheries Research* 162: 20–28.
- Abid, N. et al. 2019. "The Reproductive Biology of Swordfish (*Xiphias Gladius*) in the Strait of Gibraltar." *Journal of the Marine Biological Association of the United Kingdom* 99(3): 649–659.
- Akbari, H. et al. 2011. "Cancer Detection Using Infrared Hyperspectral Imaging." *Cancer Science* 102(4): 852–57.
- Alıçlı T. Z. et al. 2012. "Age, Sex Ratio, Length-Weight Relationships and Reproductive Biology of Mediterranean Swordfish, *Xiphias Gladius* L., 1758, in the Eastern Mediterranean." *African Journal of Biotechnology* 11(15): 3673–80.
- Anastassopoulou, J. et al. 2009. "Microimaging FT-IR Spectroscopy on Pathological Breast Tissues." *Vibrational Spectroscopy* 51(2): 270–75.
- Smith, D. et al. 2005. "Modern Raman Spectroscopy - A Practical Approach.": 1–210. <https://onlinelibrary.wiley.com/doi/book/10.1002/0470011831>.
- Arocha, F. 2002. "Oocyte Development and Maturity Classification of Swordfish from the North-Western Atlantic." *Journal of Fish Biology* 60(1): 13–27. <https://onlinelibrary.wiley.com/doi/full/10.1111/j.1095-8649.2002.tb02385.x>.
- Arocha, F. 2007. "Swordfish Reproduction in the Atlantic Ocean: An Overview." *Gulf and Caribbean Research* 19.
- Avdesh, A. et al. 2012. "Regular Care and Maintenance of a Zebrafish (*Danio Rerio*) Laboratory: An Introduction." *Journal of Visualized Experiments* (69). <http://www.jove.com/video/4196/regular-care-maintenance-zebrafish-danio-erio-laboratory-an>.
- Baker, M. J. et al. 2014. "Using Fourier Transform IR Spectroscopy to Analyze Biological Materials." *Nature Protocols* 9(8): 1771–91.
- Barth, A. 2007. "Infrared Spectroscopy of Proteins." *Biochimica et Biophysica Acta - Bioenergetics* 1767(9): 1073–1101.
- Berger, U. et al. 2009. "Fish Consumption as a Source of Human Exposure to Perfluorinated Alkyl Substances in Sweden - Analysis of Edible Fish from Lake Vättern and the Baltic Sea." *Chemosphere* 76(6): 799–804.
- Bogliolo, L. et al. 2012. "Raman Microspectroscopy as a Non-Invasive Tool to Assess the Vitrification-Induced Changes of Ovine Oocyte Zona Pellucida." *Cryobiology* 64(3): 267–72. <http://dx.doi.org/10.1016/j.cryobiol.2012.02.010>.
- Bogliolo, L. et al. 2020. "Raman Spectroscopy-Based Approach to Study the Female Gamete." *Theriogenology* 150: 268–75.
- Bonnier, F; et al. 2012. "Understanding the Molecular Information Contained in Principal Component Analysis of Vibrational Spectra of Biological Systems." *Analyst*, 137,: 322–332.

- Brown-Peterson, N. J. et al. 2011. "A Standardized Terminology for Describing Reproductive Development in Fishes." *Marine and Coastal Fisheries* 3(1): 52–70.
<https://www.tandfonline.com/action/journalInformation?journalCode=umcf20>.
- Butler, H. J. et al. 2016. "Using Raman Spectroscopy to Characterize Biological Materials." *Nature Protocols* 11(4): 664–87.
- Byrne, H. et al. 2016. "Spectral Pre and Post Processing for Infrared and Raman Spectroscopy of Biological Tissues and Cells." *Chemical Society Reviews* 45(7): 1865–78.
- Carnevali, O et al. 2010. "Melatonin Control of Oogenesis and Metabolic Resources in Zebrafish." *Journal of Applied Ichthyology* 26(5): 826–30.
- Carnevali, O et al. 2017. "Dietary Administration of EDC Mixtures: A Focus on Fish Lipid Metabolism." *Aquatic Toxicology* 185: 95–104.
- Carnevali, O. et al. 2019. "Insights on the Seasonal Variations of Reproductive Features in the Eastern Atlantic Bluefin Tuna." *General and Comparative Endocrinology* 282(July): 113216. <https://doi.org/10.1016/j.yggen.2019.113216>.
- Carnevali, O. et al. 2019. "Macromolecular Characterization of Swordfish Oocytes by FTIR Imaging Spectroscopy." *Scientific Reports* 9(1).
- Chakraborty, C. et al. 2009. "Zebrafish: A Complete Animal Model for In Vivo Drug Discovery and Development." *Current Drug Metabolism* 10: 116–24.
- Chan, J. et al. 2008. "Raman Spectroscopy and Microscopy of Individual Cells and Cellular Components." *Laser and Photonics Reviews* 2(5): 325–49.
- Chancollon, O. et al. 2006. "Food and Feeding Ecology of Northeast Atlantic Swordfish (*Xiphias Gladius*) off the Bay of Biscay." *ICES Journal of Marine Science* 63(6): 1075–85. <https://doi.org/10.1016/j.icesjms.2006.03.013>.
- Cheng, J. X. et al. 2004. "Coherent Anti-Stokes Raman Scattering Microscopy: Instrumentation, Theory, and Applications." *Journal of Physical Chemistry B* 108(3): 827–40.
- Chou, I-M. et al. 2017. "Application of Laser Raman Micro-Analyses to Earth and Planetary Materials." *Journal of Asian Earth Sciences* 145: 309–33.
<https://linkinghub.elsevier.com/retrieve/pii/S1367912017303425>.
- Clelland, E. et al. 2009. "Endocrine/Paracrine Control of Zebrafish Ovarian Development." *Molecular and Cellular Endocrinology* 312(1–2): 42–52.
- Conder, J. M. et al. 2008. "Are PFCAs Bioaccumulative? A Critical Review and Comparison with Regulatory Criteria and Persistent Lipophilic Compounds." *Environmental Science and Technology* 42(4): 995–1003.
- Conti, C. et al. 2009. "Microimaging FTIR of Head and Neck Tumors. IV." *Microscopy Research and Technique* 72(2): 67–75.
- Corriero, A et al. 2004. "Histological and Immunohistochemical Investigation on Ovarian Development and Plasma Estradiol Levels in the Swordfish (*Xiphias*

- Gladius L.)” *European Journal of Histochemistry* 48(4): 413–22.
- Czernuszewicz, R. S. et al. 2011. “Resonance Raman Spectroscopy.”
- Dahm, R. et al. 2006. “Learning from Small Fry: The Zebrafish as a Genetic Model Organism for Aquaculture Fish Species.” *Marine Biotechnology* 8(4): 329–45.
- Davidson, B. et al. 2013. “Raman Micro-Spectroscopy Can Be Used to Investigate the Developmental Stage of the Mouse Oocyte.” *PLoS ONE* 8(7).
- Delvecchio, C. et al. 2011. “The Zebrafish: A Powerful Platform for in Vivo, HTS Drug Discovery.” *Assay and Drug Development Technologies* 9(4): 354–61.
- Dewar, H. et al. 2011. “Movements and Behaviors of Swordfish in the Atlantic and Pacific Oceans Examined Using Pop-up Satellite Archival Tags.” *Fisheries Oceanography* 20(3): 219–41.
<https://onlinelibrary.wiley.com/doi/abs/10.1111/j.1365-2419.2011.00581.x>.
- Diaspro, A. 2002. “Confocal and Two-Photon Microscopy : Foundations, Applications, and Advances.” : 567. <https://www.wiley.com/doi/abs/10.1002/9780471409205.ch33>
- Driever, W. et al. 1996. “A Genetic Screen for Mutations Affecting Embryogenesis in Zebrafish A Genetic Screen for Mutations Affecting Embryogenesis in Zebrafish A Genetic Screen for Mutations Affecting Embryogenesis in Zebrafish.” *Development* 123: 37–46.
- EFSA. 2008. “Perfluorooctane Sulfonate (PFOS), Perfluorooctanoic Acid (PFOA) and Their Salts Scientific Opinion of the Panel on Contaminants in the Food Chain.” *EFSA Journal* 6(7).
- Ehrhardt, N. M. 1992. “Age and Growth of Swordfish, Xiphias Gladius, in the Northwestern Atlantic. / In: Research Output: Contribution to Journal › Article › Peer-Review.” *Bulletin of Marine Science*, Vol. 50(No. 2, 01.01): 292–301.
- Eisen, J. S. 1996. “Zebrafish Make a Big Splash Review.” *Cell* 87: 969–77.
- Engeszer, R. et al. 2007. “Zebrafish in the Wild: A Review of Natural History and New Notes from the Field.” *Zebrafish* 4(1): 21–40.
- Eriksen, K. T. et al. 2010. “Genotoxic Potential of the Perfluorinated Chemicals PFOA, PFOS, PFBS, PFNA and PFHxA in Human HepG2 Cells.” *Mutation Research - Genetic Toxicology and Environmental Mutagenesis* 700(1–2): 39–43.
- Evans, K. et al. 2014. “The Horizontal and Vertical Dynamics of Swordfish in the South Pacific Ocean.” *Journal of Experimental Marine Biology and Ecology* 450: 55–67.
- Fabian, H. et al. 2006. “Diagnosing Benign and Malignant Lesions in Breast Tissue Sections by Using IR-Microspectroscopy.” *Biochimica et Biophysica Acta - Biomembranes* 1758(7): 874–82.
- Farley, J. et al. 2014. *Determination of Southwest Pacific Swordfish Growth and*

Maturity.

- Fenton, S. E. et al. 2021. "Per- and Polyfluoroalkyl Substance Toxicity and Human Health Review: Current State of Knowledge and Strategies for Informing Future Research." *Environmental Toxicology and Chemistry* 40(3): 606–30.
- Fishman, M. C. 1999. "Commentary Zebrafish Genetics: The Enigma of Arrival." *Proc. Natl. Acad. Sci. USA* 96: 10554–56. www.pnas.org.
- Fox, G. 2020. "The Brewing Industry and the Opportunities for Real-Time Quality Analysis Using Infrared Spectroscopy." *Applied Sciences (Switzerland)* 10(2).
- Gazi, E. et al. 2007. "Direct Evidence of Lipid Translocation between Adipocytes and Prostate Cancer Cells with Imaging FTIR Microspectroscopy." *Journal of Lipid Research* 48(8): 1846–56.
- Genome, Genes, Sequence Map, and Homology Expression. "Genome Resources Workshop."
- Gioacchini, G. et al. 2012. "Probiotics Can Induce Follicle Maturation Competence: The Danio Rerio Case." *Biology of Reproduction* 86(3).
- Gioacchini, G. et al. 2014. "A New Approach to Evaluate Aging Effects on Human Oocytes: Fourier Transform Infrared Imaging Spectroscopy Study." *Fertility and Sterility* 101(1): 120–27.
- Gioacchini, G. et al. 2014. "The Influence of Probiotics on Zebrafish Danio Rerio Innate Immunity and Hepatic Stress." *Zebrafish* 11(2): 98–106.
- Gioacchini, G. et al. 2018. "Does the Molecular and Metabolic Profile of Human Granulosa Cells Correlate with Oocyte Fate? New Insights by Fourier Transform Infrared Microspectroscopy Analysis." *Molecular Human Reproduction* 24(11): 521–32.
- Giorgini, E. et al. 2014. "Vibrational Characterization of Female Gametes: A Comparative Study." *The Analyst* 139(20): 5049–60. <http://xlink.rsc.org/?DOI=C4AN00684D>.
- Giorgini, E. et al. 2010. "Effects of Lactobacillus Rhamnosus on Zebrafish Oocyte Maturation: An FTIR Imaging and Biochemical Analysis." *Analytical and Bioanalytical Chemistry* 398(7–8): 3063–72. <http://link.springer.com/10.1007/s00216-010-4234-2>.
- Giorgini, E. et al. 2011. "FT-IR Microscopic Analysis on Human Dental Pulp Stem Cells." *Vibrational Spectroscopy* 57(1): 30–34.
- Giorgini, E. et al. 2012. "The Role of Melatonin on Zebrafish Follicle Development: An FT-IR Imaging Approach." *Vibrational Spectroscopy* 62: 279–85. <http://dx.doi.org/10.1016/j.vibspec.2012.06.009>.
- Giorgini, E. et al. 2015. "Vibrational Mapping of Sinonasal Lesions by Fourier Transform Infrared Imaging Spectroscopy." *Journal of Biomedical Optics* 20(12): 125003.
- Giorgini, E. et al. 2018. "In Vitro FTIR Microspectroscopy Analysis of Primary Oral

- Squamous Carcinoma Cells Treated with Cisplatin and 5-Fluorouracil: A New Spectroscopic Approach for Studying the Drug-Cell Interaction." *Analyst* 143(14): 3317–26.
- Gorni, G. et al. 2012. "(Xiphias Gladius) Caught Off Southern Brazil : A Bayesian Analysis." 68(4): 1594–1600.
- Griffiths, P. R. et al. 2007. "Introduction to Vibrational Spectroscopy: Molecular Vibrations." *Fourier Transform Infrared Spectrometry* (171): 3–6. <https://www.wiley.com/en-us/Fourier+Transform+Infrared+Spectrometry%2C+2nd+Edition-p-97804711194040>.
- Haffter, P. et al. 1996. "The Identification of Genes with Unique and Essential Functions in the Development of the Zebrafish, Danio Rerio." *Development* 123: 1–36.
- Han, X. et al. 2003. "Binding of Perfluorooctanoic Acid to Rat and Human Plasma Proteins." *Chemical Research in Toxicology* 16(6): 775–81.
- Heraud, P. et al. 2017. "Label-Free in Vivo Raman Microspectroscopic Imaging of the Macromolecular Architecture of Oocytes." *Scientific Reports* 7(1).
- Houde, M. et al. 2006. "Biomagnification of Perfluoroalkyl Compounds in the Bottlenose Dolphin (*Tursiops Truncatus*) Food Web." *Environmental Science and Technology* 40(13): 4138–44.
- Houde, M. et al. 2011. "Monitoring of Perfluorinated Compounds in Aquatic Biota: An Updated Review." *Environmental Science and Technology* 45(19): 7962–73.
- Howe, K. et al. 2013. "The Zebrafish Reference Genome Sequence and Its Relationship to the Human Genome." *Nature* 496(7446): 498–503.
- Hu, X. et al. 2009. "Effects of Perfluorooctanoate and Perfluorooctane Sulfonate Exposure on Hepatoma Hep G2 Cells." *Archives of Toxicology* 83(9): 851–61.
- ICCAT. 2017. "Report of the 2016 Mediterranean Swordfish Stock Assessment Meeting." *Collective Volume of Scientific Papers ICCAT* 73(11-16 July): 1005–96.
- Idrissi, N. A. et al. 1986. "Swordfish." *Communication & broadcasting* (27): 43–46.
- Ingelido, A. M. et al. 2018. "Biomonitoring of Perfluorinated Compounds in Adults Exposed to Contaminated Drinking Water in the Veneto Region, Italy." *Environment International* 110: 149–59.
- Keating, M. E. et al. 2013. "Raman Spectroscopy in Nanomedicine: Current Status and Future Perspective." *Nanomedicine* 8(8): 1335–51.
- Kimmel, C. B. et al. 1995. "Stages of Embryonic Development of the Zebrafish." *Developmental Dynamics* 203(3): 253–310.
- Krafft, C. et al. 2006. "Biomedical Applications of Raman and Infrared Spectroscopy to Diagnose Tissues1." : 195 – 218.
- Larkin, P. 2011. *Infrared and Raman Spectroscopy: Principles and Spectral*

Interpretation. ed. Peter Larkin. Elsevier.

- Lasch, P. et al. 2004. "Imaging of Colorectal Adenocarcinoma Using FT-IR Microspectroscopy and Cluster Analysis." *Biochimica et Biophysica Acta - Molecular Basis of Disease* 1688(2): 176–86.
- Lau, C. et al. 2007. "Perfluoroalkyl Acids: A Review of Monitoring and Toxicological Findings." *Toxicological Sciences* 99(2): 366–94.
- Lawrence, C. 2007. "The Husbandry of Zebrafish (*Danio Rerio*): A Review." *Aquaculture* 269(1–4): 1–20.
- Lawrence, C. et al. 2012. "Generation Time of Zebrafish (*Danio Rerio*) and Medakas (*Oryzias Latipes*) Housed in the Same Aquaculture Facility." *Nature America* 41(6): 158–65. www.labanimal.com.
- Lawrence, C. et al. 2012. "The Effects of Feeding Frequency on Growth and Reproduction in Zebrafish (*Danio Rerio*)." *Aquaculture* 368–369: 103–8.
- Ledent, V. 2002. "Postembryonic Development of the Posterior Lateral Line in Zebrafish." *Development (Cambridge, England)* 129(3): 597–604.
- Lehmler, H. J. 2005. "Synthesis of Environmentally Relevant Fluorinated Surfactants - A Review." *Chemosphere* 58(11): 1471–96.
- Lindstrom, A. et al. 2011. "Polyfluorinated Compounds: Past, Present, and Future." *Environmental Science and Technology* 45(19): 7954–61.
- Lombardo, F. et al. 2012. "Melatonin Effects on *Fundulus Heteroclitus* Reproduction." *Reproduction, Fertility and Development* 24(6): 794–803.
- Lombardo, F. et al. 2014. "Melatonin-Mediated Effects on Killifish Reproductive Axis." *Comparative Biochemistry and Physiology - A Molecular and Integrative Physiology* 172: 31–38. <http://dx.doi.org/10.1016/j.cbpa.2014.02.008>.
- Loos, R. et al. 2008. "Analysis of Perfluorooctanoate (PFOA) and Other Perfluorinated Compounds (PFCs) in the River Po Watershed in N-Italy." *Chemosphere* 71(2): 306–13.
- López-Olmeda, J. F. et al. 2011. "Thermal Biology of Zebrafish (*Danio Rerio*)." *Journal of Thermal Biology* 36(2): 91–104.
- Loveless, S. E. et al. 2006. "Comparative Responses of Rats and Mice Exposed to Linear/Branched, Linear, or Branched Ammonium Perfluorooctanoate (APFO)." *Toxicology* 220(2–3): 203–17.
- Lyng, F. M. et al. 2007. "Vibrational Spectroscopy for Cervical Cancer Pathology, from Biochemical Analysis to Diagnostic Tool." *Experimental and Molecular Pathology* 82(2): 121–29.
- Lyng, F. M. et al. 2015. "Vibrational Microspectroscopy for Cancer Screening." *Applied Sciences (Switzerland)* 5(1): 23–35.
- Macías, D. et al. 2005. "Reproductive Characteristics of Swordfish (*Xiphias Gladius*) Caught in the Southwestern Mediterranean during 2003." *Col. Vol. Sci. Pap. ICCAT* 58(2): 454–69.

- MacRae, C. A. et al. 2003. "Zebrafish-Based Small Molecule Discovery." *Chemistry & biology* 10(10): 901–8.
- Mantsch, H. H. et al. 1996. *Infrared Spectroscopy of Biomolecules*. eds. Henry H Mantsch and Dennis Chapman. Wiley.
- Marisaldi, L. et al. 2020. "Maturity Assignment Based on Histology-validated Macroscopic Criteria: Tackling the Stock Decline of the Mediterranean Swordfish (Xiphias Gladius)." *Aquatic Conservation: Marine and Freshwater Ecosystems* 30(2): 303–14.
<https://onlinelibrary.wiley.com/doi/10.1002/aqc.3248>.
- Martin, J. et al. 2003. "Bioconcentration and Tissue Distribution of Perfluorinated Acids in Rainbow Trout (Oncorhynchus Mykiss)." *Environmental Toxicology and Chemistry* 22(1): 196–204.
- Matthäus, C. 2008. "Chapter 10 Infrared and Raman Microscopy in Cell Biology." *Methods in Cell Biology* 89: 275–308.
<https://linkinghub.elsevier.com/retrieve/pii/S0091679X08006109>.
- McClure, M. M. et al. 2006. "Notes on the Natural Diet and Habitat of Eight Danionin Fishes, Including the Zebrafish Danio Rerio." *Journal of Fish Biology* 69(2): 553–70.
- Megalofonou, P. et al. 1995. "Age and Growth of Juvenile Swordfish, Xiphias Gladius Linnaeus, from the Mediterranean Sea." *Journal of Experimental Marine Biology and Ecology* 188(1): 79–88.
<https://www.sciencedirect.com/science/article/pii/002209819400188J>.
- Menke, A. L. et al. 2011. "Normal Anatomy and Histology of the Adult Zebrafish." *Toxicologic Pathology* 39(5): 759–75.
- Minniti, F. et al. 2005. "Ultrastructural Features of Germ Cells in Immature Swordfish Xiphias Gladius (Teleostei, Xiphidae)." *Italian Journal of Zoology* 72(3): 217–21. <https://doi.org/10.1080/11250000509356674>.
- Movasaghi, Z. et al. 2008. "Fourier Transform Infrared (FTIR) Spectroscopy of Biological Tissues." *Applied Spectroscopy Reviews* 43(2): 134–79.
- Nakamura, I. 1985. "Vol. 5 Billfishes of the World." *Fao Species Catalogue* 5(125).
- Nakamura, I et al. 1998. "Gonadal Sex Differentiation in Teleost Fish." *The Journal Of Experimental Zoology* 281: 362–72.
- Naumann, D. 2001. "FT-Infrared and FT-Raman Spectroscopy in Biomedical Research." *Applied Spectroscopy Reviews* 36(2–3): 239.
- Neilson, J. D. et al. 2007. "Stock Structure of Swordfish (Xiphias Gladius) in the Atlantic: A Review of the Non-Genetic Evidence." *Collective Volume of Scientific Papers ICCAT*: 61, 25–60.
- Neilson, J. et al. 2013. "The Recovery of Atlantic Swordfish: The Comparative Roles of the Regional Fisheries Management Organization and Species Biology." *Reviews in Fisheries Science* 21(2): 59–97.

- Neilson, J. D. et al. 2014. "Seasonal Distributions and Migrations of Northwest Atlantic Swordfish: Inferences from Integration of Pop-Up Satellite Archival Tagging Studies." *PLoS ONE* 9(11).
- Niimi, A. J. et al. 1973. "Influence of Breeding Time Interval on Egg Number, Mortality, and Hatching of the Zebra Fish *Brachyhnio Rerio*." *Can. J. Zool.* 52: 515–17. www.nrcresearchpress.com.
- Notarstefano, V. et al. 2021. "Cytotoxic Effects of 5-Azacytidine on Primary Tumour Cells and Cancer Stem Cells from Oral Squamous Cell Carcinoma: An In Vitro FTIRM Analysis." *Cells* 10(8): 2127. <https://www.mdpi.com/2073-4409/10/8/2127>.
- Notarstefano, V. et al. 2022. "A Vibrational in Vitro Approach to Evaluate the Potential of Monoolein Nanoparticles as Isofuranodiene Carrier in MDA-MB 231 Breast Cancer Cell Line: New Insights from Infrared and Raman Microspectroscopies." *Spectrochimica Acta Part A: Molecular and Biomolecular Spectroscopy* 269: 120735. <https://linkinghub.elsevier.com/retrieve/pii/S1386142521013123>.
- Notingher, I et al. 2003. "Application of FTIR and Raman Spectroscopy to Characterisation of Bioactive Materials and Living Cells." *Spectroscopy* 17: 275–88.
- Nyquist, R. A. 1971. *Infrared Spectra of Inorganic Compounds (3800-45cm⁻¹)*. Academic Press.
- OECD *Environmental Outlook to 2030*. 2008. 46 Choice Reviews Online.
- OECD "Guideline For Testing Of Chemicals: Fish, Short-Term Toxicity Test on Embryo and Sac-Fry Stages." 1998.
- Okada, M. et al. 2012. "Label-Free Raman Observation of Cytochrome c Dynamics during Apoptosis." *Proceedings of the National Academy of Sciences of the United States of America* 109(1): 28–32. <https://www.pnas.org/content/109/1/28>.
- Olsen, G. W. et al. 2007. "Half-Life of Serum Elimination of Perfluorooctanesulfonate, Perfluorohexanesulfonate, and Perfluorooctanoate in Retired Fluorochemical Production Workers." *Environmental Health Perspectives* 115(9): 1298–1305.
- Ortiz-Delgado, J. B. et al. 2008. "Histochemical Characterisation of Oocytes of the Swordfish *Xiphias Gladius*." *Scientia Marina* 72(3): 549–564. <https://scientiamarina.revistas.csic.es/index.php/scientiamarina/article/view/1020>.
- Owens, G. L. et al. 2014. "Vibrational Biospectroscopy Coupled with Multivariate Analysis Extracts Potentially Diagnostic Features in Blood Plasma/Serum of Ovarian Cancer Patients." *Journal of Biophotonics* 7(3–4): 200–209.
- Palko et al. 1981. "Synopsis of the Biology o National Oceanic and Atmospheric Administration National Marine Fisheries Service."

- Parichy, D. M. et al. 2009. "Normal Table of Postembryonic Zebrafish Development: Staging by Externally Visible Anatomy of the Living Fish." *Developmental Dynamics* 238(12): 2975–3015.
- Parichy, D. M. et al. 2003. "Zebrafish Puma Mutant Decouples Pigment Pattern and Somatic Metamorphosis." *Developmental Biology* 256(2): 242–57.
- Pavia, D. L. et al. 2013. *Introduction to Spectroscopy*.
- Pilling, M. et al. 2016. "Fundamental Developments in Infrared Spectroscopic Imaging for Biomedical Applications." *Chem. Soc. Rev.*, 45: 1935–57.
- Poisson, F. et al. 2009. "Reproductive Dynamics of Swordfish (*Xiphias Gladius*) in the Southwestern Indian Ocean (Reunion Island). Part 1: Oocyte Development, Sexual Maturity and Spawning." *Aquatic Living Resources* 22(1): 45–58.
- Pujolar, J. et al. 2002. "A Genetic Assessment of the Population Structure of Swordfish (*Xiphias Gladius*) in the Mediterranean Sea." *Journal of Experimental Marine Biology and Ecology* 276: 19–29.
- Puppels, G. J. et al. 1991. "Laser Irradiation and Raman Spectroscopy of Single Living Cells and Chromosomes: Sample Degradation Occurs with 514.5 Nm but Not with 660 Nm Laser Light." *Experimental Cell Research* 195(2): 361–67.
- Raman, C. V. et al. 1928. "A New Type of Secondary Radiation." *Nature* 1928 121:3048 121(3048): 501–2. <https://www.nature.com/articles/121501c0>.
- Randazzo, B. et al. 2021. "Hermetia Illucens and Poultry By-Product Meals as Alternatives to Plant Protein Sources in Gilthead Seabream (*Sparus Aurata*) Diet: A Multidisciplinary Study on Fish Gut Status." *Animals* 11(3): 1–22.
- Randazzo, B. et al. 2021. "Physiological Response of Rainbow Trout (*Oncorhynchus Mykiss*) to Graded Levels of Hermetia Illucens or Poultry by-Product Meals as Single or Combined Substitute Ingredients to Dietary Plant Proteins." *Aquaculture* 538.
- Ribas, L. et al. 2014. "The Zebrafish (*Danio Rerio*) as a Model Organism, with Emphasis on Applications for Finfish Aquaculture Research." *Reviews in Aquaculture* 6(4): 209–40.
- Romeo, M. et al. 2006. "Infrared Micro-Spectroscopic Studies of Epithelial Cells." *Biochimica et Biophysica Acta - Biomembranes* 1758(7): 915–22.
- Rosenthal, N. et al. 2002. "Taking Stock of Our Models: The Function and Future of Stock Centres." *Nature Reviews Genetics* 3(9): 711–17.
- Rusciano, G. et al. 2010. "Raman Spectroscopy of *Xenopus Laevis* Oocytes." *Methods* 51(1): 27–36.
- Sabbatini, S. et al. 2013. "Infrared Microspectroscopy of Oral Squamous Cell Carcinoma: Spectral Signatures of Cancer Grading." *Vibrational Spectroscopy* 68: 196–203.
- Santangeli, S. et al. 2017. "Effects of Diisononyl Phthalate on *Danio Rerio*

- Reproduction.” *Environmental Pollution* 231: 1051–62.
- Santangeli, S. et al. 2018. “Effects of Diethylene Glycol Dibenzoate and Bisphenol A on the Lipid Metabolism of *Danio Rerio*.” *Science of the Total Environment* 636: 641–55.
- Sedberry, G. R. et al. 2001. “Satellite Telemetry Tracking of Swordfish, *Xiphias Gladius*, off the Eastern United States.” *Marine Biology* 139(2): 355–60.
- Smith, B. 2011. “Fundamentals of Fourier Transform Infrared Spectroscopy.” <https://www.taylorfrancis.com/books/mono/10.1201/b10777/fundamentals-fourier-transform-infrared-spectroscopy-brian-smith>.
- Spence, R. et al. 2008. “The Behaviour and Ecology of the Zebrafish, *Danio Rerio*.” *Biological Reviews* 83(1): 13–34.
- Spitsbergen, J. M. et al. 2003. “The State of the Art of the Zebrafish Model for Toxicology and Toxicologic Pathology Research-Advantages and Current Limitations.” *Toxicol Pathol* 31: 62–87. <http://zfin.org/ZFIN>.
- Squadrone, S. et al. 2014. “Fish Consumption as a Source of Human Exposure to Perfluorinated Alkyl Substances in Italy: Analysis of Two Edible Fish from Lake Maggiore.” *Chemosphere* 114: 181–86.
- Stahl, T. et al. 2011. “Toxicology of Perfluorinated Compounds.” *Environmental Sciences Europe* 23(1).
- Stern, H. M. et al. 2003. “Cancer Genetics and Drug Discovery in the Zebrafish.” *Nature Reviews* 3: 1–7.
- Stimson, M. M. et al. 1952. “The Infrared and Ultraviolet Absorption Spectra of Cytosine and Isocytosine in the Solid State 1,2.” *Journal of the American Chemical Society* 74(7): 1805–8. <https://pubs.acs.org/doi/abs/10.1021/ja01127a054>.
- “Stockholm Convention on Persistent Organic Pollutants (POPs).” 2017. <http://chm.pops.int/tabid/208/Default.aspx>.
- Stuart, B. H. 2006. Encyclopedia of Analytical Chemistry *Infrared Spectroscopy of Biological Applications*.
- Stuart, B. 2005. *Infrared Spectroscopy*.
- Suja, F. et al. 2009. “Contamination, Bioaccumulation and Toxic Effects of Perfluorinated Chemicals (PFCs) in the Water Environment: A Review Paper.” *Water Science and Technology* 60(6): 1533–54.
- Sunderland, E. M. et al. 2019. “A Review of the Pathways of Human Exposure to Poly- and Perfluoroalkyl Substances (PFASs) and Present Understanding of Health Effects.” *Journal of Exposure Science & Environmental Epidemiology* 29(2): 131–47. <https://doi.org/10.1038/s41370-018-0094-1>.
- Talling, J. F. et al. 1998. *Ecological Dynamics of Tropical Inland Waters*.
- Trasande, L. et al. 2016. “Burden of Disease and Costs of Exposure to Endocrine Disrupting Chemicals in the European Union: An Updated Analysis.”

Andrology 4(4): 565–72.

- Trasande, L. et al. 2015. “Estimating Burden and Disease Costs of Exposure to Endocrine-Disrupting Chemicals in the European Union.” *Journal of Clinical Endocrinology and Metabolism* 100(4): 1245–55.
- Tserpes, G. et al. 2001. “On the Reproduction of Swordfish (*Xiphias Gladius* L.) in the Eastern Mediterranean.” *ICCAT Col. Vol. Sci. Pap.* 52.
- Tserpes, G. et al. 2008. “Distribution of Swordfish in the Eastern Mediterranean, in Relation to Environmental Factors and the Species Biology.” *Hydrobiologia* 612: 241–50.
- Tserpes, G. et al. 1995. “Determination of Age and Growth of Swordfish, *Xiphias Gladius* L., 1758, in the Eastern Mediterranean Using Anal-Fin Spines.” *Fishery Bulletin* 93: 594–602.
- Turrell, G. 1996. “The Raman Effect.” *Raman Microscopy*: 1–25.
<https://linkinghub.elsevier.com/retrieve/pii/B9780121896904500211>.
- Turrell, G. et al. 1996. “Characteristics of Raman Microscopy.” *Raman Microscopy*: 27–49.
- Ulloa, P. E. et al. 2011. “Zebrafish as a Model Organism for Nutrition and Growth: Towards Comparative Studies of Nutritional Genomics Applied to Aquacultured Fishes.” *Reviews in Fish Biology and Fisheries* 21(4): 649–66.
- Uribe, M. C. et al. 2015. “Comparative Testicular Structure and Spermatogenesis in Bony Fishes.” *Spermatogenesis* 4(3): e983400.
<https://pubmed.ncbi.nlm.nih.gov/26413405/>.
- Walsh, M. J. et al. 2009. “Tracking the Cell Hierarchy in the Human Intestine Using Biochemical Signatures Derived by Mid-Infrared Microspectroscopy.” *Stem Cell Research* 3(1): 15–27.
- Wang, L. et al. 2008. “Application of Multivariate Data-Analysis Techniques to Biomedical Diagnostics Based on Mid-Infrared Spectroscopy.” *Analytical and Bioanalytical Chemistry* 391(5): 1641–54.
- Weiss, J. M. et al. 2009. “Competitive Binding of Poly- and Perfluorinated Compounds to the Thyroid Hormone Transport Protein Transthyretin.” *Toxicological Sciences* 109(2): 206–16.
- Weltzien, F. A. et al. 2004. “The Brain-Pituitary-Gonad Axis in Male Teleosts, with Special Emphasis on Flatfish (Pleuronectiformes).” *Comparative Biochemistry and Physiology - A Molecular and Integrative Physiology* 137(3): 447–77.
- Westerfield, M. 2000. “The Zebrafish Book. A Guide for the Laboratory Use of Zebrafish (*Danio Rerio*).” 4th editio.
- Willemsen, R. et al. 2011. “Zebrafish (*Danio Rerio*) as a Model Organism for Dementia.” *Neuromethods* 48: 255–69.
https://link.springer.com/protocol/10.1007/978-1-60761-898-0_14.
- Winefordner, J. D. 2005. “Raman Spectroscopy for Chemical Analysis.” *Raman*

- Wood, B. R. et al. 2008. "Shedding New Light on the Molecular Architecture of Oocytes Using a Combination of Synchrotron Fourier Transform-Infrared and Raman Spectroscopic Mapping." *Analytical Chemistry* 80(23): 9065–72. <https://pubs.acs.org/doi/10.1021/ac8015483>.
- Young, J. et al. 2003. "Reproductive Dynamics of Broadbill Swordfish, *Xiphias Gladius*, in the Domestic Longline Fishery off Eastern Australia." *Marine and Freshwater Research* 54: 315–32.
- Yu, W. G. et al. 2009. "Prenatal and Postnatal Impact of Perfluorooctane Sulfonate (PFOS) on Rat Development: A Cross-Foster Study on Chemical Burden and Thyroid Hormone System." *Environmental Science and Technology* 43(21): 8416–22.
- Zarantoniello, M. et al. 2021. "Physiological Responses of Siberian Sturgeon (*Acipenser Baerii*) Juveniles Fed on Full-Fat Insect-Based Diet in an Aquaponic System." *Scientific Reports* 11(1): 1057. <http://www.nature.com/articles/s41598-020-80379-x>.

CHAPTER 1

A NEW METHODOLOGICAL SET UP FOR SPECTROSCOPIC STUDIES ON FISH EMBRYOS

Chiara Pro, Giorgia Gioacchini, Oliana Carnevali, Elisabetta Giorgini,
Valentina Notarstefano

Department of Life and Environmental Sciences, Università Politecnica delle
Marche

Paper in preparation

Abstract

The aim of this study was to define the best fixation protocol for Raman microspectroscopy analysis of fish embryos. The experiment was carried out on zebrafish (*Danio rerio*) embryos collected from 1 to 5 days post fertilization (dpf). Once collected, samples were properly treated and fixed by using, alternatively, paraformaldehyde (PFA, 4% solution), Bouin solution (picric acid, formaldehyde, acetic acid 15:5:1), and formol (formaldehyde:glutaraldehyde 3:1). Samples were then analyzed by optical microscopy and Raman Microspectroscopy. The analysis of optical and Raman data showed that among the fixatives tested, formol allowed both to better preserve the morphology, integrity, and transparency of the sample, and to reduce the contamination of Raman spectra in terms of peaks overlapping in the regions of interest.

Introduction

Embryos' developmental stages represent a crucial process, during which the starting evolution of the fish takes place in a very rapid and susceptible to environmental conditions way (*Fleming et al. 2004*). In particular, zebrafish embryos show interesting and peculiar features, such as a fully sequenced genome, with a high degree of similarity to the human one and an easy genetic manipulation, a rapid and external development and transparency, which make them optimal for a large number of toxicological and developmental studies (*Horzmann et al. 2018; Kimmel et al. 1995; Teame et al. 2019*). In addition to histological and biomolecular assays, conventionally applied for investigating the morphology and biological processes of cells and tissues (*Romeo et al. 2006*), Raman MicroSpectroscopy (RMS) has the advantage to provide a morpho-chemical information at a molecular level on the same samples and without needing any pretreatment or labeling (*Mulvaney et al. 2000*). In fact, Raman Microspectroscopy is a very interesting analytical tool widely applied for the analysis of non-homogeneous biological samples (*Mulvaney et al. 2000*): the visual investigation let precisely characterize and target the areas of interest, while Raman scattering let provide the macromolecular fingerprint of the sample in the investigated area (*Meade et al. 2010*). Moreover, the analysis of Raman peaks in terms of position, intensity and width allows to characterize the bonding types and hence the functional groups within the analyzed sample (*Larkin 2011*).

Thanks to these peculiar features, RMS has the potentiality to become a gold standard for investigating developmental and toxicological issues related to fish embryos. In fact, this analytical tool let analyze the different compartments of the embryo, also achieving in dept information thanks to the possibility of working in a confocal way (*Caspers et al. 2003*). Up to date, only few papers are reported in this topic (*Bennet et al. 2014; Høgset et al.*

2020) RMS can be also exploited on hydrated samples, since water does not affect the Raman spectral profile, as it happens in the case of IR spectroscopy (Larkin 2011). However, even if the best practice should be to carry out the analysis on fresh specimens, immediately after their collection and without any pre-treatment like drying or staining, which could negatively affect both the sample and the spectra (Downes et al. 2010; Keating et al. 2013; Nabiev et al. 1994), this is not always possible. In these cases, to obtain reliable and objective data even after a few days from the collection of the sample, it is mandatory to define a fixation protocol that allows to maintain and preserve the collected specimens as much as possible keeping the original conditions. Previous studies dealing with the vibrational analysis of biological samples, reported the evaluation of Raman fixation protocols on healthy and neoplastic cells (Ali et al. 2013; Draux et al. 2010; Gelder et al. 2007; Mariani et al. 2009; Meade et al. 2010), mainly focusing on their effects on specific subcellular structures (cellular membrane, nucleic acids) (Srinivasan et al. 2002; Wallach et al. 1979).

In the present study, three widely used fixatives, i.e. PFA (paraformaldehyde 4% solution), Bouin's solution (picric acid, formaldehyde, acetic acid, 15:5:1), and formol (formaldehyde and glutaraldehyde, 3:1), were tested on zebrafish embryos and larvae collected from 1 to 5 days post fertilization (dpf). Samples were analyzed by optical microscopy and Raman Microspectroscopy, to evaluate the best fixation protocol that met the following requirements: (1) preserving the morphology, integrity, and transparency of the sample, and (2) reducing the contamination of Raman spectra in terms of peaks overlapping in the regions of interest.

Materials and methods

Fixative solutions preparation

The following fixative solutions were prepared.

- (i) PFA 4% solution was obtained from paraformaldehyde powder, 95% purity (Sigma Aldrich, St. Louis, MO). Preparation was carried out as follows: 50 g of paraformaldehyde powder were dissolved in 500 ml of distilled H₂O. 10 mL of 1 M NaOH were added, and the solution was gently stirred on a heating block at ~60°C until the powder was dissolved. 100 mL of 10xPBS were added and the mixture was cooled to room temperature. The pH was adjusted to 7.4 with 1 M HCl (~10 mL). Distilled H₂O was then added to reach a final volume of 1000 mL. The resulting solution was filtered through a 0.45-µm membrane to remove any particulates and stored at 4°C.
- (ii) Bouin's solution was prepared by combining 75 mL of saturated picric acid with 25 mL of formalin solution (formaldehyde 35%), and 5 mL of glacial acetic acid (100% acetic acid). The resulting solution was stored at 4°C.
- (iii) Formol solution was prepared by mixing 110 ml of formaldehyde 36,5% with 40 ml of glutaraldehyde 25%. To maintain a neutral pH, 11.6 g of sodium phosphate monobasic monohydrate and 2.7 g of sodium hydroxide 1 M were added under stirring. Distilled water was then added to reach the final volume of 1000 mL. The checking of pH was set at 7.2, and the solution was then stored at 4°C.

Sample collection

Zebrafish (*Danio rerio*) adults were maintained in 100-L aquaria (static system), with oxygenated water under the following conditions: 28 °C, pH 7.0, NO₂ concentration < 0.01 mg/L, and NH₃ concentration < 10 mg/L, with an administered photoperiod of 12 L/12D. During the spawning period, males and females were transferred to breeding tanks and from each breeding tank (about 20–30 min after the onset of light), eggs were collected. Eggs were initially observed and counted under a stereomicroscope (Leica Wild M3B; Leica Microsystems, Nussloch, Germany) for the evaluation of fertilized eggs. Only fertilized eggs, that presented a well-developed

blastodisc at 3 h after fertilization, were transferred into 10 cm diameter Petri dishes containing E3 medium (5 mM NaCl, 0.17 mM KCl, 0.33 mM CaCl₂, and 0.33 mM MgSO₄, to pH 7.0) and incubated at 28°C. A spontaneous mortality rate of 5–15±5% was observed. N. 20 embryos were withdrawn each day, from 1 dpf to 5 dpf. Once collected, samples were gently washed in deionized water and divided into 4 groups (N = 5): (A) fixation with PFA 4% solution; (B) fixation with Bouin's solution; (C) fixation with formol solution, and (D) not fixed. The experiment was carried out in triplicate.

Samples fixation

Embryos of groups A-D were fixed as follows and stored at 4°C until measurements: (A) embryos were immersed in PFA 4% solution for 1 hour, washed three times with deionized water; (B) embryos were immersed in Bouin's solution for 24 hours, washed in ethanol three times and then furtherly washed in deionized water just before measurements; (C) embryos were kept in formol solution and washed three times in deionized water just before measurements; (D) embryos were maintained in deionized water. On 2 dpf and 3 dpf embryos, the mechanical removal of chorion was performed after fixation procedure and soon before measurements.

Optical microscopy analysis

The visual investigation of fresh and fixed Zebrafish embryos (groups A-D) was performed by using the Stereomicroscope GZ 808 (Optech). The inspection was carried out in order to determine the developmental stage of the samples following Kimmel et al 1995 (*Kimmel et al. 1995*), and to evaluate the effects caused by the tested fixatives on maintenance degree.

Raman Microspectroscopy analysis

RMS measurements were carried out at the ARI Lab of the Department of Life and Environmental Sciences by a XploRA Nano MicroSpectrometer (Horiba Jobin-Yvon). On each embryo, deposited onto glass slides, N. 20 Raman spectra were collected at the depth of 100 μm within the central region of the yolk. To this purpose, the Z-profiling system was exploited together with a x100 long working distance objective (532 nm diode laser). The spectrometer was calibrated to the 520.7 cm^{-1} line of silicon prior to spectral acquisition. Raman signals were accumulated 3 times for 10 seconds in the fingerprint region 400–1800 cm^{-1} . Raw spectra were preprocessed by multi-points baseline correction and vector normalization (OPUS 7.5, Bruker Optics, Ettlingen, Germany).

Statistical analysis

Preprocessed spectra were analyzed by Principal Component Analysis (PCA; OriginPro 2018b software, OriginLab Corporation, Northampton, Massachusetts).

Results

The photomicrographs obtained by the visual investigation of not-fixed zebrafish embryos (group D) are showed in Figure 1. The morphological and physiological changes occurring during the development are well evident: with time, a general consumption of yolk is highlighted, accompanied by an elongation of the body. At 1 dpf, retina and skin start to pigment, together with the median fin fold which starts to develop; the heart starts beating. Blood circulation in arteries and veins starts at 2 dpf. At 3 dpf, the mouth makes its appearance, even still not opening. By day 3, the morphogenesis of the hatched early larva is almost completed, and its growth continues rapidly. From day 4 pf, the early larva begins to actively swim

about, and at 5 dpf it starts moving its eyes and jaws, marking the beginning of the self-feeding period of zebrafish (*Kimmel et al. 1995*).

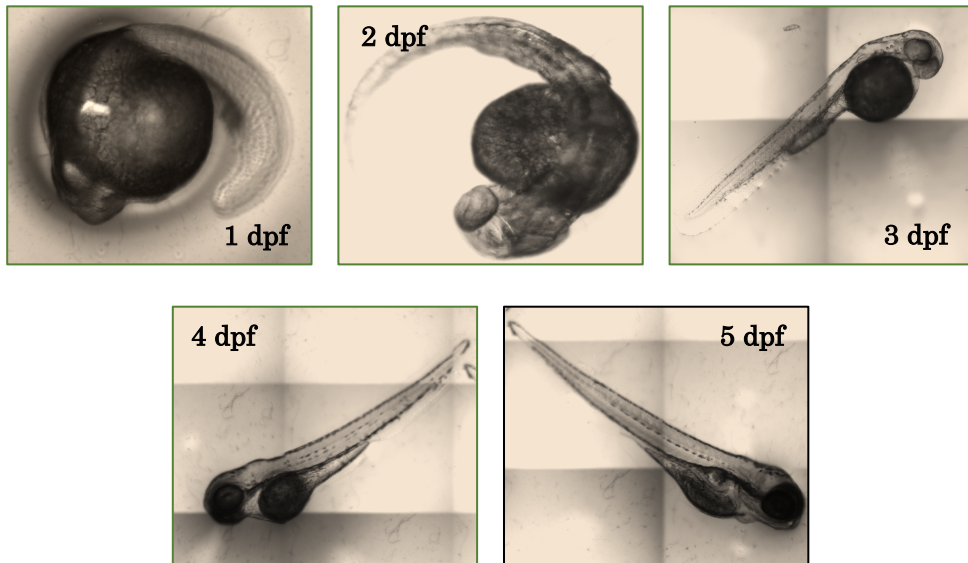


Figure 1. Photomicrographs of 1 to 5 dpf Zebrafish embryos from group D.

The comparison of fixed samples (group A-C) with not fixed ones (group D) revealed that only formol fixative guaranteed the normal morphology. In fact, while PFA-fixed samples resulted more delicate in handling, less transparent and with altered morphological features, Bouin's fixative allowed to maintain the morphology but gave samples a strong yellow colour due to the presence of picric acid. As an example, in Figure 2, the photomicrographs of 5 dpf zebrafish embryos not fixed and fixed alternatively with PFA, Bouin's, and formol are reported.



Figure 2. Photomicrographs of representative 5 dpf-embryos fixed with (A) PFA, (B) Bouin, (C) formol, and (D) not fixed.

In Figure 3, the Raman spectra of fixatives are reported. The following peaks were observed in all fixatives: 1725 cm^{-1} (stretching of C=O groups); 1450 cm^{-1} (bending of CH_2 groups); 987 cm^{-1} (bending of OH groups); 805 cm^{-1} (bending of CH_2 groups), and 550 cm^{-1} (bending of C-C-O). Moreover, in Bouin's fixative further peaks attributable to picric acid were identified: 1550 cm^{-1} and 1330 cm^{-1} (stretching of NO_2 groups); 1276 cm^{-1} and 1165 cm^{-1} (stretching of benzene ring), and 890 cm^{-1} (stretching of C-N bonds).

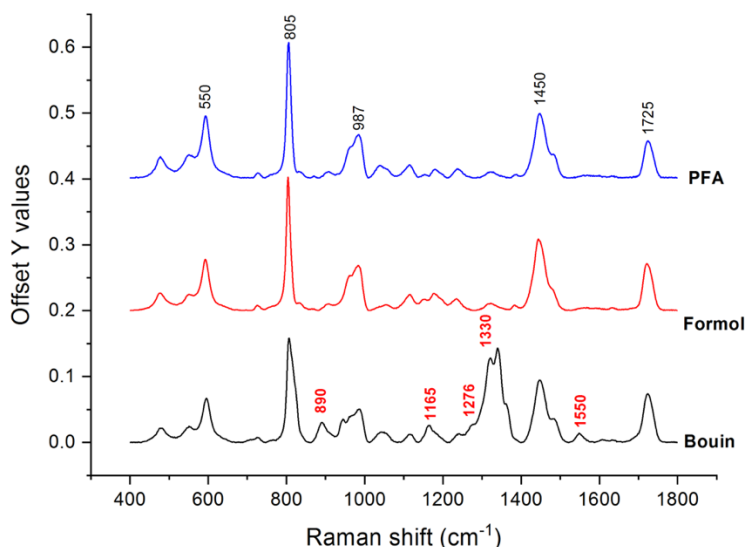
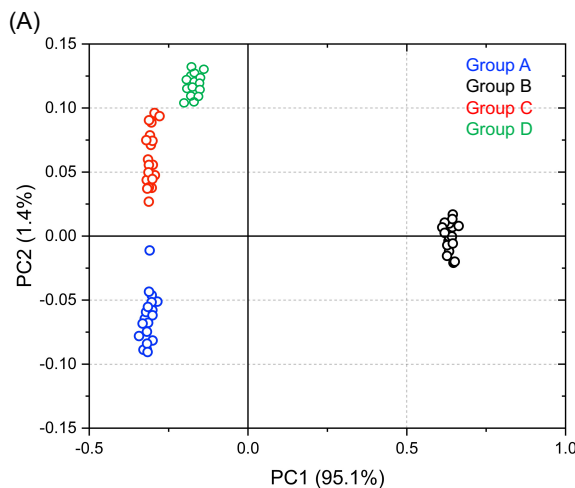


Figure 3. Raman spectra of PFA (blue line), Formol (red line) and Bouin (black line) fixatives. The main Raman peaks are reported above spectra.

To evaluate the contamination due to tested fixation procedures, Raman spectra were also collected on the yolk region of 2-5 dpf fixed embryos (groups A-C) and compared with those of controls (group D) and Raman data were submitted to Principal Component Analysis (Figure 4A). A complete segregation was observed between the Raman spectra of Bouin-fixed samples (group B) and both PFA (group A) and formol (group C) ones along PC1 axis (explained variance 95.1%). Moreover, PFA (group A) and formol (group C) samples were split by PC2, with a lower percentage of variance (explained variance 1.4%). Noteworthy, embryos fixed with formol (group C) and control ones (group D) showed the lowest degree of dissimilarity. The analysis of loadings (Figure 4B) confirmed relevant spectral differences between Bouin's fixed samples and PFA and formol ones (PC1 loadings), while no differences were observed between PFA and formol fixed samples (PC2 loadings).



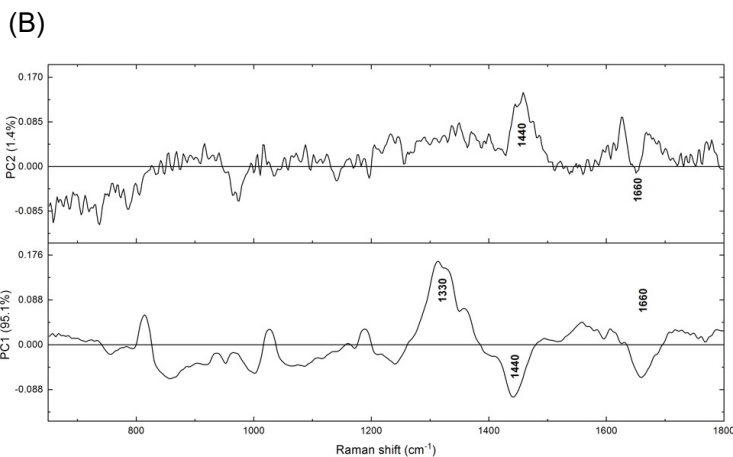


Figure 4. (A) PCA scatter plot of spectra of 1 dpf-embryos not fixed (green) and fixed by using PFA (blue), Bouin's fixative (black), and Formol (red). (B) PC1 and PC2 loading profiles; numbers corresponding to the highest peaks differences.

Discussion

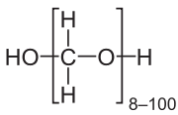
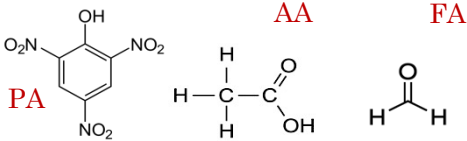
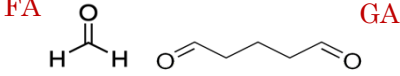
Raman Microspectroscopy presents the great advantage to let acquire samples in hydrated conditions, since this technique is sensible to polarizable electron clouds and hence Raman spectra are not affected by water (Czamara *et al.* 2015; Movasaghi *et al.* 2007; Talari *et al.* 2015; Turrell *et al.* 1996). Nevertheless, it is not always possible to perform Raman measurements soon after sample collection; furtherly, over time, fresh samples could be subjected to degeneration processes. Hence, the use of fixatives is mandatory to preserve the biological sample, but these procedures could introduce some artifact compromising the whole analysis (Downes *et al.* 2010; Keating *et al.* 2013; Nabiev *et al.* 1994). In this perspective, to perform reliable and objective Raman measurements, it appears crucial to define a specific fixation protocol which let preserve samples in term of morphology and composition and at the same time, does not affect the spectral profile.

The present study wants to give some preliminary advice about this topic, testing some routinely used fixation protocols, in order to evaluate the most fitting both morphological and vibrational issues, and without overturn laboratory practice (*Hobro et al. 2017; Meade et al. 2010*).

At this purpose, the following commercially fixatives were tested on zebrafish embryos: paraformaldehyde, Bouin's fixative and formol. All these compounds have a quite different chemical composition, from which their behaviour derives. As regards paraformaldehyde, it results from the polymerization of formaldehyde monomers and is formed by the assembly of 8–100 units: formaldehyde reacts with primary amines on proteins and nucleic acids to form partially reversible methylene bridges. Bouin's fixative consists of a solution containing picric acid, formaldehyde and glacial acetic acid in a ratio 15:5:1; picric acid slowly penetrates in tissues and forms picrates basic proteins which precipitate; acetic acid coagulates nucleic acids, while formaldehyde forms cross-linkage in proteins. Formol is a solution of formaldehyde and glutaraldehyde, with a ratio of 3:1; formaldehyde, as just said, reacts with primary aminic groups present both in proteins and nucleic acids and forms methylene cross-bridges, while glutaraldehyde is a dialdehyde compound that reacts with amino and sulfhydryl groups and possibly with aromatic ring structures (*Table 1*).

Zebrafish samples were analyzed in terms of morphology and spectral profiles. As regards the maintenance of the morphological features, only formol kept the original conditions of the embryos, both in colour and in morphology, while Bouin and PFA did not give successful results. Bouin's fixation procedure immediately resulted in an alteration of the colour of both embryos, due to the effect of picric acid, while PFA made embryos very delicate in handling and with altered morphological features.

Table 1. Chemical composition of the tested fixatives.

Fixative	Chemical structure
Paraformaldehyde (PFA)	
Bouin's fixative: <ul style="list-style-type: none"> picric acid (PA) glacial acetic acid (AA) formaldehyde (FA) 	
Formol: <ul style="list-style-type: none"> formaldehyde (FA) glutaraldehyde (GA) 	

PFA and formol fixed samples resulted in very similar Raman spectra, with no relevant peaks, attributable to fixatives contamination. Conversely, Bouin's fixative massively affects the spectral profiles of zebrafish embryos, mainly due to picric acid. In fact, this compound contains an aromatic ring substituted with three nitro groups. All these chemical moieties are very Raman active, producing high signals which interfere with the sample signal.

Conclusions

Fish embryos are a valuable model to study relevant environmental issues, including the toxicological effects of emerging contaminants. In this framework, Raman spectroscopy can be considered an optimal analytical tool thanks to its potential to produce morpho-chemical information at high resolution and at a molecular level on the different embryos' compartments. Nevertheless, the need to obtain robust and reliable information is strictly related to the preparation of the sample, since any fixation procedure applied to the sample before the RMS analysis could affect the final results.

For this reason, the assessment of a reliable protocol for Raman analysis of fish embryos is crucial. As regards the fixatives, the obtained results let define the protocol employing formol as the optimal one, both regarding the morphology and the Raman profiles of fixed zebrafish embryos. In fact, (i) it let preserve the morphology, integrity and transparency of the sample and (ii) it less affects Raman spectra in terms of peaks overlapping in the regions of interest.

References

- Ali, S. M. et al. 2013. "A Comparison of Raman, FTIR and ATR-FTIR Micro Spectroscopy for Imaging Human Skin Tissue Sections." *Analytical Methods* 5(9): 2281–91.
- Bennet, M. et al. 2014. "Simultaneous Raman Microspectroscopy and Fluorescence Imaging of Bone Mineralization in Living Zebrafish Larvae." *Biophysical Journal* 106(4): L17–19.
- Caspers, P. J. et al. 2003. "Combined In Vivo Confocal Raman Spectroscopy and Confocal Microscopy of Human Skin." *Biophysical Journal* 85(1): 572–80.
- Czamara, K. et al. 2015. "Raman Spectroscopy of Lipids: A Review." *Journal of Raman Spectroscopy* 46(1): 4–20.
- Downes, A. et al. 2010. "Raman Spectroscopy and Related Techniques in Biomedicine." *Sensors* 10(3): 1871–89.
- Draux, F. et al. 2010. "Raman Spectral Imaging of Single Cancer Cells: Probing the Impact of Sample Fixation Methods." *Analytical and Bioanalytical Chemistry* 397(7): 2727–37.
- Fleming, T. P. et al. 2004. "The Embryo and Its Future." *Biology of Reproduction* 71(4): 1046–54.
<https://academic.oup.com/biolreprod/article/71/4/1046/2666924>.
- Gelder, J. D. et al. 2007. "Reference Database of Raman Spectra of Biological Molecules." *Journal of Raman Spectroscopy* 38(9): 1133–47.
- Hobro, A. J. et al. 2017. "An Evaluation of Fixation Methods: Spatial and Compositional Cellular Changes Observed by Raman Imaging." *Vibrational Spectroscopy* 91: 31–45.
- Høgset, H. et al. 2020. "In Vivo Biomolecular Imaging of Zebrafish Embryos Using Confocal Raman Spectroscopy." *Nature Communications* 11(1).
- Horzmann, K. A. et al. 2018. "Making Waves: New Developments in Toxicology With the Zebrafish." *Toxicological Sciences* 163(1): 5–12.
<https://academic.oup.com/toxsci/article/163/1/5/4870163>.
- Keating, M. E. et al. 2013. "Raman Spectroscopy in Nanomedicine: Current Status and Future Perspective." *Nanomedicine* 8(8): 1335–51.
- Kimmel, C. B. et al. 1995. "Stages of Embryonic Development of the Zebrafish." *Developmental Dynamics* 203(3): 253–310.
- Larkin, P. 2011. *Infrared and Raman Spectroscopy: Principles and Spectral Interpretation*. ed. Peter Larkin. Elsevier.
- Mariani, M. M. et al. 2009. "Impact of Fixation on in Vitro Cell Culture Lines Monitored with Raman Spectroscopy." *Analyst* 134(6): 1154–61.
- Meade, A. D. et al. 2010. "Studies of Chemical Fixation Effects in Human Cell Lines Using Raman Microspectroscopy." *Analytical and Bioanalytical Chemistry*

396(5): 1781–91.

- Movasaghi et al. 2007. “Raman Spectroscopy of Biological Tissues.” *Applied Spectroscopy Reviews* 42(5): 493–541.
- Mulvaney, S. P. et al. 2000. “Raman Spectroscopy.” *Analytical Chemistry* 72(12).
- Nabiev, I. et al. 1994. “Applications of Raman and Surface-Enhanced Raman Scattering Spectroscopy in Medicine.” *Journal Of Raman Spectroscopy* 25: 13–23.
- Romeo, M. J. et al. 2006. “Infrared and Raman Microspectroscopic Studies of Individual Human Cells.”
- Srinivasan, M. et al. 2002. “Effect of Fixatives and Tissue Processing on the Content and Integrity of Nucleic Acids.” *American Journal of Pathology* 161(6): 1961–71.
- Talari, A. C. S. et al. 2015. “Raman Spectroscopy of Biological Tissues.” *Applied Spectroscopy Reviews* 50(1): 46–111.
- Teame, T. et al. 2019. “The Use of Zebrafish (*Danio Rerio*) as Biomedical Models.” *Animal Frontiers* 9(3): 68–77.
<https://academic.oup.com/af/article/9/3/68/5522877>.
- Turrell, G. et al. 1996. “Characteristics of Raman Microscopy.” *Raman Microscopy*: 27–49.
- Wallach, D. F. H. et al. 1979. “Application of Laser Raman and Infrared Spectroscopy to the Analysis of Membrane Structure.” *Biochimica et Biophysica Acta (BBA) - Reviews on Biomembranes* 559(2): 153–208.
<https://www.sciencedirect.com/science/article/pii/0304415779900017>.

CHAPTER 2

METABOLISM ALTERATION IN FISH EMBRYOS EXPOSED TO ENVIRONMENTAL CONTAMINANTS: WHAT CAN WE LEARN FROM MOLECULES' VIBRATIONAL CHANGES

Chiara Pro, Giorgia Gioacchini, Oliana Carnevali, Elisabetta Giorgini,
Valentina Notarstefano

Department of Life and Environmental Sciences, Università Politecnica delle
Marche

Paper in preparation

Abstract

The aim of this study is to evaluate the effects caused by the emerging contaminants PFOS and PFOA on zebrafish embryos in terms of alterations in the developmental morphology and macromolecular composition and uptake of yolk. To this purpose, zebrafish embryos were treated for 1 to 4 days with different concentrations of PFOA and PFOS. Microphotographs of embryos and Raman spectra of the yolk region were collected, and data were compared with those from control samples. The results clearly showed that PFOS and PFOA induces some alterations not only in terms of embryos morphology but also at the level of yolk composition and uptake. In fact, the visual investigation showed some cases of malformations at the higher administered doses, while the spectral analysis revealed an altered consumption of yolk's components over time, sided by changes in almost all the bands related to the main biomolecules of the yolk.

Introduction

Polyfluorinated compounds (PFCs) are emerging contaminants with adverse effects on the environment. Among them, perfluorooctane sulfonate (PFOS) and perfluorooctanoic acid (PFOA) are the most studied, since they present peculiar features, such as an extreme stability and resistance to degradation, which make them able to bioaccumulate in food chains, reaching also animals and humans (*Conder et al. 2008; Lehmler 2005; Lindstrom et al 2011; Suja et al. 2009*).

As already mentioned, zebrafish represents a well-established experimental model, widely used in toxicological and developmental studies (*Cassar et al. 2019; Cassar et al. 2021; Chakraborty et al. 2009*). In fact, *Danio rerio* embryos and early-stage larvae are completely lecithotrophic, thus meaning that they entirely rely on a finite supply of yolk; for this reason, embryonic nutrition can be evaluated observing the rate of yolk consumption (*Fraher et al. 2016*). Proteins and lipids represent the major constituents of zebrafish yolk. Lipids are crucial for mediating cell signalling and for providing building blocks for plasma and cell membranes; the most represented is cholesterol (40% of total lipid), followed by phosphatidylcholine (17%), triacylglycerols (9%), phosphatidylinositol (8%), phosphatidylethanolamine (5%), diacylglycerol (4%), cholesteryl esters (3%), and sphingomyelins (3%) (*Sant et al. 2018*). The observation of the dynamic profile of lipids within the yolk throughout embryo development showed that yolk lipids are not simply consumed by the embryo: in fact, although previous research described the yolk as a metabolically inactive reserve of maternally deposited nutrients, it is now clear that the yolk and the yolk sac are metabolically active (*et al. 2018*). For example, the amount of triacylglycerols increases in the yolk from 0 to 24 hpf (hours post fertilization) and then progressively declines; conversely, the level of diacylglycerols remain constant during embryogenesis, suggesting they are produced and used at

the same rate (*Fraher et al. 2016*). Regarding the proteins present in the yolk, the most important are vitellogenin-derived proteins, including lipovitellin and phosvitin, which are essential for oocyte maturation (*Link et al. 2006*). Interestingly, it has been demonstrated that lipophilic xenobiotics in the surrounding aquatic environment can penetrate the yolk and aggregate (*Scholz et al. 2008*): this can result in an alteration of the rate at which yolk's nutrients are used. At this purpose, measuring the dimensions of yolk during embryogenesis can be related to the rate of nutrient uptake, in order to identify chemicals that may interfere with nutrient mobilization from the yolk sac to the embryo (*Fraher et al. 2016*). It has been reported that exposure to PFOS during embryonic and larval development determines an increase in the rate of yolk utilization over the first four days post fertilization (*Sant et al. 2017*). More in detail, the yolk sac area measured at 5 dpf revealed that PFOS-treated zebrafish embryos and larvae were significantly smaller than the one of control samples; conversely, the treatment with PFOA had an opposite effect, with bigger yolk sac areas measured at 5 dpf, suggesting a decreased yolk nutrients utilization by larvae (*Jantzen et al. 2016*).

Raman MicroSpectroscopy (RMS) is a powerful vibrational technique, widely applied in life sciences for the study of the biomolecular building and composition of cells and tissues (*Giorgini et al. 2014; Lyng et al. 2015; Matthäus et al. 2008*). It presents the advantage to be label-free, since each molecule has a proper Raman spectrum, which is composed by peaks and bands, constituting the molecular fingerprint of the sample (*Ferraro et al. 2003*). The analysis of the position, intensity and width of the bands allows the identification and characterization of functional groups, bonding types and molecular conformations of the most important biological molecules of the sample, in terms of proteins, lipids, carbohydrates, and nucleic acids content (*Baena et al. 2004; Baker et al. 2014; Wolkers et al. 2010*). This

chemical information can be directly related to specific biological processes, such as cellular activity, metabolism and oxidative stress (*Downes et al. 2010; Giorgini et al. 2010; Giorgini et al. 2018*).

In the present study, RMS was used on zebrafish embryos (1) to evaluate the consumption of the single yolk components during embryo development, and (2) to detect the impairment caused by PFOS and PFOA treatments in these processes, in terms of both time exposure and concentration. The use of this vibrational approach presents some advantages; in fact, by working in a confocal mode, it let perform an in-depth analysis, providing relevant information on the uptake and consumption of yolk single components (such as lipids, proteins, phosphates and carbohydrates); moreover, it let correlate the macromolecular changes due to the exposure to these environmental contaminants with the morphological alterations.

Materials and methods

PFOS and PFOA solutions preparation

PFOS [$\text{CF}_3(\text{CF}_2)_7\text{SO}_3\text{H}$] and PFOA [$\text{CF}_3(\text{CF}_2)_6\text{COOH}$] were purchased by Sigma Aldrich, as powder 95-98% (St. Louis, MO). PFOS and PFOA were added to ultrafiltered distilled water to obtain 0.02 μM , 0.2 μM and 2 μM solutions, that were maintained at 4°C.

Sample collection

Zebrafish (*Danio rerio*) adults were maintained in 100-L aquaria (static system), with oxygenated water under the following conditions: 28 °C, pH 7.0, NO_2 concentration < 0.01 mg/L, and NH_3 concentration < 10 mg/L, with an administered photoperiod of 12 L/12D. During the spawning period, males and females were transferred to breeding tanks and from each breeding tank (about 20–30 min after the onset of light), eggs were collected.

Eggs were initially observed and counted under a stereomicroscope (Leica Wild M3B; Leica Microsystems, Nussloch, Germany) for the evaluation of fertilized eggs. Only fertilized eggs, that presented a well-developed blastodisc at 3 h after fertilization, were transferred into 10 cm diameter Petri dishes containing E3 medium (5 mM NaCl, 0.17 mM KCl, 0.33 mM CaCl₂, and 0.33 mM MgSO₄, to pH 7.0) and incubated at 28°C. A spontaneous mortality rate of 5–15±5% was observed.

Samples treatment with PFOS and PFOA

1-dpf embryos were collected, counted under a stereomicroscope (GZ 808, Optech) and randomly divided into the following groups (N=7): (A) control group; (B) embryos treated with PFOA 0.02 µM; (C) embryos treated with PFOA 0.2 µM; (D) embryos treated with PFOA 2.0 µM; (E) embryos treated with PFOS 0.02 µM; (F) embryos treated with PFOS 0.2 µM, and (G) embryos treated with PFOS 2.0 µM.

From each experimental group, embryos were collected each day from 2 to 5 dpf, gently washed in deionized water and fixed in formol solution, as described in Chapter 1. Samples were kept in the fixative solution until measurements; just before measurements, embryos were washed three times in deionized water. On 2 dpf and 3 dpf embryos, the mechanical removal of chorion was performed after fixation procedure and soon before measurements. The concentration and times of exposure of both contaminants were chosen according to literature data (*Jantzen et al. 2016*). The experiment was performed in triplicate.

Optical microscopy analysis

The visual investigation of embryos of A-G groups was performed by using the Stereomicroscope GZ 808 (Optech). The inspection was carried out in order to evaluate the effects caused by PFOS and PFOA treatments.

Raman microspectroscopy measurements and data analysis

Raman measurements were performed by a XploRA Nano MicroSpectrometer (Horiba Jobin-Yvon) at the ARI Lab of the Department of Life and Environmental Sciences. On each embryo, deposited onto glass slides, N. 20 Raman spectra were collected at the depth of 100 μm within the central region of the yolk. The Z-profiling system was exploited together with a x100 long working distance objective (532 nm diode laser). The spectrometer was calibrated to the 520.7 cm^{-1} line of silicon prior to spectral acquisition. Raman signals were accumulated 3 times for 10 seconds in the fingerprint region 400–1800 cm^{-1} . Raw spectra were preprocessed by multi-points baseline correction and vector normalization (OPUS 7.5, Bruker Optics, Ettlingen, Germany). Preprocessed spectra were analysed in terms of position and height of bands of interest (Integration mode K, OPUS 7.5, Bruker Optics, Ettlingen, Germany).

Statistical analysis

Normally distributed data deriving from RMS spectra were presented as mean \pm S.D. Significant differences among groups were determined by means of a factorial analysis of variance (one-way ANOVA) followed by Tukey's multiple comparison test, by the statistical software Prism6 (Graphpad Software, Inc. USA). Statistical significance was set at $p < 0.05$.

Results

In Figure 1, the microphotographs of zebrafish embryos belonging to the CTRL group (Group A), and after 1, 2, 3, and 4 days of treatment with PFOA 0.02 μM , 0.2 μM and 2 μM (Groups B-D) and PFOS 0.02 μM , 0.2 μM and 2 μM (Groups E-G) are showed. The images clearly display the growing steps of the embryos, with the elongation of the body, and the reduction of

the overall yolk volume. More in detail, in CTRL embryos, at 2 dpf, after retina and skin starting pigmentation, it begins the blood circulation in arteries and veins; mouth appears at 3 dpf, even still not opening; by day 3, embryo growth continues rapidly, since morphogenesis of the hatched early larva is almost completed. The early larva begins to actively swim about from 4 dpf, and at 5 dpf it starts moving its eyes and jaws, with the beginning of the self-feeding period of zebrafish (*Kimmel et al. 1995*).

In general, no visible morphological alterations were observed in most of the treated embryos. However, some modifications were found in few specimens (ca. 5% of total embryos) related to the development and growth with modifications in the somite development, occurrence of pericardial edema, vitelline cysts, bent tail, and bent spine were found; moreover, in some cases, hatching modifications were observed, with samples without chorion loss (Figure 2). It is noteworthy that the lowest concentration of both the administered compounds seemed to not produce adverse effects on the morphology. More in detail, as regards PFOA, alterations were observed only at the highest dose (2 μ M), while PFOS negative effects were displayed at both 0.2 and 2 μ M.

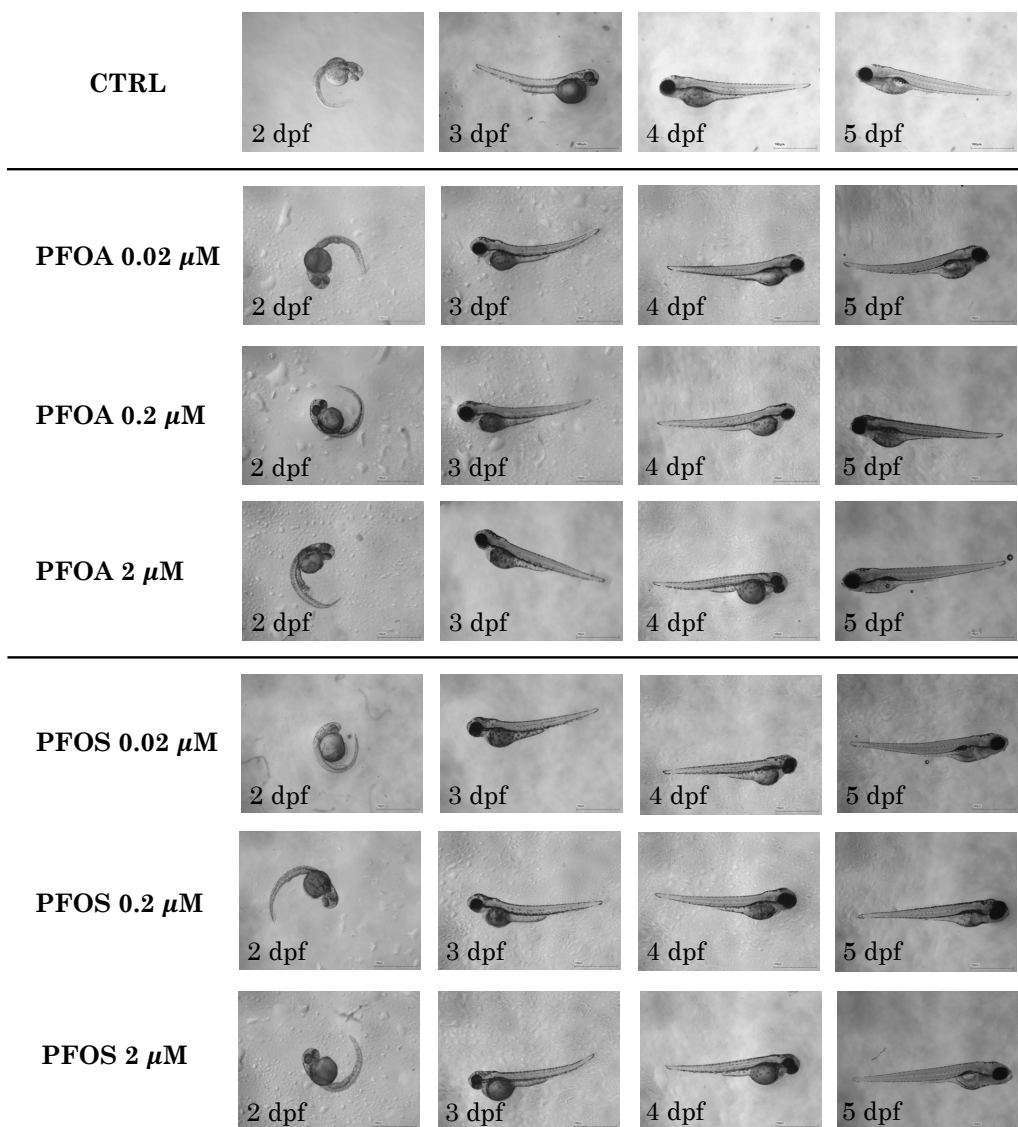


Figure 1. Photomicrographs of 2 to 5 dpf-embryos. The CTRLs and the treated samples are displayed, with the three different administered doses (0.02, 0.2 and 2 μ M) for each of the two tested compounds (PFOA and PFOS).

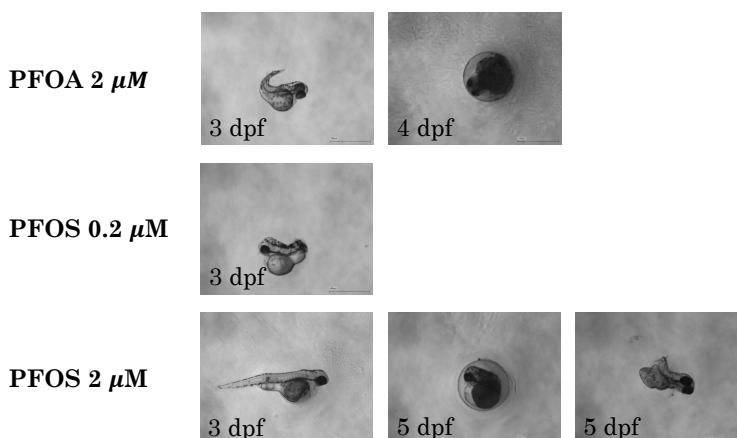


Figure 2. Photomicrographs of malformed embryos. Some of the evidenced malformations are shown, with the corresponding dose and administered compound.

In Figure 3, the Raman spectra collected on the yolk region of 2 to 5 dpf CTRL embryos are showed. The following Raman bands, representative of the biomolecules composing the yolk, were detected (*Czamara et al. 2015; Talari et al. 2015*): (i) 1740 cm^{-1} : lipid ester groups vibration; (ii) 1655 cm^{-1} : amidic C=O groups stretching (Amide I); (iii) 1442 cm^{-1} : lipid chains CH_2 bending; (iv) 1259 cm^{-1} : lipids CH_2 in-plane deformation/Amide III; (v) 1080 cm^{-1} : PO_2^- groups stretching; (vi) 1000 cm^{-1} : phenylalanine ring breathing; (vii) 850 cm^{-1} : tyrosine ring breathing; (viii) 704 cm^{-1} : cholesterol/cholesteryl esters ring deformation; (ix) 590 cm^{-1} : PO_4^{3-} groups stretching.

Raman spectra evidenced how the fingerprint region of yolk is mainly attributable to lipids and proteins. In fact, the bands at 1740 cm^{-1} and 1655 cm^{-1} are due to the stretching of C=O groups respectively in the lipid and protein component, whereas the band at 1442 cm^{-1} is assigned to the scissoring mode of the CH_2 groups, and hence to deformations of long hydrocarbon chains. Moreover, the presence of the bands at 1080 cm^{-1} and 590 cm^{-1} indicates the presence of phosphate groups attributable to phospholipids and phosphorylated compounds, while the band at 704 cm^{-1} is

attributable to cholesterol and cholesteryl esters. In general, a decreasing trend of most of these bands was observed with time, confirming the consumption of yolk during embryo development. An exception was detected as regards the band centred at 590 cm^{-1} , attributable to phosphate groups in the phosvitin molecule, which remained almost unchanged with time: this finding suggests that the amount of this component, which derives from the proteolytic cleavage of vitellogenin, remains constant during embryogenesis (Figure 3) (Prescott *et al.* 1986).

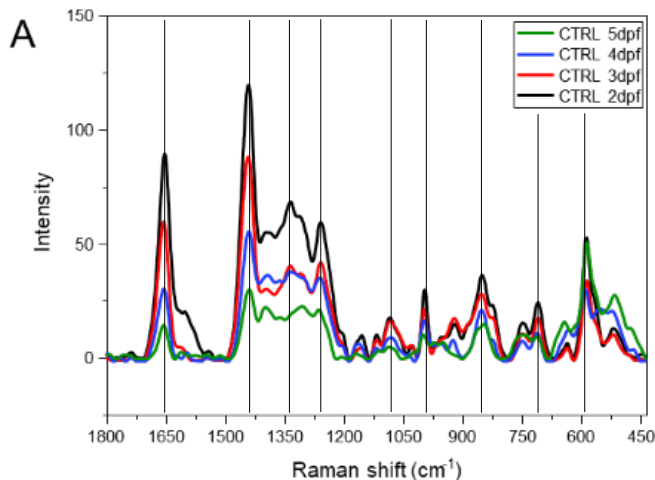


Figure 3. Average spectra of the yolk of CTRL embryos collected at 2, 3, 4, and 5 dpf (group A). Vertical lines indicate the Raman peaks referred mainly to lipid content, protein content and phosphate components.

Then, Raman spectra of all the PFOA (groups B-D) and PFOS (groups E-G) treated samples were analyzed and compared with those of CTRL ones (Group A) (Figure 4). In general, treated embryos showed a different trend of consumption with respect to CTRLs at all time points, with spectra having altered peaks corresponding to the yolk biomolecules. However, this was more evident in embryos submitted to PFOS, respect to PFOA and

differences resulted more evident as far as the administered dose of compound increases. These findings are in agreement with the data reported in literature, which show PFOS with a higher toxicity respect to PFOA (*Jantzen et al. 2016; Jantzen et al. 2016*).

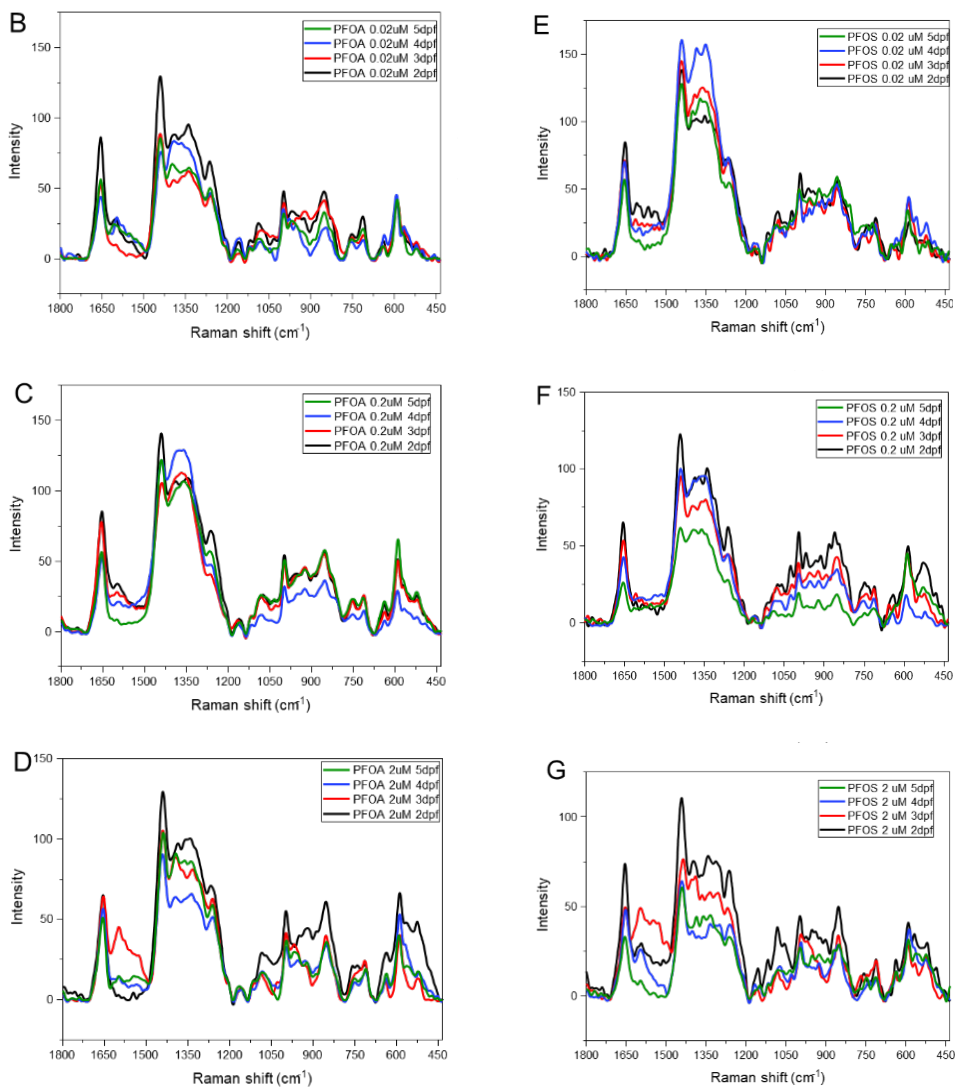


Figure 4. Average spectra of the yolk of embryos and larvae collected at 2, 3, 4, and 5 dpf, after treatment with PFOA 0.02 μ M (B), PFOS 0.2 μ M (C), PFOS 2 μ M (D), and PFOS 0.02 μ M (E), PFOS 0.2 μ M (F), PFOS 2 μ M (G).

For a deeper understanding of the effects of the treatments with PFOA and PFOS on yolk nutrients utilization, the height of the major Raman bands was investigated and compared along the four days of treatment. As regards control embryos (group A), in the spectra from 2 dpf embryos, a major amount of lipids (bands centered at 1442 and 704 cm^{-1}), phosphate groups (bands centered at 1086 and 590 cm^{-1}), and proteins (1655, 1259, and 1000 cm^{-1}) was observed; moreover, the analysis of band heights confirmed in this group the constant and almost linear decreasing trend for all the studied Raman bands. By concerning treated embryos, all the doses of PFOA and PFOS displayed a lower starting amount of lipids, proteins, and phosphates, and their decrease along the four analyzed days appeared less constant: in particular, the decrease was more evident until day 3, while days 4 and 5 were characterized by a minor slope of the decreasing trend, suggesting a slowdown of the utilization of yolk's biomolecules.

More in detail, in Figure 5, the line plots representative of the proteic region of the spectrum are reported (Amide I, 1655 cm^{-1} ; Amide III, 1259 cm^{-1} , and phenylalanine, 1000 cm^{-1}); for clarity, in each box, the black dotted line represents CTRL samples (Group A), while yellow, orange and red lines the PFOA-treated embryos and light green, green and dark green lines the PFOS-ones. Considering CTRL embryos, an overall and constant decreasing trend is evident with time; in treated samples, the starting point at 2 dpf presents a lower value in all the protein-related bands, with an evident decrease until 3 dpf, and a slowdown corresponding to 4 and 5 dpf.

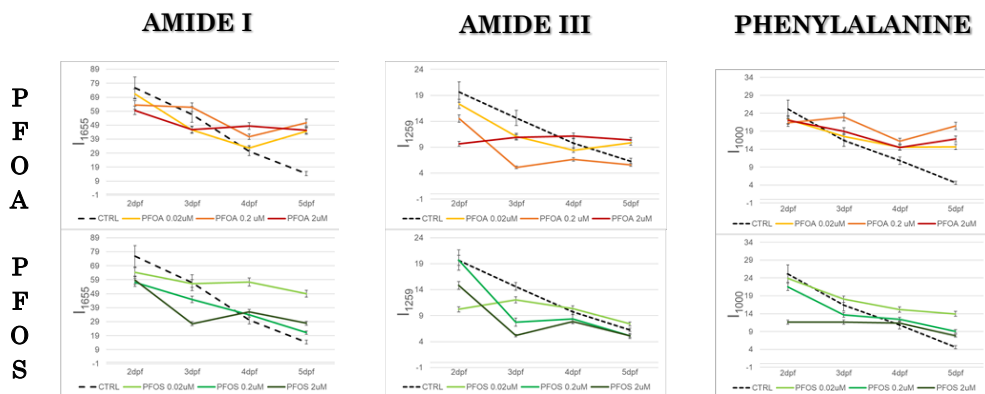


Figure 5. Line plots displaying average \pm SD values of the heights of the following Raman bands: 1655 cm^{-1} (Amide I), 1259 cm^{-1} (Amide III), and 1000 cm^{-1} (phenylalanine). CTRL (dotted black), PFOS $0.02\ \mu\text{M}$ (yellow), PFOS $0.2\ \mu\text{M}$ (orange), PFOS $2\ \mu\text{M}$ (red), PFOA $0.02\ \mu\text{M}$ (light green), PFOA $0.2\ \mu\text{M}$ (green), and PFOA $2\ \mu\text{M}$ (dark green).

As for proteins, also the line plots of lipid-related bands (CH_2 groups, 1442 cm^{-1} , and cholesterol and cholesteryl esters, 704 cm^{-1}) showed a general decreasing trend in CTRLs, considering all the time points (Figure 6). Conversely, in treated samples, a lower starting point at 2 dpf was found for CH_2 moieties, with similar amounts at 3, 4 and 5 dpf, suggesting a lower consumption of yolk lipids respect to CTRL. As regards cholesterol, higher and constant amounts respect to CTRL were displayed, especially by PFOA-treated embryos.

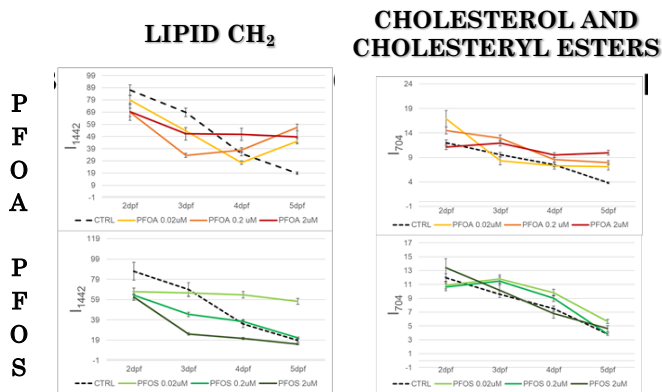


Figure 6. Line plots displaying average \pm SD values of the heights of the following Raman bands: 1442 cm^{-1} (lipid CH_2), and 704 cm^{-1} (cholesterol and cholesteryl esters). CTRL (dotted black), PFOS $0.02\ \mu\text{M}$ (yellow), PFOS $0.2\ \mu\text{M}$ (orange), PFOS $2\ \mu\text{M}$ (red), PFOA $0.02\ \mu\text{M}$ (light green), PFOA $0.2\ \mu\text{M}$ (green), and PFOA $2\ \mu\text{M}$ (dark green).

Finally, by considering the phosphates-related bands (phosphate groups, 1086 cm^{-1} , and phosvitin, 590 cm^{-1}) (Figure 7), mainly due to vitellogenin and its derivatives (*Hiramatsu et al. 2002*), the general decreasing trend was observed in CTRL, while different and not consisting values were found in treated embryos. Phosvitin levels are low, if compared to CTRL at 2 dpf, and with similar values at all time points, suggesting a decreasing consumption of phosvitin inside the yolk.

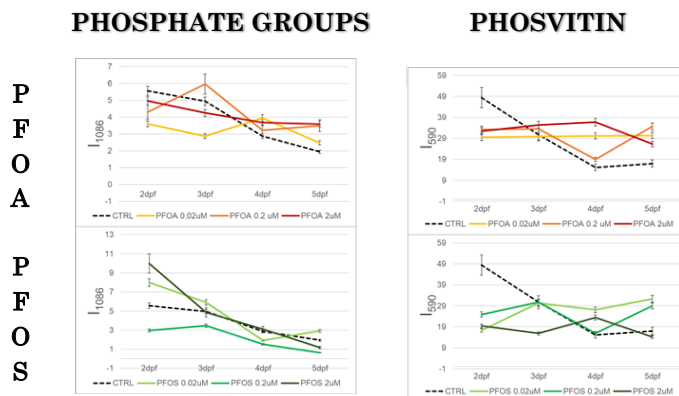


Figure 7. Line plots displaying average \pm SD values of the heights of the following Raman bands: 1086 cm^{-1} (phosphate groups), and 590 cm^{-1} (PO_4^{3-} of phosphvinitin). CTRL (dotted black), PFOS $0.02\ \mu\text{M}$ (yellow), PFOS $0.2\ \mu\text{M}$ (orange), PFOS $2\ \mu\text{M}$ (red), PFOA $0.02\ \mu\text{M}$ (light green), PFOA $0.2\ \mu\text{M}$ (green), and PFOA $2\ \mu\text{M}$ (dark green).

Discussion

The presence of PFCs is ubiquitous, and there are certainties both in seawater (Ahrens *et al.* 2010; Brumovský *et al.* 2016; Concha-Graña *et al.* 2018; Zhang *et al.* 2019) and in freshwater (Post *et al.* 2013; Rumsby *et al.* 2009; Sun *et al.* 2018). Their presence has been detected even in drinking water (Andrews *et al.* 2020; Ericson *et al.* 2009; Post *et al.* 2009; Wilhelm *et al.* 2010; Yim *et al.* 2009), thus meaning that these compounds are widespread in all water compartments, all over the world. Their occurrence is manmade, because the origin of PFCs is due to chemical synthesis: they are used as additives to guarantee impermeability of coatings, inertial surfactancy, oxidative protection coatings, and thermal stability of lubricants (Lehmler 2005; Lindstrom *et al.* 2011). PFOA and PFOS belong to the PFCs compounds, and their chemical structure and behaviour makes them amphiphilic (i.e. they have an affinity for both hydrophilic and hydrophobic substances). In addition, they possess a shape similar to fatty acids, and they can mimic their activity, triggering a large number of

pathologies. The diffusion of PFCs, particularly concerning PFOA and PFOS, raised as an unknown issue, due to the capability of these compounds to combine environmental pollution with endocrine disrupting activity. Several studies on PFOA and PFOS on the aqueous biota are present (*Augustsson et al. 2021; Gallochio et al. 2021; Goodrow et al. 2020; Lanza et al. 2017; Stahl et al. 2014*), presenting data which indicate that PFCs have been detected in all kinds of fish, from arctic cetaceans to harbour fish inhabitants (*Houde et al. 2011*). The present study wants to insert in this scenario, by evaluating the effects, in terms of Raman spectra differences, of the water exposure to PFOA and PFOS of zebrafish embryos. Some preliminary results of the altered evolution that undergo zebrafish embryos and larvae subsequently to the exposure to emerging environmental contaminants have been achieved, by applying RMS vibrational technique. The analysis was performed from 2 to 5 dpf on the embryos and larvae' yolk: it contains finite food supply (*Sant et al. 2018*) and plays a fundamental role as nutritional cache for the development of fish (*Schwartz et al. 2021*). In addition, the yolk is the only cell compartment who can be found in all the first 5 days after the fertilization of the oocyte, and it is perfectly visible, both because of its dimensions and thanks to the transparency of zebrafish embryos (*Kimmel et al. 1995*). The obtained Raman data, as regards CTRLs, showed a constant decrease in bands height along the observed days, except for the band centred at 590 cm^{-1} (PO_4^{3-} groups stretching). This can be explained by the presence of the phosvitin molecule, which derives from the proteolytic cleavage of vitellogenin present in the yolk of the embryos (*Prescott et al. 1986*). In addition, for the treated samples, a similar decreasing trend was evidenced, even if completed altered with respect to CTRLs. Considering the height of the major Raman bands along the four days of treatment, the investigation evidenced at 2 dpf a larger amount of lipids, phosphate groups and proteins, corresponding to the bands centered at 1442 and 704 cm^{-1} , at

1086 and 590 cm^{-1} and at 1655, 1259, and 1000 cm^{-1} , respectively. The decreasing trend of consumption of the biomolecules shown from the comparison of the total spectra was validated: it was more evident until day 3, while a downward path characterized days 4 and 5. This suggests a slowdown of the utilization of yolk's biomolecules, starting from the 4th dpf (*Kimmel et al. 1995; Sant et al. 2018; Singleman et al. 2014*) and confirms the active role of Zebrafish yolk until 3-4 dpf (*Fraher et al. 2016; Miyares et al. 2014*) in the metabolism and degradation of PFOA and PFOS.

Conclusions

Concluding, this preliminary study gives new evidence on yolk consumption by zebrafish embryos during the first 5 days of development, highlighted by RMS, which allowed to investigate the single uptake of each macromolecular component (proteins, lipids, cholesterol and phosphatidylcholine). Furthermore, as regards the embryonic exposure to PFOA and PFOS at three different doses, the spectral data suggest that these contaminants can cause alterations not only in embryos morphology, but also in the macromolecular composition and uptake of yolk. In fact, lower contents of lipids, proteins and phosphates were observed in 2 dpf treated embryos, respect to control ones. In addition, an altered trend of consumption related to a slowdown of the utilization of yolk's proteins, lipids, and phosphates mainly at 4 and 5 dpf was displayed.

These spectral results let validate the use of Raman Microspectroscopy to assess the effects on embryo development of PFOS and PFOA, thus paving the way to a future exploitation of this approach to in vitro screen the effects triggered by other emerging chemical contaminants.

References

- Ahrens, L. et al. 2010. "Distribution of Perfluoroalkyl Compounds in Seawater from Northern Europe, Atlantic Ocean, and Southern Ocean." *Chemosphere* 78(8): 1011–16.
<https://www.sciencedirect.com/science/article/pii/S0045653509013952>.
- Andrews, D. Q. et al. 2020. "Population-Wide Exposure to Per- And Polyfluoroalkyl Substances from Drinking Water in the United States." *Environmental Science and Technology Letters* 7(12): 931–36.
<https://pubs.acs.org/doi/abs/10.1021/acs.estlett.0c00713>.
- Augustsson, A. et al. 2021. "Consumption of Freshwater Fish: A Variable but Significant Risk Factor for PFOS Exposure." *Environmental Research* 192: 110284.
- Baena, J. R. et al. 2004. "Raman Spectroscopy in Chemical Bioanalysis." *Current Opinion in Chemical Biology* 8(5): 534–39.
- Baker, M. J. et al. 2014. "Using Fourier Transform IR Spectroscopy to Analyze Biological Materials." *Nature Protocols* 9(8): 1771–91.
- Brumovský, M. et al. 2016. "Per- and Polyfluoroalkyl Substances in the Western Mediterranean Sea Waters." *Chemosphere* 159: 308–16.
- Cassar, S. et al. 2019. "Use of Zebrafish in Drug Discovery Toxicology." *Chemical Research in Toxicology* 33(1): 95–118.
<https://pubs.acs.org/doi/abs/10.1021/acs.chemrestox.9b00335>.
- Cassar, S. et al. 2021. "Zebrafish as an Animal Model for Ocular Toxicity Testing: A Review of Ocular Anatomy and Functional Assays." *Toxicologic Pathology* 49(3): 438–54.
- Chakraborty, C. et al. 2009. "Zebrafish: A Complete Animal Model for In Vivo Drug Discovery and Development." *Current Drug Metabolism* 10: 116–24.
- Concha-Graña, E. et al. 2018. "Fast and Sensitive Determination of Per- and Polyfluoroalkyl Substances in Seawater." *Journal of Chromatography A* 1555: 62–73.
- Conder, J. M. et al. 2008. "Are PFCAs Bioaccumulative? A Critical Review and Comparison with Regulatory Criteria and Persistent Lipophilic Compounds." *Environmental Science and Technology* 42(4): 995–1003.
- Czamara, K. et al. 2015. "Raman Spectroscopy of Lipids: A Review." *Journal of Raman Spectroscopy* 46(1): 4–20.
- Downes, A. et al. 2010. "Raman Spectroscopy and Related Techniques in Biomedicine." *Sensors* 10(3): 1871–89.
- Ericson, I. et al. 2009. "Levels of Perfluorinated Chemicals in Municipal Drinking Water from Catalonia, Spain: Public Health Implications." *Archives of Environmental Contamination and Toxicology* 57(4): 631–38.
- Ferraro, J. R. et al. 2003. "Introductory Raman Spectroscopy: Second Edition."

Introductory Raman Spectroscopy: Second Edition: 1–434.

- Fraher, D. et al. 2016. “Zebrafish Embryonic Lipidomic Analysis Reveals That the Yolk Cell Is Metabolically Active in Processing Lipid.” *Cell Reports* 14(6): 1317–29. <http://dx.doi.org/10.1016/j.celrep.2016.01.016>.
- Gallocchio, F. et al. 2021. “Investigation of Levels of Perfluoroalkyl Substances in Freshwater Fishes Collected in a Contaminated Area of Veneto Region, Italy.” *Environmental Science and Pollution Research* 1: 1–16. <https://link.springer.com/article/10.1007/s11356-021-17236-5>.
- Giorgini, E. et al. 2014. “Vibrational Characterization of Female Gametes: A Comparative Study.” *Analyst* 139(20): 5049–60.
- Giorgini, E. et al. 2010. “Effects of Lactobacillus Rhamnosus on Zebrafish Oocyte Maturation: An FTIR Imaging and Biochemical Analysis.” *Analytical and Bioanalytical Chemistry* 398(7–8): 3063–72. <http://link.springer.com/10.1007/s00216-010-4234-2>.
- Giorgini, E. et al. 2018. “In Vitro FTIR Microspectroscopy Analysis of Primary Oral Squamous Carcinoma Cells Treated with Cisplatin and 5-Fluorouracil: A New Spectroscopic Approach for Studying the Drug-Cell Interaction.” *Analyst* 143(14): 3317–26.
- Goodrow, S. M. et al. 2020. “Investigation of Levels of Perfluoroalkyl Substances in Surface Water, Sediment and Fish Tissue in New Jersey, USA.” *Science of The Total Environment* 729: 138839.
- Hiramatsu, N. et al. 2002. “Vitellogenesis in Aquatic Animals.” *Fisheries science* 68(sup1): 694–99.
- Houde, M. et al. 2011. “Monitoring of Perfluorinated Compounds in Aquatic Biota: An Updated Review.” *Environmental Science and Technology* 45(19): 7962–73.
- Jantzen, C. E. et al. 2016. “PFOS, PFNA, and PFOA Sub-Lethal Exposure to Embryonic Zebrafish Have Different Toxicity Profiles in Terms of Morphometrics, Behavior and Gene Expression.” *Aquatic Toxicology* 175: 160–70. <http://dx.doi.org/10.1016/j.aquatox.2016.03.026>.
- Jantzen, C. E. et al. 2016. “Behavioral, Morphometric, and Gene Expression Effects in Adult Zebrafish (Danio Rerio) Embryonically Exposed to PFOA, PFOS, and PFNA.” *Aquatic Toxicology* 180: 123–30.
- Kimmel, C. B. et al. 1995. “Stages of Embryonic Development of the Zebrafish.” *Developmental Dynamics* 203(3): 253–310.
- Lanza, H. A. et al. 2017. “Temporal Monitoring of Perfluorooctane Sulfonate Accumulation in Aquatic Biota Downstream of Historical Aqueous Film Forming Foam Use Areas.” *Environmental Toxicology and Chemistry* 36(8): 2022–29.
- Lehmler, H. J. 2005. “Synthesis of Environmentally Relevant Fluorinated Surfactants - A Review.” *Chemosphere* 58(11): 1471–96.
- Lindstrom, A. B. et al. 2011. “Polyfluorinated Compounds: Past, Present, and

- Future.” *Environmental Science and Technology* 45(19): 7954–61.
- Link, V. et al. 2006. “Proteomics of Early Zebrafish Embryos.” *BMC Developmental Biology* 6: 1–9.
- Lyng, F. M. et al. 2015. “Vibrational Microspectroscopy for Cancer Screening.” *Applied Sciences (Switzerland)* 5(1): 23–35.
- Matthäus, C. et al. 2008. “Chapter 10 Infrared and Raman Microscopy in Cell Biology.” *Methods in Cell Biology* 89: 275–308. <https://linkinghub.elsevier.com/retrieve/pii/S0091679X08006109>.
- Miyares, R. L. et al. 2014. “Zebrafish Yolk Lipid Processing: A Tractable Tool for the Study of Vertebrate Lipid Transport and Metabolism.” *DMM Disease Models and Mechanisms* 7(7): 915–27.
- Post, G. B. et al. 2009. “Occurrence and Potential Significance of Perfluorooctanoic Acid (PFOA) Detected in New Jersey Public Drinking Water Systems.” *Environmental Science and Technology* 43(12): 4547–54.
- Post, G. B. et al. 2013. “Occurrence of Perfluorinated Compounds in Raw Water from New Jersey Public Drinking Water Systems.” *Environmental Science and Technology* 47(23): 13266–75.
- Prescott, B et al. 1986. “A Raman Spectroscopic Study of Hen Egg Yolk Phosvitin: Structures in Solution and in the Solid State.” *Biochemistry* 25(10): 2792–98.
- Rumsby, P. C. et al. 2009. “Perfluorooctane Sulphonate and Perfluorooctanoic Acid in Drinking and Environmental Waters.” *Philosophical Transactions of the Royal Society A: Mathematical, Physical and Engineering Sciences* 367(1904): 4119–36.
- Sant, K. E. et al. 2017. “Embryonic Exposures to Perfluorooctanesulfonic Acid (PFOS) Disrupt Pancreatic Organogenesis in the Zebrafish, *Danio Rerio*.” *Environmental Pollution* 220: 807–17. <https://www.sciencedirect.com/science/article/pii/S0269749116318437>.
- Sant, K. E. et al. 2018. “Zebrafish as a Model for Toxicological Perturbation of Yolk and Nutrition in the Early Embryo.” *Current environmental health reports* 5(1): 125–33.
- Scholz, S. et al. 2008. “The Zebrafish Embryo Model in Environmental Risk Assessment - Applications beyond Acute Toxicity Testing.” *Environmental Science and Pollution Research* 15(5): 394–404.
- Schwartz, A. V. et al. 2021. “Mathematical Modeling of the Interaction between Yolk Utilization and Fish Growth in Zebrafish, *Danio Rerio*.” *Development (Cambridge)* 148(9).
- Singleman, C. et al. 2014. “Growth and Maturation in the Zebrafish, *Danio Rerio*: A Staging Tool for Teaching and Research.” *Zebrafish* 11(4): 396. [/pmc/articles/PMC4108942/](https://pubmed.ncbi.nlm.nih.gov/24108942/).
- Stahl, L. L. et al. 2014. “Perfluorinated Compounds in Fish from U.S. Urban Rivers and the Great Lakes.” *Science of the Total Environment* 499: 185–95.

- Suja, F. et al. 2009. "Contamination, Bioaccumulation and Toxic Effects of Perfluorinated Chemicals (PFCs) in the Water Environment: A Review Paper." *Water Science and Technology* 60(6): 1533–54.
- Sun, R. et al. 2018. "Perfluorinated Compounds in Surface Waters of Shanghai, China: Source Analysis and Risk Assessment." *Ecotoxicology and Environmental Safety* 149: 88–95.
- Talari, A. C. S. et al. 2015. "Raman Spectroscopy of Biological Tissues." *Applied Spectroscopy Reviews* 50(1): 46–111.
- Wilhelm, M. et al. 2010. "Occurrence of Perfluorinated Compounds (PFCs) in Drinking Water of North Rhine-Westphalia, Germany and New Approach to Assess Drinking Water Contamination by Shorter-Chained C4-C7 PFCs." *International Journal of Hygiene and Environmental Health* 213(3): 224–32.
- Wolkers, W. F. et al. 2010. "In Situ FTIR Studies on Mammalian Cells." *Spectroscopy* 24(5): 525–34.
- Yim, L. M. et al. 2009. "Perfluorinated Compounds in Tap Water from China and Several Other Countries." *Environmental Science and Technology* 43(13): 4824–29.
- Zhang, G. et al. 2019. "Distribution of Perfluorinated Compounds in Surface Water and Soil in Partial Areas of Shandong Province, China." *Soil and Sediment Contamination: An International Journal* 28(5): 502–12. <https://doi.org/10.1080/15320383.2019.1635079>.

CHAPTER 3

NEW INSIGHTS FROM FTIRI ON *Xiphias gladius* REPRODUCTION: A CORRELATION BETWEEN OOCYTES MORPHO-CHEMICAL FEATURES AND THE FISHING AREA

Chiara Pro, Luca Marisaldi, Valentina Notarstefano, Edoardo Acri, Oliana Carnevali, Elisabetta Giorgini, Giorgia Gioacchini

Department of Life and Environmental Sciences, Università Politecnica delle Marche

Paper in preparation

Abstract

Swordfish is a large and epipelagic fish, with high commercial and ecological value. It has a worldwide geographical distribution, and it usually lives in sea areas comprised from the latitudes 45° N and 45° S. As regards the Mediterranean Sea too, spawning takes place from June to August in specific areas, i.e. the Balearic Islands, the south of the Tyrrhenian Sea and the Strait of Messina and the Ionian Sea. Swordfish females have asynchronous ovaries, with oogonia and oocytes at several stages of development simultaneously present. A crucial role in fertilization is played by the zona radiata (ZR), a glycoprotein layer surrounding the plasma membrane of mature eggs. ZR is mainly composed by three glycoproteins, and it changes in composition, thickness, and structure during oogenesis, becoming highly ordered and architecturally complex in the mature stage.

The aim of this study is to evaluate a possible correlation between ZR thickness and macromolecular composition and the geographical fishing area. At this purpose, vitellogenic and mature oocytes of swordfish specimens caught in three different regions of the Mediterranean Sea (such as Balearic Islands, Sicily, and Sardinia) were submitted to histological and FTIR Imaging (FTIRI) analyses. In particular, a different thickness of ZR, in relation with both the developmental stage (i.e., oocyte diameter) and the fishing zone was observed. These morphological differences were further investigated by FTIRI analysis which let detect changes in the topographical distribution and relative amounts of the most relevant biomolecules not only between vitellogenic and mature oocytes, but also in relation with the fishing area.

Introduction

Swordfish (*Xiphias gladius*) is a large epipelagic fish, with a high commercial and ecological value. It has a worldwide distribution between 45°N and 45°S (*Palko et al. 1981*), going from temperate to tropical and subtropical regions. In addition, it is highly migratory, and capable of long-distance movements (*Dewar et al. 2011; Neilson et al. 2007; Sedberry et al. 2001*). The complexity of its management claimed for an International Commission for the Conservation of Atlantic Tunas (ICCAT), which, as the name predicts, has in charge many migrating species, including tuna-like species, sharks and swordfish (*Saber et al. 2020*).

Living in temperate climates, swordfish is present in the Mediterranean Sea too, where a stock model area has been identified (*Smith et al. 2015*). Here, the strong fishery traditions brought to severe overfishing in the 30 past years, leading to the enacting of fishery surveillance and recovery plan establishment: it included measures such as total allowable catches (TAC), fleet capacity limitations, closed fishing season, maximum number of hooks on longlines and minimum size of the specimen caught (*ICCAT 2017*).

Swordfish has a great and rapid development and reaches sexual maturation at about 1-2 years in males and 2-3 years in females, considering the Mediterranean Sea (*Taylor 1992*). Swordfish reproduction has been widely studied (*Arocha 2002; Arocha 2007*): it is a sexually dimorphic and gonochoric species, and females have asynchronous ovaries, thus meaning that oogonia and oocytes at different maturation stages are simultaneously present in the ovaries. The key process for reproduction is oogenesis, during which the oocyte grows and differentiates (*Brooks et al. 1997; Kjørsvik et al. 1990*).

The different stages of oocyte have been described and characterized using histology (*Abid et al. 2019; Arocha 2002; Corriero et al. 2004; Farley et*

al. 2014; Macías et al. 2005; Marisaldi et al. 2020; Poisson et al. 2009; Young et al. 2003), immunohistochemistry, histochemistry (*Corriero et al. 2004; Ortiz-Delgado et al. 2008*), Fourier Transform Infrared (FTIR) Imaging spectroscopy (*Carnevali et al. 2019*), transmission (*Minniti et al. 2005*) and electron (*Corriero et al. 2004*) microscopy.

Zona Radiata (ZR) is a mainly proteic region located in the external part of the oocyte (*Litscher et al. 2018*). In teleosts, it forms the eggshell that provides mechanical protection against external disturbances, but it is shed when hatching is induced. ZR is involved in the processes of oogenesis, egg deposition, fertilization, and embryogenesis (*Litscher et al. 2014*), and it is useful to enable gas exchange, excretion and transport of nutrients from the external environment (*Arukwe et al. 1997; Fossi et al. 2001; Yamagami et al. 1992; Zelazowska 2010*).

In the present study, Fourier Transform Infrared Imaging (FTIRI) spectroscopy was exploited to obtain reliable morpho-chemical information of this important region in vitellogenic and mature oocytes from swordfish specimens caught in three different areas of the Mediterranean Sea: Balearic Islands, Sicily, and Sardinia. Spectral data were compared with those from histological assays. FTIRI is a well-established technique for the analysis of cells and tissues (*Baker et al. 2014; Butler et al. 2016; Chan et al. 2008; Matthäus et al. 2008; Naumann 2001; Romeo et al. 2006*) and it allows the spectroscopical mapping of biological, even non-homogeneous, samples. The areas to investigate can be chosen, thanks to the coupling of IR spectrometers with bidimensional arrays detectors, and this provides both anatomic and biochemical information of the sample (*Sreedhar et al. 2015; Chan et al. 2016*). In addition, FTIRI has already been applied to the study of fish, showing its ability to provide a characterization of the biochemical changes associated with oocyte growth and maturation (*Carnevali et al. 2019; Gioacchini et al. 2014; Giorgini et al. 2014; Mazzeo et al. 2016; Wood*

et al. 2008) As reported by Carnevali et al 2019, it has been a powerful tool to identify and study the differences in oocytes structure in swordfish population caught in the Mediterranean Sea (*Carnevali et al. 2019*).

Materials and methods

Swordfish samples collection

For this experiment, N 60 swordfish females captured in the period May–July 2017 were analyzed. Swordfish were caught in the central (Sardinia and Sicily) and western Mediterranean Sea (Balearic Islands) by commercial vessels using longlines and tuna traps. All the samples had a Lower Jaw-Fork Length (LJFL) >100 cm. As indicated by the ICCAT manual for fish caught for commercial purpose, samples were collected in compliance with the guidelines for biological samples. In accordance with the Italian legislation (D.L. 4 of Mars 2014, n. 26, art. 2) ethics approval is not necessary. Soon after capture, ovaries were removed, and gonad portions (~2 cm³ in volume) were picked up from the middle part of the ovary of all specimens for histology and FTIRI analyses.

Histological analysis

Gonad portions (2 cm³ in volume) were fixed in formol solution, dehydrated with a series of increasing EtOH baths, cleared in xylene, and embedded in paraffin. Sections of 5 µm in width were cut with a microtome (RM2125 RTS; Leica Biosystems, Wetzlar, Germany), stained with Mayer's haematoxylin/eosin, and examined under microscope (Axio Imager 2; Zeiss, Oberkochen, Germany) (*Gioacchini et al 2019*). The analysis was focused on vitellogenic (VTG) and mature (MAT) oocytes. A total amount of 452 oocytes has been withdrawn: 196 from Sardinia, 198 from Sicily and 58 from the Balearic Islands.

FTIRI measurements and data analysis

Gonad portions were immediately frozen at -80°C without any further fixation protocol. By using a cryomicrotome, five thin sections ($\sim 10\ \mu\text{m}$ thickness) were cut from each frozen sample, by a distance of $200\ \mu\text{m}$ from each other. Sections were deposited onto CaF_2 optical windows ($1\ \text{mm}$ thickness, $13\ \text{mm}$ diameter) and let air-drying for 30 min. No fixation process was applied. N. 20 ovaries from each geographical region were analyzed, containing both vitellogenic (VTG) and mature (MAT) oocytes. FTIRI measurements were performed at the Laboratory of Advanced Research Instrumentation (ARI) of the Department of Life and Environmental Sciences, Università Politecnica delle Marche (Ancona, Italy).

A Bruker INVENIO-R interferometer coupled with a Hyperion 3000 Vis-IR microscope and equipped with a liquid nitrogen cooled bidimensional Focal Plane Array (FPA) detector was used. FPA allows to acquire IR images of non-homogeneous biological samples by the simultaneous acquisition of 4096 spectra on an area of $164 \times 164\ \mu\text{m}^2$. A 15X condenser/objective was used to obtain the visible image of each section and to select the areas. IR maps were collected on the Zona Radiata (ZR) of vitellogenic (VTG) and mature (MAT) oocytes (transmission mode; $4000\text{--}900\ \text{cm}^{-1}$ MIR range; spatial resolution $\sim 2.56\ \mu\text{m}$; spectral resolution $4\ \text{cm}^{-1}$; 256 scans). Background spectra were acquired on clean regions of the CaF_2 optical windows. Raw IR maps were corrected by applying the Atmospheric Compensation routine, to remove the contribution of atmospheric carbon dioxide and water vapour, and then Vector Normalization routine in the $4000\text{--}900\ \text{cm}^{-1}$ spectral range, to avoid possible artefacts due to differences in thickness (OPUS 7.5 software, Bruker Optics, Ettlingen, Germany).

False colour images representing the topographical distribution of the most relevant biochemical features were generated by integrating IR maps under the following spectral regions: $3000\text{--}2829\ \text{cm}^{-1}$ (vibrational modes of

lipids, named LIP); 1765–1719 cm^{-1} (vibrational modes of fatty acids, named FA); 1719–1487 cm^{-1} (vibrational modes of proteins, named PRT); 1290–1192 cm^{-1} (vibrational modes of phosphates groups, named PH), and 1135–1001 cm^{-1} (vibrational modes of glycosylated compounds, named GLY). An arbitrary “rainbow” colour scale was used: white/light pink colour indicates areas with the highest absorbance values, while blue colour areas with the lowest ones.

From the Zona Radiata of each IR map, ~200 IR spectra each were extracted; spectra were then vector normalized, two-points baseline linear fitted and integrated under the same above defined spectral regions by using the Integration routine (OPUS 7.5 software package, Bruker Optics, Ettlingen, Germany) (*Giorgini et al. 2018; Talari et al. 2017*). The integrated areas were ratioed against the sum of the integrated areas 3050–2800 and 1770–950 cm^{-1} to calculate the following parameters: LIP (relative amount of total lipids); FA (relative amount of fatty acids); PRT (relative amount of total proteins); GLY (relative amount of glycosylated compounds) and PH (relative amount of phosphate groups).

Statistical Analysis

Spectral data were submitted to one-way analysis of variance (ANOVA) to determine the presence of statistically significant differences among groups (Software package Prism 6.0, GraphPad Software, San Diego, CA). Statistical significance was set at $p < 0.05$.

Results

The histological analysis of swordfish ovary section was focused on the zona radiata of vitellogenic and mature oocytes (Figures 1 and 2, respectively), revealing that ZR thickness depends on the region of capture.

In particular, a smaller ZR thickness was found in oocytes of specimens caught in Sardinia, and this trend was observed for both development stages.

Together with the morphological structure of the oocytes, the overall diameter for each oocyte was measured, and as expected, an increasing trend between Zona Radiata and the overall diameter of the oocytes from the three geographical regions was found.

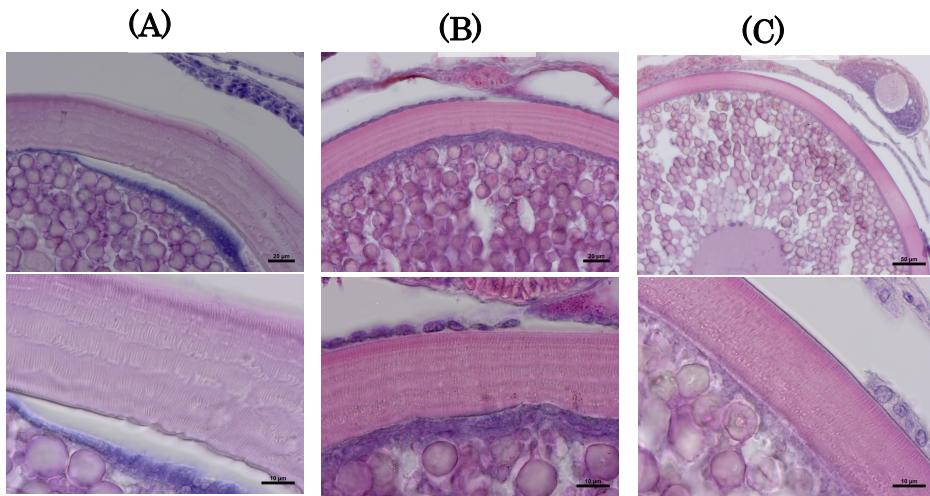


Figure 1. Histological analysis of vitellogenic swordfish oocytes collected in: (A) Balearic Islands, (B) Sicily, and (C) Sardinia (top, low magnification; bottom, high magnification).

In Figure 3, the correlation between the diameter of oocytes and the width of zona radiata is reported; Sardinian oocytes (red dots) showed a much shorter zona radiata width, with respect to the oocytes coming from Sicily (green dots) and Balearic Islands (blue dots).

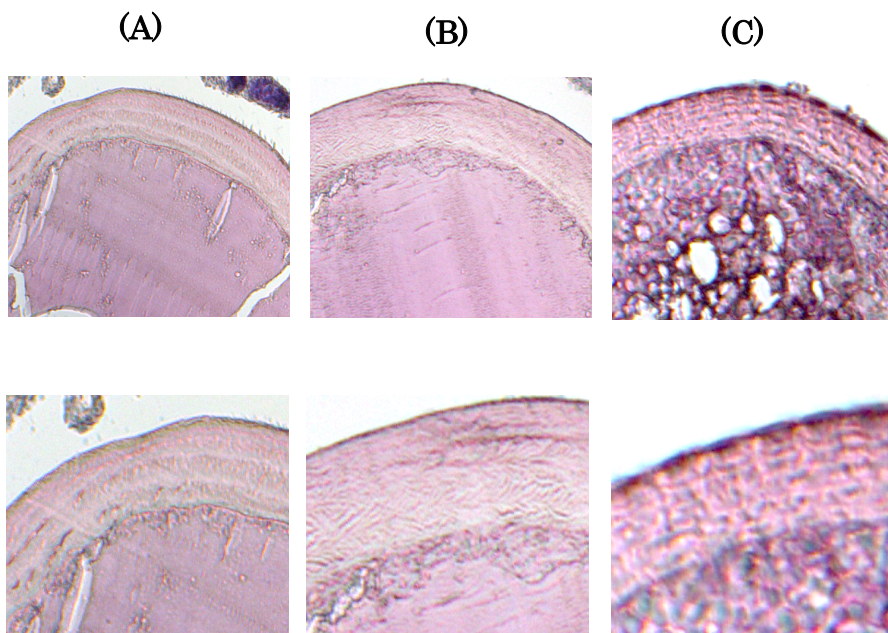


Figure 2. Histological analysis of mature swordfish oocytes collected in: (A) Balearic Islands, (B) Sicily, and (C) Sardinia (top, low magnification; bottom, high magnification).

These results were also confirmed by the hyperspectral imaging analysis, which showed the topographical distribution specific biomolecules (such as lipids, fatty acids, proteins, glycosylated compounds, and phosphates) within the mapped areas: each pixel corresponds to an IR spectrum, and its signal, integrated in a specific IR band/region, gives information about amount and localization of the corresponding molecular/chemical group. As regards vitellogenic oocytes, a different distribution of lipids and fatty acids was observed with respect to proteins, carbohydrates, and phosphates: glycosylated proteins (GLY and PRT maps) are more present in the zona radiata, while the lipid distribution describes the uptake of vitellogenin and fatty acids through ZR pores (LIP and FA maps). The same hyperspectral analysis has been performed on mature oocytes originating from the three areas (Figure 4). In mature oocytes a

similar distribution of glycosylated proteins on zona radiata is observed (GLY and PRT maps). As regards lipids and fatty acids, their presence is found only in the ooplasm since their uptake in this maturation phase is over (LIP and FA maps). Imaging results do not evidence differences in the localization of the macromolecules in the 3 geographical different areas.

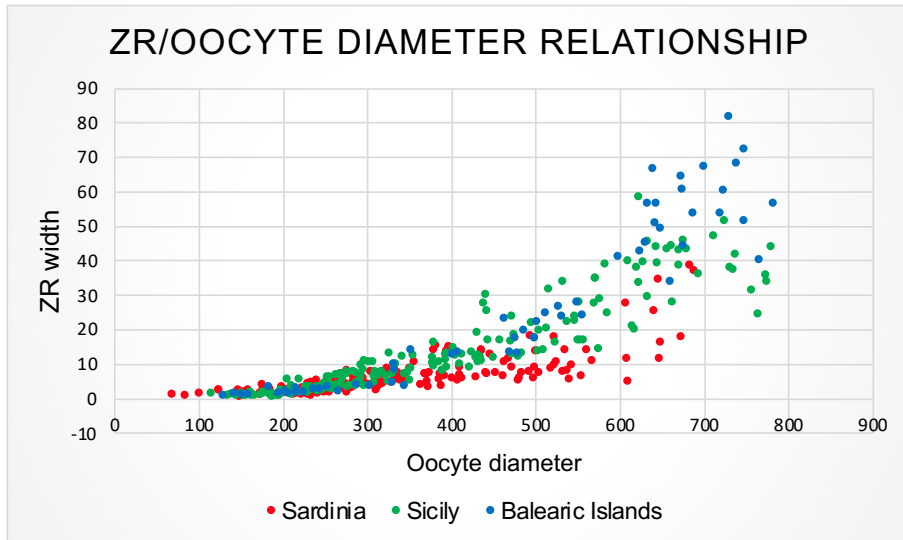


Figure 3. Correlation between oocyte diameter and ZR thickness in Balearic Islands (blue), Sicily (green), and Sardinia (red).

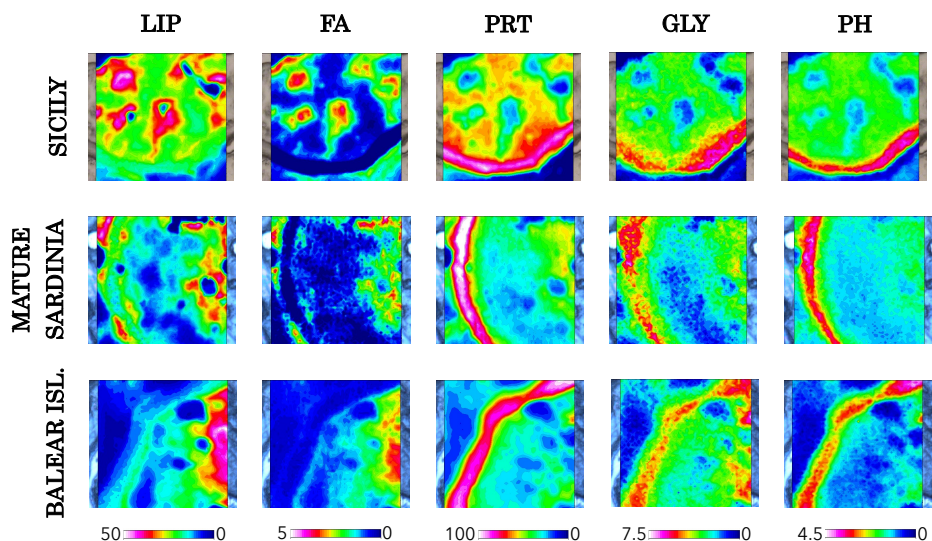


Figure 4. Hyperspectral Imaging analysis of ZR of mature swordfish oocytes from Sicily, Sardinia and Balearic Islands. The columns represent the topographical distribution of (LIP) lipids, (FA) fatty acids, (PRT) proteins, (GLY) glycosylated compounds, and (PH) phosphates. Different colour scales were adopted for each parameter.

Univariate analysis has been performed on the previously considered parameters (lipids, fatty acids, phosphates, proteins and glycosylated compounds) to evaluate differences in the macromolecular composition of zona radiata in oocytes from three different geographical regions. As regards vitellogenic oocytes (Figure 5), the highest amounts of lipids and fatty acids were found in Balearic Island samples, while the lowest in Sardinia samples. Proteins were higher in Sardinia and Balearic oocytes and lower in Sicily samples; a similar trend was observed for glycosylated compounds, with the highest amount observed for Balearic samples, followed by Sardinia and Sicily ones. A similar content in phosphates was detected.

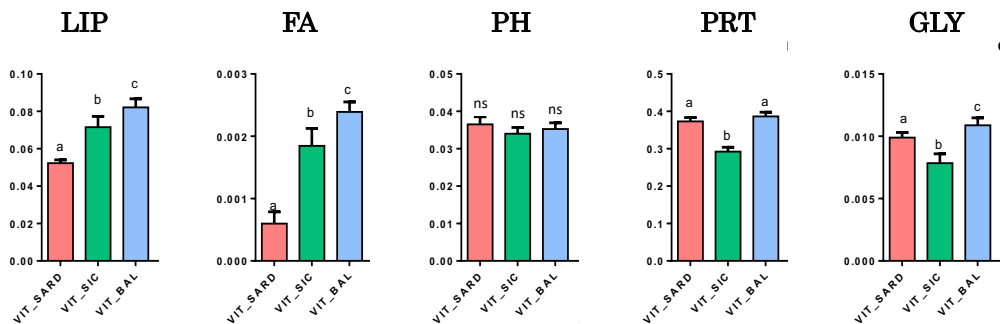


Figure 5. Macromolecular composition of vitellogenic oocytes belonging to (red) Sardinia, (green) Sicily, and (blue) Balearic Islands Univariate analysis of the following parameters: (LIP) lipids, (FA) fatty acids, (PRT) proteins, (GLY) glycosylated compounds, and (PH) phosphates. Different letters indicate statistically significant differences among experimental groups ($p < 0.05$). n.s. indicates that no statistically significant difference is evidenced among the considered groups.

The same analysis, performed on mature oocytes, gave different results (Figure 6): no statistically significant differences were observed in the relative amounts of lipids, fatty acids, and phosphates among the three geographical regions. Proteins displayed a significant difference, with higher amounts in samples from Sardinia and Balearic Islands with respect to Sicily samples. Glycosylated compounds were statistically significant higher in Sardinia samples with respect to both Sicily and Balearic ones.

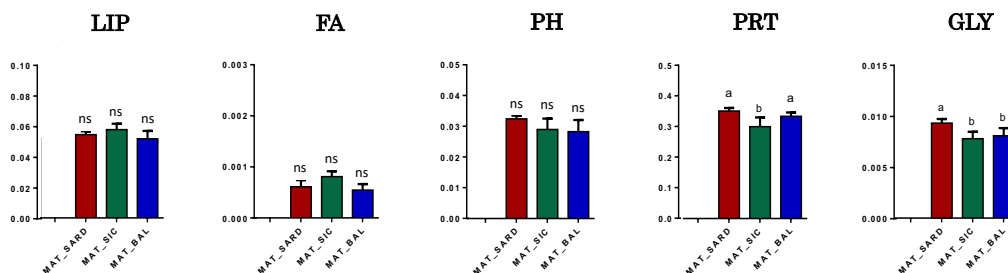


Figure 6. Macromolecular composition of mature oocytes belonging to (red) Sardinia, (green) Sicily, and (blue) Balearic Islands. Univariate analysis of the following parameters: (LIP) lipids, (FA) fatty acids, (PRT) proteins, (GLY) glycosylated compounds, and (PH) phosphates. Different letters indicate statistically significant differences among experimental groups ($p < 0.05$). n.s. indicates that no statistically significant difference is evidenced among the considered groups.

Discussion

The female swordfish is a multiple pelagic spawner with asynchronous ovaries, thus meaning that it is possible to find and identify simultaneously oocyte at different developmental stages: oogonia, previtellogenic, vitellogenic, mature/hydrated and atretic follicles (Abid et al. 2019; Poisson et al. 2009). Swordfish reproduction is a known process, but it is important to continue deepening its mechanisms in order to obtain as many information as possible to understand, preserve and protect this endangered species. Egg quality is an important parameter in reproduction perspective, is based on egg quality and the development of the different stages involves the development of Zona Radiata around the oocyte. In this light, our focus has been this specific structure.

ZR varies in thickness and complexity in a gradual way during oocyte developmental stages (Marisaldi et al. 2020): it becomes more and more ordered and architecturally complex during later maturational stages, even if it starts to differentiate throughout the growth of the oocyte (Hara et al. 2016; Menn et al. 2007). During the primary oocyte stage, a thin zona radiata

(~5 μm) begins to form at the periphery of the oocyte. Then, upon entering the vitellogenic phase, oocytes begin to accumulate small vitellogenin globules toward the periphery of the cytoplasm and during the early stages of vitellogenesis, the zona radiata began to be clearly visible, reaching up to 10 μm . As vitellogenesis proceed, during the middle to late vitellogenic stages, the zona radiata becomes prominent, with a remarkable increase in thickness up to 30 μm . At this stage, the ZR is constituted by two layers: an external layer (zona radiata externa, ZRE) and an internal one (zona radiata interna, ZRI). In mature oocytes, the zona radiata becomes particularly evident in this stage, with a thickness up to 40-50 μm . Finally, in atretic oocyte, the zona radiata breakdown was among the first structural events that could be identified, according to previous findings (*Corriero et al. 2004; Poisson et al. 2009; Tyler et al. 1996*).

The development and differentiation from stage to stage depend on several biochemical changes, which lead to the maturation of the follicle reaching ovulation and then fertilization (*Gioacchini et al. 2019*). The role ZR plays is fundamental during fertilization: in fact, the external part of ZR, composed by glycoproteins, has an affinity for spermatozoa and is used as a guide for the single sperm to reach the egg cell going through the micropyle. In addition, after fertilization ZR is able to protect the embryo in the aquatic environment and it is useful to enable gas exchange, excretion and transport of nutrients from the external environment (*Zelazowska 2010*).

The monitoring of ZR evolution process can be monitored by applying Infrared Spectroscopy techniques: FTIRI allows to identify the biochemical composition of the analysed sample. Infrared Imaging spectroscopy has already been applied to obtain information about the macromolecular shaping and arrangement of swordfish oocytes at different developmental stages, in terms of composition and topographical distribution of biologically

interesting macromolecules, such as lipids, proteins, carbohydrates and phosphates (*Carnevali et al. 2019*).

A specific focus on ZR obtained by applying FTIRI spectroscopy has been considered in the present work, in order to distinguish between the two developmental stages of ZR and the three considered geographical regions.

The results achieved by the hyperspectral imaging analysis of vitellogenic, and mature Zona Radiata were highlighted by applying the univariate analysis of the most meaningful bands. Considering vitellogenic oocytes, the phosphates (PH) had a similar content in three different geographical regions. Conversely, lipids (LIP) and fatty acids (FA) had the highest amounts in Balearic Island samples, lower amount in Sicily oocytes and the lowest in Sardinia samples. Proteins (PRT) were higher in Sardinia and Balearic oocytes and lower in Sicily samples; a similar trend was observed in glycosylated compounds (GLY), with the highest amount observed for Balearic samples, followed by Sardinia and Sicily ones. Taking into account mature oocytes, no statistically significant differences were observed in the relative amounts of Lipids (LIP), fatty acids (FA), and phosphates (PH) among the three geographical regions. Proteins (PRT) showed a significant difference, with higher amounts in samples from Sardinia and Balearic Islands with respect to Sicily samples. Glycosylated compounds (GLY) were statistically significant higher in Sardinia samples with respect to both Sicily and Balearic ones.

These results evidence that the biochemical composition of ZR of oocytes is different considering the three west Mediterranean regions of swordfish, and that the developmental phase too influences ZR biomolecule presence. Among the most interesting parameters there are LIP and FA presence: they are generally present in the vitellogenic stage of ZR, due to the passage through ZR, but they are significantly low in Sardinian samples with respect to both Sicily and Balearic Islands ones. Correlating to what

reported by literature, during the vitellogenic stage, the presence of proteins and glycosylated compounds are evident in ZR: they show a comparable trend, due to the fact that ZR is a proteic region composed by glycosylated aminoacids. On the contrary, in mature oocytes, there seems to be a statistically significative difference in the proteic and glycosylated presence, more present in Sardinian ZR samples: in mature oocytes, the increase of the Zona Radiata is evident, and it is accompanied by a decrease in fatty acids, lipids and phosphates (*Carnevali et al. 2019*).

Conclusions

Concluding, this study represents a successful application of a multidisciplinary approach based on histological and FTIR Imaging techniques for the analysis to swordfish species. Differences in swordfish ZR thickness and macromolecular composition in relation with fishing area, both as regards vitellogenic and mature oocytes, have been identified and analyzed, and the obtained results could be attributed to the presence of different genetic stocks in the Mediterranean Sea, which is still under debate. This can constitute an improvement of knowledge in reproductive biology of swordfish, considered as a threatened species, and could be useful for better elucidating oocyte quality and fertility success rate.

The combined approach based on histological and FTIR Imaging analyses of vitellogenic and mature swordfish oocytes let confirm our hypothesis about the influence of fishing area on the ZR thickness and macromolecular composition. Considering that these parameters are strictly related to oocyte quality and fertility success rate, these preliminary results are very encouraging to better understand reproductive biology of swordfish.

References

- Abid, N. et al. 2019. "The Reproductive Biology of Swordfish (*Xiphias Gladius*) in the Strait of Gibraltar." *Journal of the Marine Biological Association of the United Kingdom* 99(3): 649–659.
- Arocha, F. 2002. "Oocyte Development and Maturity Classification of Swordfish from the North-Western Atlantic." *Journal of Fish Biology* 60(1): 13–27. <https://onlinelibrary.wiley.com/doi/full/10.1111/j.1095-8649.2002.tb02385.x>.
- Arocha, F. 2007. "Swordfish Reproduction in the Atlantic Ocean: An Overview." *Gulf and Caribbean Research* 19.
- Arukwe, A. et al. 1997. "Fish Zona Radiata (Eggshell) Protein: A Sensitive Biomarker for Environmental Estrogens." *Environmental Health Perspectives* Vol. 105.
- Baker, M. J. et al. 2014. "Using Fourier Transform IR Spectroscopy to Analyze Biological Materials." *Nature Protocols* 9(8): 1771–91.
- Brooks, S. et al. 1997. "Egg Quality in Fish: What Makes a Good Egg?" *Reviews in Fish Biology and Fisheries* 1997 7:4 7(4): 387–416. <https://link.springer.com/article/10.1023/A:1018400130692>.
- Butler, H. J. et al. 2016. "Using Raman Spectroscopy to Characterize Biological Materials." *Nature Protocols* 11(4): 664–87.
- Carnevali, O. et al. 2019. "Macromolecular Characterization of Swordfish Oocytes by FTIR Imaging Spectroscopy." *Scientific Reports* 9(1): 1–9.
- Chan, J. et al. 2008. "Raman Spectroscopy and Microscopy of Individual Cells and Cellular Components." *Laser and Photonics Reviews* 2(5): 325–49.
- Chan, K. L. A. et al. 2016. "Attenuated Total Reflection Fourier-Transform Infrared (ATR-FTIR) Imaging of Tissues and Live Cells." *Chemical Society Reviews* 45(7): 1850–64.
- Corriero, A. et al. 2004. "Histological and Immunohistochemical Investigation on Ovarian Development and Plasma Estradiol Levels in the Swordfish (*Xiphias Gladius* L.)." *European Journal of Histochemistry* 48(4): 413–22.
- Dewar, H. et al. 2011. "Movements and Behaviors of Swordfish in the Atlantic and Pacific Oceans Examined Using Pop-up Satellite Archival Tags." *Fisheries Oceanography* 20(3): 219–41. <https://onlinelibrary.wiley.com/doi/abs/10.1111/j.1365-2419.2011.00581.x>.
- Farley, J. et al. 2014. *Determination of Southwest Pacific Swordfish Growth and Maturity*.
- Fossi, M. C. et al. 2001. "Do Endocrine Disrupting Chemicals Threaten Mediterranean Swordfish? Preliminary Results of Vitellogenin and Zona Radiata Proteins in *Xiphias Gladius*." *Marine Environmental Research* 52(5): 477–83.
- Gioacchini, G. et al. 2014. "A New Approach to Evaluate Aging Effects on Human

- Oocytes: Fourier Transform Infrared Imaging Spectroscopy Study.” *Fertility and Sterility* 101(1): 120–27. <http://dx.doi.org/10.1016/j.fertnstert.2013.09.012>.
- Gioacchini, G. et al. 2019. “A de Novo Transcriptome Assembly Approach Elucidates the Dynamics of Ovarian Maturation in the Swordfish (*Xiphias Gladius*.)” *Scientific Reports* 9(1).
- Giorgini, E. et al. 2014. “Vibrational Characterization of Female Gametes: A Comparative Study.” *Analyst* 139(20): 5049–60. <http://dx.doi.org/10.1039/C4AN00684D>.
- Giorgini, E. et al. 2018. “In Vitro FTIR Microspectroscopy Analysis of Primary Oral Squamous Carcinoma Cells Treated with Cisplatin and 5-Fluorouracil: A New Spectroscopic Approach for Studying the Drug-Cell Interaction.” *Analyst* 143(14): 3317–26.
- Hara, A. et al. 2016. “Vitellogenesis and Choriogenesis in Fishes.” *Fisheries Science* 82(2): 187–202. <https://doi.org/10.1007/s12562-015-0957-5>.
- ICCAT. 2017. “Report of the 2016 Mediterranean Swordfish Stock Assessment Meeting.” *Collective Volume of Scientific Papers ICCAT* 73(11-16 July): 1005–96.
- Kjørsvik, E. et al. 1990. “Egg Quality in Fishes.” *Advances in Marine Biology* 26(C): 71–113.
- Litscher, E. S. et al. 2014. “Evolution, Structure, and Synthesis of Vertebrate Egg-Coat Proteins.” *Trends in developmental biology* 8: 65–76.
- Litscher, E. S. et al. 2018. “The Fish Egg’s Zona Pellucida.” *Current Topics in Developmental Biology* 130: 275–305. <https://linkinghub.elsevier.com/retrieve/pii/S0070215318300024>.
- Macías, D. et al. 2005. “Reproductive Characteristics of Swordfish (*Xiphias Gladius*) Caught in the Southwestern Mediterranean during 2003.” *Col. Vol. Sci. Pap. ICCAT* 58(2): 454–69.
- Marisaldi, L. et al. 2020. “Maturity Assignment Based on Histology-validated Macroscopic Criteria: Tackling the Stock Decline of the Mediterranean Swordfish (*Xiphias Gladius*).” *Aquatic Conservation: Marine and Freshwater Ecosystems* 30(2): 303–14. <https://onlinelibrary.wiley.com/doi/10.1002/aqc.3248>.
- Matthäus, C. et al. 2008. “Chapter 10 Infrared and Raman Microscopy in Cell Biology.” *Methods in Cell Biology* 89: 275–308. <https://linkinghub.elsevier.com/retrieve/pii/S0091679X08006109>.
- Mazzeo, I. et al. 2016. “A Comparison of Techniques for Studying Oogenesis in the European Eel *Anguilla Anguilla*.” *Journal of Fish Biology* 89(4): 2055–69.
- Menn, F. L. et al. 2007. “Ultrastructural Aspects of the Ontogeny and Differentiation of Ray-Finned Fish Ovarian Follicles BT - The Fish Oocyte: From Basic Studies to Biotechnological Applications.” In eds. Patrick J Babin, Joan Cerdà, and Esther Lubzens. Dordrecht: Springer Netherlands, 1–37.

https://doi.org/10.1007/978-1-4020-6235-3_1.

- Minniti, F. et al. 2005. "Ultrastructural Features of Germ Cells in Immature Swordfish *Xiphias Gladius* (Teleostei, Xiphidae)." *Italian Journal of Zoology* 72(3): 217–21. <https://doi.org/10.1080/11250000509356674>.
- Naumann D. 2001. "FT-Infrared and FT-Raman Spectroscopy in Biomedical Research." *Applied Spectroscopy Reviews* 36(2–3): 239.
- Neilson, J. D. et al. 2007. "Stock Structure of Swordfish (*Xiphias Gladius*) in the Atlantic: A Review of the Non-Genetic Evidence." *Collective Volume of Scientific Papers ICCAT*: 61, 25–60.
- Ortiz-Delgado, J. B. et al. 2008. "Histochemical Characterisation of Oocytes of the Swordfish *Xiphias Gladius*." *Scientia Marina* 72(3): 549–564. <https://scientiamarina.revistas.csic.es/index.php/scientiamarina/article/view/1020>.
- Palko et al. 1981. "Synopsis of the Biology o National Oceanic and Atmospheric Administration National Marine Fisheries Service."
- Poisson, F. et al. 2009. "Reproductive Dynamics of Swordfish (*Xiphias Gladius*) in the Southwestern Indian Ocean (Reunion Island).Part 1: Oocyte Development, Sexual Maturity and Spawning." *Aquatic Living Resources* 22(1): 45–58.
- Romeo, M. et al. 2006. "Infrared Micro-Spectroscopic Studies of Epithelial Cells." *Biochimica et Biophysica Acta - Biomembranes* 1758(7): 915–22.
- Saber, S. et al. 2020. "A Preliminary Analysis of the Maturity of ICCAT Swordfish Stocks." *Collect. Vol. Sci. Pap. ICCAT* 77(3): 537–51.
- Sedberry, G. R. et al. 2001. "Satellite Telemetry Tracking of Swordfish, *Xiphias Gladius*, off the Eastern United States." *Marine Biology* 139(2): 355–60.
- Smith, B. L. et al. 2015. "Multilocus Bayesian Estimates of Intra-Oceanic Genetic Differentiation, Connectivity, and Admixture in Atlantic Swordfish (*Xiphias Gladius* L.)." *PLoS ONE* 10(6).
- Sreedhar, H. et al. 2015. "High-Definition Fourier Transform Infrared (FT-IR) Spectroscopic Imaging of Human Tissue Sections towards Improving Pathology." *JoVE* (95): e52332. <https://www.jove.com/t/52332>.
- Talari, A. C. S. et al. 2017. "Advances in Fourier Transform Infrared (FTIR) Spectroscopy of Biological Tissues." *Applied Spectroscopy Reviews* 52(5): 456–506.
- Taylor, R. G. et al. 1992. *Reproductive Biology of the Swordfish Xiphias Gladius in the Straits of Florida and Adjacent Waters*.
- Tyler, C. R. et al. 1996. "Measurement of Vitellogenin, a Biomarker for Exposure to Oestrogenic Chemicals, in a Wide Variety of Cyprinid Fish." *Journal of Comparative Physiology B* 166(7): 418–26. <https://doi.org/10.1007/BF02337886>.
- Wood, B. R. et al. 2008. "Shedding New Light on the Molecular Architecture of

Oocytes Using a Combination of Synchrotron Fourier Transform-Infrared and Raman Spectroscopic Mapping.” *Analytical Chemistry* 80(23): 9065–72. <https://pubs.acs.org/doi/10.1021/ac8015483>.

Yamagami, K. et al. 1992. “Molecular and Cellular Basis of Formation, Hardening, and Breakdown of the Egg Envelope in Fish.” *International review of cytology* 136(C): 51–92. <https://pubmed.ncbi.nlm.nih.gov/1506146/>.

Young, J. et al. 2003. “Reproductive Dynamics of Broadbill Swordfish, *Xiphias Gladius*, in the Domestic Longline Fishery off Eastern Australia.” *Marine and Freshwater Research* 54: 315–32.

Zelazowska, M. 2010. “Formation and Structure of Egg Envelopes in Russian Sturgeon *Acipenser Gueldenstaedtii* (Acipenseriformes: Acipenseridae).” *Journal of Fish Biology* 76(3): 694–706.

CONCLUSIONS

Basic research in teleost fish species is crucial not only for the comprehension of sea life aspects but also to deepen topics related to human health. The present PhD project took into account physiological mechanisms, related to environmental issues, of wild and laboratory model fish species, evidencing how the vibrational approach can be useful to investigate a large number of specimens, without depending on their dimensions, complexity and diffusion. The vibrational approach combined with the visual and/or histological analysis showed its successful application in detecting and evidencing meaningful biochemical aspects, obtaining a great amount of information about the distribution of the most relevant biomolecules of tissues and cells with the corresponding biochemical composition of the sample.

In particular, Raman Microspectroscopy was applied for the identification of the spectral features of Zebrafish embryos, in the specific context of their treatment with a proper fixative solution, in order to achieve and obtain the best spectral quality and conservation of the sample. The vibrational fingerprint of the fixatives was evaluated and statistically correlated with the corresponding visual outcome. This could represent a new, reliable and fast tool to be applied in Zebrafish embryos treatment and maintenance, as far as RMS measurements cannot always be performed as soon as the specimen is ready to be analyzed.

In addition, and subsequently to the previous one, RMS analysis was performed to evaluate and detect several aspects related to the impairment on Zebrafish embryos after their exposure in water medium to two widely diffused perfluorinated compounds: PFOA and PFOS. RMS analyses highlighted several signals of metabolic stress, mainly at the higher doses of administered compounds, which impacted the biochemical composition of

yolk's embryo, in terms of proteins, lipids, cholesterol and phospholipid bands. The spectral data suggest that the two observed compounds can penetrate the yolk sac, inducing alterations in all the just mentioned components, causing a lowering in the contents of lipids, proteins and phosphates and an altered trend of consumption related to a slowdown of the utilization of yolk's proteins, lipids and phosphates.

Besides this main topic, the impairment induced by endogenous and exogenous factors on the biochemical composition of swordfish oocytes was also investigated by applying Fourier Transform Infrared Imaging spectroscopy, evidencing the differences in composition in oocytes belonging to different geographical regions of the Mediterranean Sea, shedding a new light on the possibility of presence of different genetic stocks in the Mediterranean Sea. The differences in swordfish ZR thickness and macromolecular composition in relation with the fishing area, both as regards vitellogenic and mature oocytes, can improve knowledge in reproductive biology of swordfish, considered as a threatened species, and could further be useful for better elucidating oocyte quality and fertility success rate of this specie.

In conclusion, the overall results of the present PhD project show that vibrational spectroscopies can provide rapid and precious information about different fish species, confirming and enriching histological and visual analyses: hence, these techniques revealed to be valuable tools for basic research studies in the field of fish metabolic and reproductive biology.